New directions in the theory of spin-polarized atomic hydrogen and deuterium

NEW DIRECTIONS IN THE THEORY OF SPIN-POLARIZED ATOMIC HYDROGEN AND DEUTERIUM

VIANNEY KOELMAN

NEW DIRECTIONS IN THE THEORY OF SPIN-POLARIZED ATOMIC HYDROGEN AND DEUTERIUM

Proefschrift

ter verkrijging van de graad van doctor aan de Technische Universiteit Eindhoven, op gezag van de Rector Magnificus, Prof. ir. M. Tels, voor een commissie aangewezen door het college van dekanen in het openbaar te verdedigen op dinsdag 13 december 1988 te 14.00 uur

door

JOHANNES MARIA VIANNEY ANTONIUS KOELMAN

geboren te Heerlen

Druk: Boek en Offsetdrukkerij Letru, Helmond, 04920-37797

Dit proefschrift is goedgekeurd door de promotoren:
Prof. dr. B.J. Verhaar
Prof. dr. J.T.M. Walraven

The work described in this thesis was carried out at the Physics Department of the Eindhoven University of Technology and was part of a research program of the 'Stichting voor Fundamenteel Onderzoek der Materie' (FOM) which is financially supported by the 'Nederlandse Organisatie voor Wetenschappelijk Onderzoek' (NWO).

CONTENTS

CHAPTER 1
INTRODUCTION

Section 1.1
Atomic hydrogen and deuterium gases: Two novel quantum fluids

Virtually all substances solidify at low temperatures. This is due, in particular, to the universal Van der Waals attraction. During many decades the only known examples of substances which do not solidify were the helium isotopes ^{3}He and ^{4}He. They remain liquid down to zero temperature because their interatomic Van der Waals attraction is to a large extent compensated by the zero-point kinetic energy of the atoms. As the zero-point motion which prevents them to crystalize has a quantum-mechanical origin, they are generally called quantum fluids.

As first pointed out by Hecht,[1] hydrogen and deuterium atoms with polarized electronic spins would constitute even more extreme examples of quantum fluids. Due to their lower mass, H and D have a larger zero-point energy than the helium isotopes, while the attraction strength of the triplet potential acting between spin-polarized hydrogen or deuterium atoms is comparable in weakness to the He-He attraction. Hecht concluded that whereas due to the quantum mechanical zero-point motion the helium isotopes do not solidify, spin polarized H and D not even liquefy.

Spin-polarized bosonic H and fermionic D would therefore provide us with weakly interacting gas phase quantum fluids in which the many surprising phenomena which were discovered with the Bose liquid ^{4}He and the Fermi liquid ^{3}He are expected to take place in a much clearer form. This particularly applies to the effects which occur in the quantum degeneracy regime: the low-temperature, high-density regime where the thermal De Broglie wavelength of the particles is larger than the interparticle spacing. For instance, the phenomenon of Bose-Einstein condensation in the degenerate Bose gas H should occur with a condensate fraction reaching values close to 100%.[2] This figure is to be compared to that for the degenerate Bose system ^{4}He in which the Bose-Einstein condensation is sharply suppressed by the strong interaction effects: its condensate fraction is measured to be below 15%.[3]

Moreover, the dilute H and D gases enable comparison of experimental results with *ab initio* theoretical results of any desired precision. This in contrast to the dense quantum fluids ^{3}He and ^{4}He for which no *ab initio* microscopic theories have been developed. This particularly applies to the Fermi system ^{3}He which, up to now, can only be described by phenomenological theories.[4] For the Bose liquid ^{4}He one can perform Monte Carlo simulations[5] which are however of limited accuracy.

Moreover, comparison between experimental and theoretical results is considerably

facilitated for the H and D systems as the interatomic interactions for these elementary atoms are known with a very high degree of accuracy.[6] Spectroscopic experiments have confirmed the accuracy of these *ab initio* potentials to high precision.[7] From the experimental point of view an important advantage of spin-polarized H and D is that with these systems, temperature and density can be controlled independently over large ranges of values. Furthermore, thanks to their large (electronic) magnetic moments, H and D can be manipulated using magnetic fields (see next section). In the bosonic H gas one might expect interesting phenomena associated with the dynamics of a non-vanishing nuclear spin ($I=\frac{1}{2}$) to occur. This in contrast to the Bose fluid ^{4}He which carries no spin. The fermionic D gas in this respect should display very rich behavior: it bears a nuclear spin I=1, to be compared to the nuclear spin $I=\frac{1}{2}$ of the Fermi fluid ^{3}He.

For many years the idea of Hecht to use spin polarized H or D in order to create degenerate quantum gases received little attention as it was by no means clear how to create spin polarized atomic hydrogen or deuterium gas in stable form. This changed drastically when two decades after Hecht's prediction Silvera and Walraven succeeded in stabilizing spin polarized hydrogen for the first time.[8] Since that time a large number of experimentalists as well as theoreticians, recognizing the potential richness of these new quantum systems, put effort in the study of spin polarized quantum gases. In the next section we discuss the techniques for stabilizing spin polarized atomic hydrogen and deuterium which form the basis of all research on these systems.

References

(1) C.E. Hecht, Physica 25, 1159 (1959).

(2) N. Bogoliubov, J. Phys. (U.S.S.R.) 11, 23 (1947).

(3) V.F. Sears, E.C. Svensson, P. Martel and A.D.B. Woods, Phys. Rev. Lett. 49, 279 (1982).

(4) L.D. Landau, Zh. Eksp. Teor. Fiz. 30, 1058 (1956) [English translation: Soviet Phys. JETP 3, 920 (1957)].

(5) D.M. Ceperly and E.L. Pollock, Phys. Rev. Lett. 56, 351 (1986).

(6) W. Kolos and L. Wolniewicz, J. Chem. Phys. 43, 2429 (1965); W. Kolos and L. Wolniewicz, Chem. Phys. Lett. 24, 457 (1974); L. Wolniewicz, J. Chem. Phys. 78, 6173 (1983).

(7) I. Dabrowski, Can. J. Phys. 62, 1639 (1984).

(8) I.F. Silvera and J.T.M. Walraven, Phys. Rev. Lett. 44, 164 (1980).

Section 1.2
Stabilization of H and D gas

Molecular hydrogen or deuterium can easily be dissociated in an electric discharge. However, the resulting atoms are at high temperatures, not spin-polarized and usually very short-lived due to adsorption and subsequent rapid recombination on surfaces. Experimental attempts to create stable spin-polarized hydrogen or deuterium gases therefore all focus on the problems of how to polarize their electronic spins and how to cool and confine them without inducing a rapid decay.

The use of liquid-helium covered walls formed the key to the successful stabilization of atomic hydrogen. The first successful stabilization experiments[1,2] showed that hydrogen and deuterium atoms can thermalize with liquid-helium covered walls at sub-kelvin temperatures without undergoing a rapid recombination. The use of liquid-helium lined walls solved the cooling problem, and also the confinement problem. Furthermore, having cold atoms, the spins can be polarized in a straightforward manner by exploiting the separation of spin-up and spin-down atoms in strong magnetic field gradients. This can be understood in more detail by examining the ground-state hyperfine energy levels for hydrogen and deuterium as functions of magnetic field strength (Fig.1).

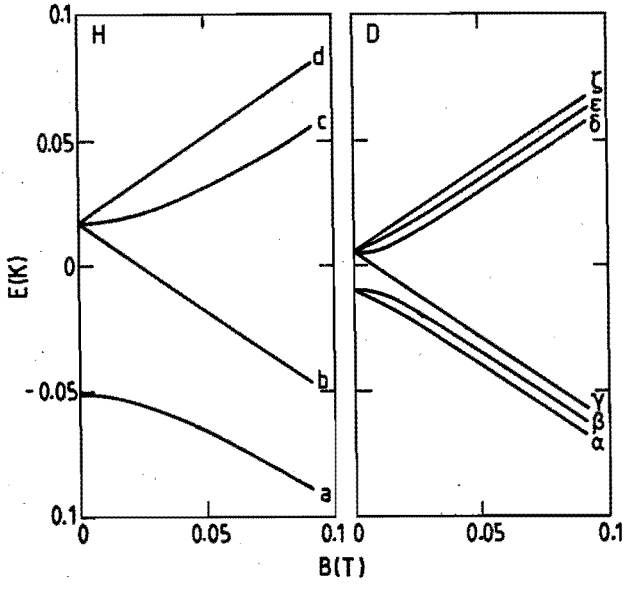

Fig.1. a) Hyperfine energy levels for the ground electronic state of hydrogen in a magnetic field, b) same for deuterium.

The upper half of the hyperfine states are "low-magnetic-field seekers": their energies decrease with magnetic field strength as they are essentially electron spin "up" states denoted by H↑ or D↑. The lower half of the hyperfine states are "high-magnetic-field seekers": their energies decrease with magnetic field strength as they have essentially their electron spin in the "down" state: H↓ or D↓.

The standard type of experiments utilize this behavior by locating the cell in which the spin-polarized atoms are to be stabilized in high field, while the dissociator is located at a low field region (Fig.2). This configuration attracts the "high-field seekers" to the stabilization cell and repels the "low-field seekers" from it. For large magnetic fields and cold atoms so that the energy separation between the "high-field seeking" states and the "low-field seeking" states (approximately two times the electronic Zeeman energy) is much larger than the thermal kinetic energy of the atoms, this separation is in fact complete. In this way, only the "high-field-seeking" state atoms (H↓ or D↓) are confined.

Experiments showed that this scheme is especially useful in stabilizing atomic hydrogen. It soon turned out[3,4] that the H↓ gas consisting of an admixture of a- and b-state atoms (Fig.1) rapidly purifies into a b-state atom gas: the so–called "doubly spin-polarized" atomic hydrogen gas, denoted H↓↓. This H↓↓ gas is very stable. There is a decay due to nuclear spin relaxation in two-body collisions, but this decay is extremely slow[5] as the interactions which couple to the nuclear spin are very weak. Three-body recombination reactions are also very slow, especially at low atom densities. In fact, at magnetic fields of approximately 8 Tesla and temperatures close to 0.5 Kelvin three-body loss mechanisms were found to be more than six orders of magnitude slower than the zero field room-temperature three-body decay.[6] Accordingly, many interesting experiments have been carried out with spin-polarized hydrogen atoms at high magnetic field (see next section).

For deuterium the situation is quite different. Up to now only two successful experiments with D↓ have been reported.[2,7] In these experiments no high atom density could be built up, as the samples decayed very rapidly. The origin of this rapid decay is attributed to[2,7] the building up of a two-dimensional adsorbed D atom gas on the helium surfaces: As discussed above, liquid-helium-lined walls provide us with a very efficient means for confining spin-polarized hydrogen gas. This is because a liquid helium surface has a very small adsorption energy for hydrogen atoms (approximately 1 K in temperature units), which prevents a large building up of adsorbed-atom density down to very low temperatures. The adsorption energy of deuterium atoms on a ^{4}He film is measured to be approximately 2.6 K,[2] much larger than the value for H, so that at typical temperatures of a few hundreds of millikelvins a considerable adsorbed atom density builds up. In combination with an anomalously large two-body decay rate for adsorbed D↓ atoms,[7] this yields a very rapid decay.

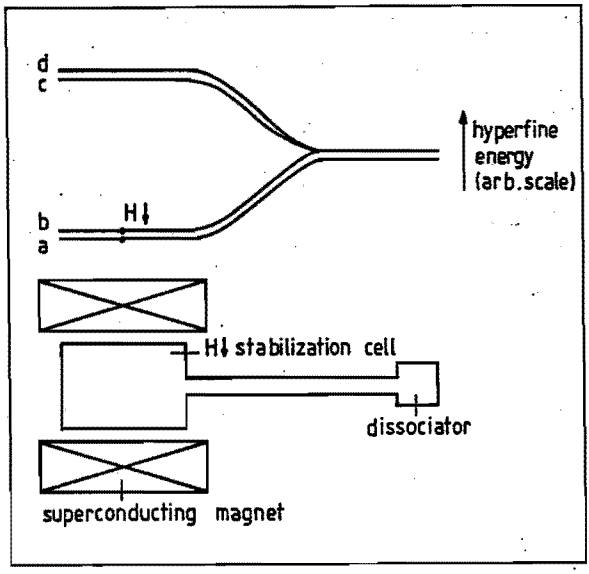

Fig.2. Lower part: experimental setup for H↓ stabilization (schematic). The walls are covered with a superfluid helium film. Upper part: hyperfine energy levels at various locations.

Although the situation for H↓ is more favorable to observe degenerate quantum behavior, the degeneracy regime in which Bose-Einstein condensation should occur has never been achieved. Attempts to enter this low-temperature, high-density regime are also hampered by surface adsorption. This is because, in order to achieve Bose-Einstein condensation in a bulk gas in thermodynamic equilibrium with an adsorbed gas, a saturated surface density has to be built up in the latter.[8] This surface density is roughly given by: $n_s \simeq \mu E_a/\hbar^2$ (μ is the reduced atomic mass of the H-H system and E_a the adsorption energy), which is approximately 10^{14} atoms/cm^2 for H on a ^{4}He film. Such large adsorbed atom densities give rise to a very fast decay due to three-body recombination events.[6,9] Due to this three-body recombination the adsorbed atoms at saturated density have a mean lifetime of only some tens of microseconds. The resulting large recombination heat load warms up the sample, thereby preventing the degeneracy regime to be reached.

Several proposals have been put forward to overcome these difficulties.At Harvard[10] experimental efforts are going on which explore the possible existence of a B-field "window" with a low enough three-body decay rate. Guided by theoretical results[11] these efforts aim at very high magnetic fields (B ≃ 25 Tesla).

An entirely new approach is to get rid of the walls by using a wall free confinement

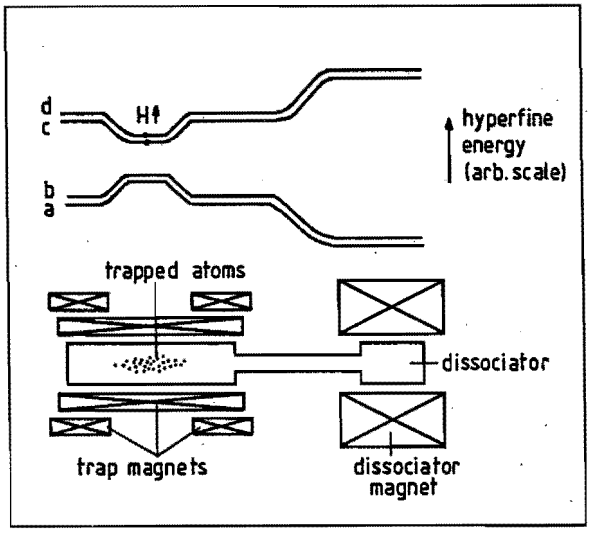

Fig.3. Lower part: experimental setup for H↑ stabilization (schematic). All walls are covered with a superfluid helium film. Upper part: hyperfine energy levels at various locations.

scheme. This should open up the intriguing possibility of working at very low (sub-millikelvin) temperatures and low atom densities to reach the degeneracy regime. The large magnetic moments of the hydrogen atoms could be used as "handles" to manipulate and confine them with magnetic fields. Unfortunately, the Maxwell equations forbid a static magnetic field maximum in free space[12]. Hence, it is not possible to trap H↓ in a static magnetic field. A way out might be the use of a dynamic magnetic trap. This possibility has been analyzed by Lovelace *et al.*[13] They find that fields of the order of 1 Tesla at a few kilohertz are needed to provide a trap for H↓ of a few millikelvin deep. One may doubt whether such fields can be realized without excessive eddy-current heating in the refrigeration system. Besides, it is not clear how the low energetic atoms required to fill the very shallow trap are to be produced.

Much more promising is the proposal[14] to trap H↑ atoms (c and d atoms, Fig.1) instead of H↓ atoms. These "low-field-seeking" atoms can be trapped in a static magnetic field minimum which can be created in free space. Low-field-seeking H↑ atoms can be made using a dissociator located in a high B-field region (Fig.3), so that the "low-field-seekers", being attracted to the confinement region, are separated from the "high-field-seekers". The H↑ atoms in the low field region become trapped as they thermalize amongst themselves in two-body collisions and with the helium covered walls (at temperatures of 50-100 mK). Working with H↑ instead of H↓ can only be

done at the expense of introducing a rapid decay due to electronic spin relaxation to "high-field-seeking" H↓ states. It appears that[15] especially spin-exchange collisions between two c-state atoms or between a c-state and a d-state atom lead to a rapid relaxation to a- and b-state atoms which are repelled from the trap. Fortunately, very rapidly these spin-exchange processes become ineffective as they lead to the disappearance of the c-state atoms, thereby creating a doubly-polarized d-state atom (H↑↑) gas. The lifetime of the H↑↑ gas is limited by dipolar spin relaxation.[15] Analyses of the behavior of trapped H↑↑ gas undergoing evaporative cooling and magnetic compression in the presence of the dipolar relaxation process[16] indicate that the degeneracy regime might be reached marginally at temperatures of a few tens of microkelvins. Most troublesome in this respect is the behavior of the ratio of thermalization rate (due to elastic collisions between the atoms) over decay rate (due to dipolar spin-relaxation collisions). This ratio is proportional to the square root of temperature, so that at lower temperatures evaporative cooling, relying on a rapid thermalization of the atoms, becomes less efficient. In fact, the H↑↑ gas cannot be cooled below a critical temperature typically of the order of a few microkelvin, where thermalization and relaxation rates become of comparable magnitude.

In relation to this an interesting novel development is discussed in chapter 2 of this thesis. In analyzing the behavior of magnetically trapped deuterium atoms (D↑) very exciting possibilities, associated with the Fermi character of D, show up. It appears that under the influence of fast spin-exchange processes also D↑ purifies into doubly spin-polarized deuterium gas: D↑↑. But, in contrast to the case of trapped H↑↑, the dipolar relaxation limited stability of D↑↑ increases with decreasing temperature. Also the ratio of thermalization rate over relaxation rate increases with lowering temperature, making evaporative cooling more and more efficient at lower temperatures.

Recently, two groups have succeeded in magnetically trapping spin polarized H gas.[17] Using evaporative cooling, temperatures of about 1 mK have been realized in trapped H↑↑ gas.[18] Many exciting developments, including optical detection and manipulation of trapped H and D,[19] may be expected in the near future.

References

(1) I.F. Silvera and J.T.M. Walraven, Phys. Rev. Lett. 44, 164 (1980).

(2) I.F. Silvera and J.T.M. Walraven, Phys. Rev. Lett. 45, 1268 (1980).

(3) B.W. Statt and A.J. Berlinsky, Phys. Rev. Lett. 45, 2105 (1980).

(4) R.W. Cline, T.J. Greytak and D. Kleppner, Phys. Rev. Lett. 47, 1195 (1981).

(5) R.M.C. Ahn, J.P.H.W. van den Eijnde, C.J. Reuver, B.J. Verhaar and I.F. Silvera, Phys. Rev. B 26, 452 (1982).

(6) R. Sprik, J.T.M. Walraven and I.F. Silvera, Phys. Rev. Lett. 51, 479, 942 (1983); H.F. Hess, D.A. Bell, G.P. Kochanski, R.W. Cline, D. Kleppner and T.J.Greytak, Phys. Rev. Lett. 51, 483 (1983); T. Tommila, S. Jaakola, M. Krusius, I. Krylov and E. Tjukanov, Phys. Rev. Lett. 56, 941 (1986).

(7) I. Shinkoda, M.W. Reynolds, R.W. Cline and W.N. Hardy, Phys. Rev. Lett. 57, 1243 (1986).

(8) D.O. Edwards and I.B. Mantz, J. Phys. (Paris) 41, C7–257 (1980); I.F. Silvera and V.V. Goldman, Phys. Rev. Lett. 45, 915 (1980).

(9) L.P.H. de Goey, J.P.J. Driessen, B.J. Verhaar and J.T.M. Walraven, Phys. Rev. Lett. 53, 1919 (1984).

(10) J.D. Gillaspy, I.F. Silvera and J.S. Brooks, preprint.

(11) H.T.C. Stoof, L.P.H. de Goey, B.J. Verhaar and W. Glöckle, Phys. Rev. B 38, (Dec. 1988).

(12) W.H. Wing, Prog. Quant. Electr. 8, 181 (1984).

(13) R.V.E. Lovelace, C. Mehanian, T.J. Tommila and D.M. Lee, Nature 318, 30 (1985).

(14) H.F. Hess, Bull. Am. Phys. Soc. 30, 854 (1985).

(15) A. Lagendijk, I.F. Silvera and B.J. Verhaar, Phys. Rev. B 33, 626 (1986); H.T.C. Stoof, J.M.V.A. Koelman and B.J. Verhaar, Phys. Rev. B. 38, 4688 (1988).

(16) H.F. Hess, Phys. Rev. B 34, 3476 (1986); T.J. Tommila, Europhys. Lett. 2, 789 (1986).

(17) H.F. Hess, G.P. Kochanski, J.M. Doyle, N. Masuhara, D. Kleppner and T.J. Greytak, Phys. Rev. Lett. 59, 672 (1987); R. van Roijen, J.J. Berkhout, S. Jaakkola and J.T.M. Walraven, Phys. Rev. Lett. 61, 931 (1988).

(18) N. Masuhara, J.M. Doyle, J.C. Sandberg, D. Kleppner, T.J. Greytak, H.F. Hess and .P. Kochanski, Phys. Rev. Lett. 61, 935 (1988).

(19) T.W. Hijmans, O.J. Luiten, I.D. Setija and J.T.M. Walraven, Proc. of the Third International Conf. on Spin-Polarized Quantum Systems, Torino, 1988 (World-Scientific Publ.).

Section 1.3
Scientific opportunities and applications

In the physical regimes already studied, spin-polarized atomic hydrogen has proven to be a very rich system (for a comprehensive overview the reader is referred to Refs. 1 and 2). Much has been learned about the decay mechanisms of spin-polarized hydrogen and deuterium (see previous section). Very interesting experiments have been carried out which increased our knowledge on the interaction of low energetic H and D atoms with helium surfaces. Also the exceptional properties of spin-polarized hydrogen gas have clearly shown up in their transport properties, especially in the observation of nuclear spin waves.[3]

Yet there remain many interesting scientific opportunities and technological applications of spin-polarized H and D which have only partially been studied, or even unstudied. For instance, the interaction of very low energetic H and D atoms with helium surfaces is still only partially understood. A theoretical analysis[4] leaves a very large uncertainty in the sticking probability of slow H atoms incident on a helium film. Having very cold atoms (for instance H$\uparrow\ddagger$ or D$\uparrow\dagger$ atoms produced in a magnetic trap) one might experimentally study this problem.

Also associated with the helium film is the possibility of observing nuclear spin waves in a two-dimensional gas (see chapter 4 of this thesis). Such an experimental observation should provide direct information on the peculiar effects of the negative centrifugal "barrier" typical for 2D low energy scattering.[5] At higher surface densities the adsorbed gas becomes degenerate and is expected to undergo a Kosterlitz-Thouless transition.[6]

In general, the hope to observe gas phase degenerate quantum behavior, i.e. the observation of Fermi-pressure effects in D gas (see chapter 2) and particularly Bose-Einstein condensation in H gas, are very important motivations for spin-polarized hydrogen and deuterium research.

One of the most impressive applications of spin-polarized hydrogen is the cryogenic hydrogen maser. By making use of several peculiarities of cold H gas in a helium-lined cell, a very stable frequency standard can be built. Actual maser oscillation of hydrogen atoms at sub-kelvin temperatures has been observed by a number of groups.[7] The cryogenic hydrogen maser is extensively discussed in chapter 3.

Another important application is the possibility of doing ultrahigh-resolution spectroscopy with very cold H or D gases in which all Doppler effects are considerably reduced. In this respect it is interesting to note that the results of chapter 2 indicate that with magnetically trapped deuterium unheard-of low temperatures can be reached, far below the cooling limit of a few microkelvin for magnetically trapped hydrogen.

Other applications involve: the use of spin-polarized hydrogen or deuterium to create polarized proton or deuteron targets for nuclear and particle scattering (possibly by using doubly-polarized H or D to create solid nuclear-polarized H_2 or D_2[2]), and the use of doubly spin-polarized deuterium to enhance the efficiency of plasma fusion reactors.[8]

References

(1) I.F. Silvera and J.T.M. Walraven,in *Progress in Low Temp. Phys.*, edited by D.F.Brewer, (North–Holl., Amsterdam 1986) Vol. 10, 139.

(2) T.J. Greytak and D. Kleppner, in *New Trends in Atomic Phys.*, edited by G. Grynberg and R. Stora, (North–Holl., Amsterdam 1984) p. 1125.

(3) B.R. Johnson, J.S. Denker, N. Bigelow, L.P. Levy, J.H. Freed and D.M. Lee, Phys. Rev. Lett. 52, 1508 (1984).

(4) V.V. Goldman, Phys. Rev. Lett. 56, 612 (1986).

(5) B.J. Verhaar, L.P.H. de Goey, J.P.H.W. van den Eijnde and E.J.D. Vredenbregt, Phys. Rev. A 32, 1424 (1985).

(6) D.O. Edwards and I.B. Mantz, J. Phys. (Paris) 41, C7–257 (1980).

(7) M.D. Hürlimann, W.N. Hardy, A.J. Berlinsky and R.W. Cline, Phys. Rev. A 34, 1605 (1986); R.L. Walsworth, I.F. Silvera, H.P. Godfried, C.C. Agosta, R.F.C. Vessot and E.M. Mattison, Phys. Rev. A 34, 2550 (1986); H.F. Hess, G.P. Kochanski, J.M. Doyle, T.J. Greytak and D. Kleppner, Phys. Rev. A 34, 1602 (1986).

(8) R.M. Kulsrud, H.P. Furth, E.J. Valeo and M. Goldhaber, Phys. Rev. Lett. 49, 1248 (1982).

Section 1.4
This thesis

The following three chapters of this thesis each treat a different recent development in the theory of atomic hydrogen or deuterium gas. They have in common that, on a microscopic level, they deal with collisions between hydrogen (or deuterium) atoms in their ground electronic state. At first sight, collisions between ground-state hydrogen atoms might seem a trivial problem, being a standard example in textbooks on atomic collision theory. However, as will become clear in the next chapters, this is certainly not the case for the problem of collisions at very low energy. In that case the dynamics of all four spins involved in the collision is manifest. The quantum-mechanical analysis of the complicated spin dynamics shows many surprises and provides a challenge common to the three subjects treated in this thesis.

The above can be illustrated with the phenomenon of nuclear spin waves studied in chapter 4. As will be shown, despite the fact that interactions between two atoms are nuclear-spin independent, the outcome of an scattering event does depend on the nuclear spins involved due to particle indistinguishability effects at low collision energies. This subtle effect gives rise to quantum phenomena on a macroscopic scale via the occurrence of nuclear spin waves.

The interaction between the nuclear and the electronic spins plays an important role in the calculation of the decay rates of magnetically trapped H and D gases. As will become clear in chapter 2, care must be taken in the way the hyperfine interaction is taken into account in the calculation of inelastic two-body collisions. For instance, a complete neglect of this hyperfine interaction in the calculation of the decay rates for $H\uparrow$ and $D\uparrow$ gases yields rates which vanish in the low-temperature limit, whereas the exact low-temperature rates are large and independent of temperature.

The nuclear spin dynamics plays a very decisive role in spin-exchange collisions between H atoms in a maser. In chapter 3 it will be shown that the nuclear spin dynamics due to the hyperfine interaction during spin-exchange collisions puts severe limits on the frequency stability level achievable with low temperature H masers.

CHAPTER 2
MAGNETICALLY TRAPPED ATOMIC DEUTERIUM

Section 2.1
Fermionic D gas versus bosonic H gas

In the past decade a great number of exciting experiments have been carried out with spin-polarized hydrogen.[1,2] Spin-polarized deuterium however, has attracted relatively little attention of experimentalists as, even in liquid-helium-lined cells, this gas was found to be very hard to stabilize.[3,4] This probably accounts for the fact that by the time the opportunity of surface-free magnetic confinement was recognized in the field of spin-polarized hydrogen research,[5] nobody put effort in the analysis of the stability of magnetically trapped deuterium. Yet, a little thinking already reveals the exceptional properties of such a system. Wall-free confinement of deuterium atoms not only eliminates surface adsorption and subsequent recombination, which cause the rapid decay of deuterium in helium-lined cells, but also, if the deuterium atoms are all in the same hyperfine state, the Pauli exclusion principle suppresses at low temperatures all collision processes thereby enhancing the stability of the gas. As in the absence of wall adsorption sample temperatures can be lowered considerably this suppression of collisions may be very strong.

We show in the present chapter, that the difference in behavior between magnetically-trapped bosonic H gas and fermionic D gas is remarkable. The decay rate of magnetically trapped H is fast and, to lowest order, independent of temperature. In trapped D gas however, the decay rate decreases dramatically with decreasing temperature. As a result, at sub-millikelvin temperatures the lifetime of trapped D is orders of magnitude larger than that of trapped H. Furthermore, in the hydrogen case the ratio of thermalization rate over decay rate decreases with lowering temperature, thereby putting a fundamental lower limit on temperatures achievable with trapped H. This in contrast to the deuterium case where this ratio increases with lowering temperature yielding the possibility of reaching unheard-of low temperatures, and the observation of gas-phase degenerate quantum behavior.

By now, two groups have reported successful experiments with magnetically trapped H.[6,7] Having trapped H, the trapping of D is by no means a trivial extension. Due to the larger adsorption energy of D on helium films and the higher surface decay rate, deuterium atoms are more difficult to load in a trap than hydrogen. Once the problem of loading has been overcome, for instance by using deeper magnetic traps, magnetically trapped deuterium provides us with a highly ideal gaseous quantum system.

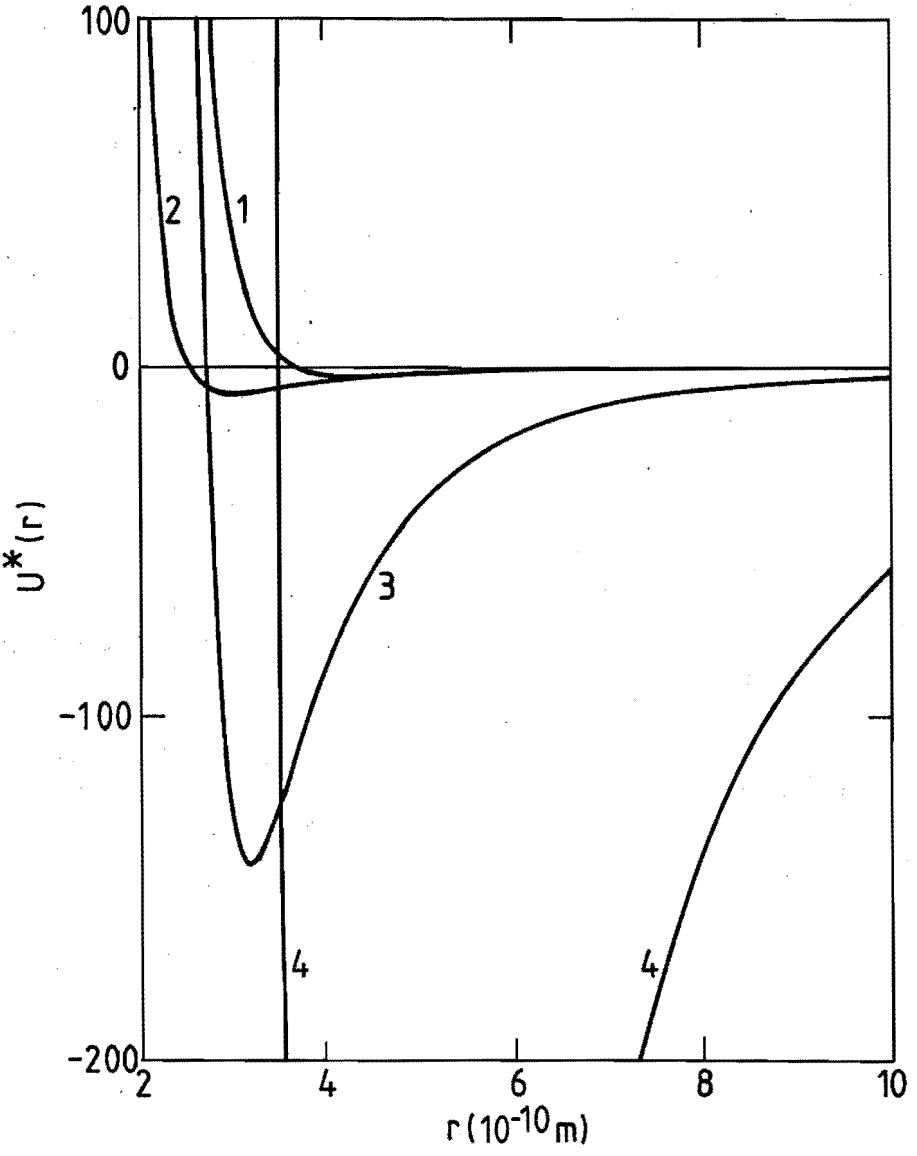

Fig. 1. Dimensionless interaction $U^*(r)=mr^2V(r)/\hbar^2$ *as a function of interatomic separation for various groundstate atoms. Curve 1: spin-polarized hydrogen atoms, curve 4: spin-polarized lithium atoms. For the sake of comparison also the dimensionless interaction between helium atoms (curve 2) and neon atoms (curve 3) is shown. For atomic species with minima in the dimensionless interaction much deeper than unity a large number of scattering resonances contribute to the recombination decay down to very low temperatures.*

The large difference in behavior between bosonic and fermionic isotopes applies to all B-field trappable atoms. Hydrogen and deuterium are however unique, as without any doubt among all B-field-trappable atomic bosons and fermions, they have the highest intrinsic stability. Other atomic systems such as the alkalis, have the distinct advantage that they can be laser cooled relatively easily. However, as pointed out by Vigué,[8] due to fast resonance recombination associated with their strong interatomic interactions and their large atomic masses, the alkalis are considerably less stable. Fig.1 illustrates the exceptional smallness of interaction effects in magnetically trapped hydrogen.

References

(1) I.F. Silvera and J.T.M. Walraven,in *Progress in Low Temp. Phys.*, edited by D.F.Brewer, (North-Holl., Amsterdam 1986) Vol. 10, 139;

(2) T.J. Greytak and D. Kleppner, in *New Trends in Atomic Phys.*,edited by G. Grynberg and R. Stora, (North-Holl., Amsterdam 1984) p. 1125.

(3) I.F. Silvera and J.T.M. Walraven, Phys. Rev. Lett. 45, 1268 (1980).

(4) I. Shinkoda, M.W. Reynolds, R.W. Cline and W.N. Hardy, Phys. Rev. Lett. 57, 1243 (1986).

(5) H.F. Hess, Bull. Am. Phys. Soc. 30, 854 (1985).

(6) H.F. Hess, G.P. Kochanski, J.M. Doyle, N. Masuhara, D. Kleppner, and T.J. Greytak, Phys. Rev. Lett. 59, 672 (1987); N. Masuhara, J.M. Doyle, J.C. Sandberg, D. Kleppner, T.J. Greytak, H.F. Hess, and G.P. Kochanski, Phys. Rev. Lett. 61, 931 (1988).

(7) R. van Roijen, J.J. Berkhout, S. Jaakkola, and J.T.M. Walraven, Phys. Rev. Lett. 61, 935 (1988).

(8) J. Vigué, Phys. Rev. A 34, 4476 (1986).

Section 2.2

Spin-polarized deuterium in magnetic traps

J.M.V.A. Koelman, H.T.C. Stoof, B.J. Verhaar, and J.T.M. Walraven*

Department of Physics, Eindhoven University of Technology,
5600 MB Eindhoven, The Netherlands
**Natuurkundig Laboratorium, Universiteit van Amsterdam,*
1018 XE Amsterdam, The Netherlands

[Published in Phys. Rev. Lett. 59, 676 (1987)]

We have calculated the spin-exchange two-body rate constants associated with the population dynamics of the hyperfine levels of atomic deuterium as a function of magnetic field in the Boltzmann zero-temperature limit. Results indicate that a gas of low-field-seeking deuterium atoms trapped in a static magnetic field minimum decays rapidly into an ultrastable gas of doubly spin-polarized deuterium. We also discuss the temperature dependence of various effects.

The interesting physics of the gaseous spin-polarized quantum systems has been primarily studied for the Bose system spin-polarized hydrogen and the Fermi system spin-polarized ^{3}He.[1] Although the extreme quantum nature of these spin-polarized systems has been established in a variety of experiments, the observation of degenerate quantum behavior so far has been out of reach of the experimentalists. For spin-down polarized hydrogen (H$\downarrow$) it was established[2] that the critical density for Bose-Einstein condensation (BEC) can only be approached up to a factor 10 due to the presence of a third-order recombination process which is dominant on the surfaces of the helium-covered sample cells. Also for gaseous ^{3}He the degeneracy regime ($T \ll T_F$, where T_F is the Fermi temperature) is far out of reach of experiments as a result of the relatively strong interaction effects which lead to the formation of the liquid state.[1]

Spin-polarized deuterium (D$\downarrow$) has attracted relatively little attention of the experimentalists as this gas was found to be much less stable than hydrogen.[3,4] Nevertheless the theoretical interest in this system is considerable. To establish the nature of the ground state of D$\downarrow$ is a subtle problem which stimulated the use of the advanced methods of Fermi-fluid theory.[5,6] It is predicted that the doubly-polarized state (D$\downarrow\downarrow$) should be gaseous down to $T = 0$ K. Also the Landau parameters have been calculated,[6] and extensive theoretical effort was put in calculating the transport properties of gaseous D$\downarrow$ as a function of temperature.[7]

Recently, surface-free confinement schemes were proposed[8] which offer new

prospects to observe BEC by studying spin-up polarized hydrogen (H↑) in magnetic traps similar to those used for confining laser-cooled spin-polarized alkalis.[9] In this letter we show that D↑‡ is especially suited for confinement in a minimum-B-field trap and may well prove to be the purest experimental realization of the nearly ideal degenerate Fermi gas in which to a large extent density and temperature can be controlled independently. As such it is a most interesting model system enabling comparison with *ab initio* theoretical results of any desired precision. This in contrast to dense, strongly interacting Fermi systems as nuclear matter, liquid ^{3}He, and the electron gas in metals.

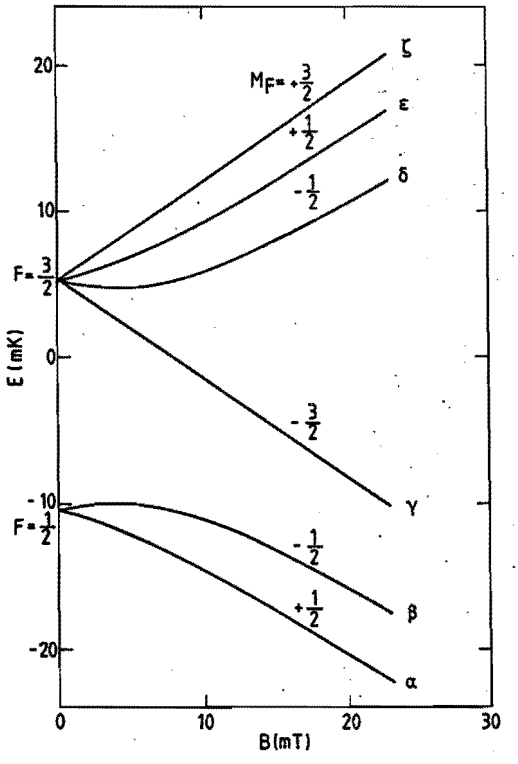

Fig.1. Energies of the deuterium hyperfine states as a function of magnetic field.

We discuss the stability of D↑, a mixture of the hyperfine states δ, ϵ, and ζ (Fig.1), confined in a static minimum-B-field trap. We calculate both spin-exchange and dipolar two-body rate constants in the low-field, T=0 K limit, and estimate the temperature and field dependence of these effects. We show that spin exchange causes

D↑ to decay rapidly towards the doubly-polarized gas D↑‡ of only ζ-state atoms. This gas may be cooled with a similar evaporative scheme as proposed[8] for H↑‡. However, in contrast to the hydrogen case where dipolar relaxation is predicted to be very fast and, to lowest order independent of temperature,[10] the stability of the fermion D↑‡ against dipolar relaxation is expected to grow with decreasing temperature because of the absence of s-wave scattering, ultimately leading to an *ultrastable* state. D↑‡ is not only likely to be the most stable B-field-trappable spin-polarized system (including the alkalis), but may also be cooled well into the degeneracy regime. We briefly discuss how Fermi statistics affects the properties of D↑‡. As a last point we address the stability of D↑‡ against resonance recombination.

We first discuss the various relaxation processes in a gaseous mixture of δ-, ε-, and ζ-state atoms (D↑). The lifetimes of these low-magnetic-field seekers are primarily limited by inelastic spin-exchange relaxation events. Dipolar relaxation only becomes competitive at high magnetic fields[10] ($B \gtrsim 0.2$ Tesla for D↑) and as such is not relevant in the current context. As in the hydrogen case an important exception to this rule is collisions between fully polarized atoms (ζ-ζ collisions) which are unaffected by spin-exchange. Considering the low values of the relevant temperatures and Fermi-Dirac statistics only low energy s-wave scattering between atoms in antisymmetrical spin states occurs. We therefore calculated the eighteen rate constants corresponding to the allowed downward spin exchange transitions between the fifteen antisymmetrized spin states $(\alpha\beta-\beta\alpha)/\sqrt{2}$, ... , $(\varepsilon\zeta-\zeta\varepsilon)/\sqrt{2}$ for s-wave scattering in the Boltzmann zero-temperature limit. These rate constants can be expressed in terms of the two-body spin-exchange T-matrix elements for vanishing kinetic energy in the incoming channel. When the splittings of the internal energy levels are not too large, we may also assume that the kinetic energy in the final channel vanishes. This approximation[11] applies when the time interval in which the interaction associated with the internal degrees of freedom is interrupted by the exchange interaction is small compared to the time scales at which precessions associated with the internal-energy-level splittings take place. For low collision energies, this interruption time is determined by the time interval in which the colliding atoms can be localized within the interaction range: $\Delta t \simeq \mu r_0^2/\hbar$ (μ being the reduced atomic mass and r_0 the range of the interaction). Using the above approximation, we find that the relaxation rates in the Boltzmann zero-temperature limit can be expressed in terms of the triplet and singlet scattering lengths a_T and a_S:

$$G_{i\to f} = 4\pi v_f \left[\frac{a_T - a_S}{2}\right]^2 |\langle f|P_T - P_S|i\rangle|^2,$$

in which $|i\rangle$ and $|f\rangle$ are normalized antisymmetric two-body spin states, P_T (P_S) is the projection operator on the triplet (singlet) spin subspace, and $v_f = [2(E_i - E_f)/\mu]^{1/2}$ is

the relative velocity in the final spin channel.

Using the above expression in case of spin exchange relaxation in atomic hydrogen with $a_T=1.34a_0$ and $a_S=0.32a_0$ we reproduce the values of the H+H spin-exchange relaxation rates obtained with a coupled channel calculation[10] within a few percent up to magnetic field strengths of 0.1 Tesla. In case of atomic deuterium we calculate $a_T=-6.8a_0$ and $a_S=13.0a_0$ and obtain the values for the 18 zero-temperature spin-exchange relaxation rates displayed in Fig.2. Interestingly enough for the present purposes, these rates are typically two orders of magnitude larger than the H+H spin-exchange rates.[10] This is due to the larger value for $|a_T-a_S|$ entering in the expression for the rates.

We now consider low-field-seeking deuterium atoms in a magnetic trap. If we use the notations n_δ, n_ϵ, and n_ζ for the densities of these states, and assume all high-field-seeking atoms and a fraction P of the low-field-seeking atoms formed in inelastic spin-exchange events to escape to a perfect adsorber outside the trapping region, the population dynamics of the various hyperfine levels is described by

$$\dot{n}_\delta = -(G_{\delta\zeta\to\alpha\epsilon}+G_{\delta\zeta\to\beta\zeta})\,n_\delta n_\zeta-(G_{\delta\epsilon\to\zeta\gamma}+G_{\delta\epsilon\to\beta\epsilon}+P\,G_{\delta\epsilon\to\delta\alpha}+G_{\delta\epsilon\to\beta\alpha})\,n_\delta n_\epsilon,$$

$$\dot{n}_\epsilon = -G_{\zeta\epsilon\to\zeta\alpha}\,n_\epsilon n_\zeta-(G_{\delta\epsilon\to\zeta\gamma}+P\,G_{\delta\epsilon\to\beta\epsilon}+G_{\delta\epsilon\to\delta\alpha}+G_{\delta\epsilon\to\beta\alpha})\,n_\delta n_\epsilon$$

$$+(1-P)\,G_{\delta\zeta\to\alpha\epsilon}\,n_\delta n_\zeta,$$

$$\dot{n}_\zeta = -P\,G_{\zeta\epsilon\to\zeta\alpha}\,n_\epsilon n_\zeta-(G_{\delta\zeta\to\alpha\epsilon}+P\,G_{\delta\zeta\to\beta\zeta})n_\delta n_\zeta+(1-P)\,G_{\delta\epsilon\to\zeta\gamma}\,n_\delta n_\epsilon.$$

In general, a decay described by these equations yields a stable state consisting of one single hyperfine component. Which hyperfine state will survive depends on the relative magnitudes of the various decay rates, as well as on the the escape probability P and on the ratios between the initial populations. Substituting the above calculated relaxation rates, we find a preferential decay of δ and ϵ atoms. Hence, equal initial populations will lead to a trapped gas of ζ atoms ("doubly spin-polarized" deuterium). The fraction of ζ atoms which survive the spin-exchange decay process when starting with equal initial populations decreases with increasing P: At B = 0.1 T, we find that 88 % of the initial number of ζ atoms survive for P = 0, while for P = 1, this figure is 12 %.

The trapped ζ-atom gas will be ultralong lived as, in the zero-temperature limit, two-body collisions can be ruled out because of the Pauli principle. For nonzero temperatures, two-body electronic dipolar relaxation is dominant. Using plane-wave Born expressions[12] we estimate the corresponding cross section to be $\sigma_{rel}\simeq (E/E')^{1/2}\times 10^{-22}$ m^2, with E (E') the kinetic energy in the initial (final) spin channel. For low

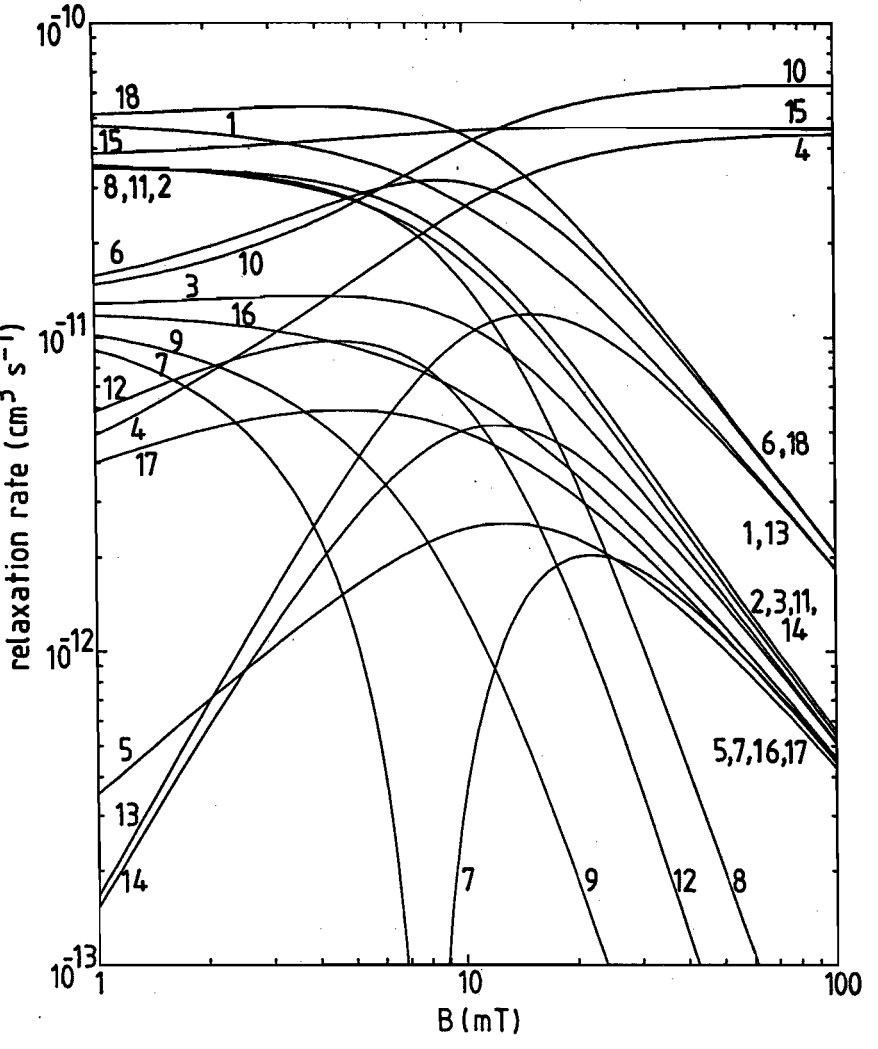

Fig.2. The zero temperature spin exchange relaxation rates $G_{i\to f}$ *as a function of magnetic field. The curves correspond to the following rates,* i→f*: 1:* $\zeta\epsilon\to\zeta\alpha$*, 2:* $\delta\zeta\to\alpha\epsilon$*, 3:* $\delta\zeta\to\beta\zeta$*, 4:* $\beta\zeta\to\alpha\epsilon$*, 5:* $\delta\epsilon\to\zeta\gamma$*, 6:* $\delta\epsilon\to\beta\epsilon$*, 7:* $\delta\epsilon\to\delta\alpha$*, 8:* $\delta\epsilon\to\beta\alpha$*, 9:* $\zeta\gamma\to\epsilon\beta$*, 10:* $\zeta\gamma\to\delta\alpha$*, 11:*$\zeta\gamma\to\beta\alpha$*, 12:* $\beta\epsilon\to\alpha\delta$*, 13:* $\beta\epsilon\to\beta\alpha$*, 14:* $\alpha\delta\to\alpha\beta$*, 15:* $\epsilon\gamma\to\delta\beta$*, 16:* $\epsilon\gamma\to\alpha\gamma$*, 17:* $\beta\delta\to\alpha\gamma$*, 18:* $\delta\gamma\to\beta\gamma$*.*

collision energies, E' tends to a constant yielding the dipolar relaxation rate at low temperatures to be proportional to temperature. For B≃0.1T we estimate $G_{dip}/T \simeq 10^{-14}$ $cm^3s^{-1}K^{-1}$ ($T \lesssim 0.05$ K). Notice that this energy dependence favors relaxation of fast atoms leading to a self-cooling contribution associated with relaxation which is absent in the hydrogen case.

Interestingly enough, though the thermalization rate also vanishes in the low-temperature limit, we find that the system still achieves thermal equilibrium on a time scale substantially smaller than the dipolar lifetime of D↑‡. Thermalization of the trapped ζ gas may occur through elastic triplet potential scattering or via elastic dipolar collisions. At low temperatures ($T \lesssim 0.03$ K) dipolar thermalizing collisions dominate because the short-ranged triplet potential becomes ineffective due to the Pauli principle. Again using plane-wave Born expressions[12] we estimate the dipolar collision cross section to be $\sigma_{th,dip} \simeq 10^{-22}$ m^2. At higher collision energies, where the Pauli principle becomes less effective, gas-phase thermalization takes place predominantly through elastic scattering via the strong short-ranged triplet potential. A phase-shift analysis yields the corresponding cross section to be proportional to the energy squared: $\sigma_{th,trip}/E^2 \simeq 10^{-19}$ m^2K^{-2}. For density $n = 10^{14}$ cm^{-3} and temperature equal to the corresponding Fermi temperature $T_F \simeq 39$ μK, the above expressions yield a lifetime due to dipolar relaxation of several hours and a gas-phase thermalization time of several seconds. Under similar conditions the lifetime of H↑‡ is some seconds.[10] In contrast to the case of H↑‡ where in the limit $T \to 0$ the ratio of the thermalization rate to the relaxation rate vanishes, in case of D↑‡ this ratio increases as $T^{-1/2}$. This shows the possibility to use evaporative cooling as an efficient means for cooling the trapped gas down to the degeneracy regime.

In the foregoing, degeneracy effects were left out of consideration. An accurate description of such effects depends in a subtle manner on the evaporation scheme and requires a detailed analysis. In a naive picture, the Fermi pressure limits the density for decreasing temperatures, in contrast to the hydrogen case where higher densities are favored, ultimately leading to BEC. In contrast to relaxation, the thermalization rate is affected by blocking effects in the final state. Still, the evaporative cooling scheme may be expected to be very efficient, if we take into account that, for low temperatures, the differences in occupation of the single-particle levels, compared with the T=0 state, are concentrated at the highest energy levels near the Fermi energy. Cooper pairing in D↑‡ is way out of reach as only p-wave pairing is possible,[13] requiring extremely high densities.

Resonance recombination[14] and resonance-enhanced relaxation, which are probably the dominant decay mechanisms in magnetically trapped alkalis, are not expected to disturb the above described decay of D↑. The (v=21, j=0) and the (v=21, j=1) molecular levels are just bound, so that resonance recombination can play a role

in the decay of D↓. In D↑, however, recombination via these levels is inefficient thanks to the positive sign of the Zeeman energies for the low-field-seeking states. Unbound singlet states also play a negligible role at temperatures of interest as the lowest resonant state (v=20, j=6) is calculated to be 10 K above threshold. Also the slow decay of D↑‡ is not disturbed by resonance-enhanced processes as collisions proceed via the triplet potential which does not support (almost) bound states.

In the foregoing we discussed the behavior of the trapped gas in some detail but we did not treat the problem of the loading of the trap and only mentioned some facts relevant to the cooling of the trapped gas. As in the hydrogen case, the development of an efficient filling and cooling scheme is a major project, which is left as a challenge to experimentalists.

This work is part of a research program of the Stichting voor Fundamenteel Onderzoek der Materie (FOM), which is financially supported by the Nederlandse organisatie voor Zuiver Wetenschappelijk Onderzoek (ZWO).

References

(1) T.J. Greytak and D. Kleppner, in *New Trends in Atomic Physics*, Proceedings of the Les Houches Summer School, 1982, edited by G. Grynberg and R. Stora (North-Holland, Amsterdam, 1984) p. 1125; I.F. Silvera and J.T.M. Walraven, in *Progress in Low Temperature Physics*, edited by D. Brewer (North-Holland, Amsterdam, 1986), Vol. 10, p. 139; P.J. Nacher G. Tastevin, M. Leduc, S.B. Crampton and F. Laloë, J. Phys. Lett. (Paris) 45, L441 (1984), and references therein.

(2) R. Sprik, J.T.M. Walraven and I.F. Silvera, Phys. Rev. Lett. 51, 479, 942 (1983); H.F. Hess, D.A. Bell, G.P. Kochanski, R.W. Cline, D. Kleppner and T.J. Greytak, Phys. Rev. Lett. 51, 483 (1983); T. Tommila, S. Jaakkola, M. Krusius, I. Krylov and E. Tjukanov, Phys. Rev. Lett. 56, 941 (1986).

(3) I.F. Silvera and J.T.M. Walraven,Phys. Rev. Lett. 45, 1268 (1980).

(4) I. Shinkoda, M.W. Reynolds, R.W. Cline and W.N. Hardy, Phys. Rev. Lett. 57, 1243 (1986).

(5) E. Krotscheck, R.A. Smith, J.W. Clark and R.M. Panoff, Phys. Rev. B 24, 6383 (1981); R.M. Panoff, J.W. Clark, M.A. Lee, K.E. Schmidt, M.H. Kalos and G.V. Chester, Phys. Rev. Lett. 48, 1675 (1982).

(6) H.R. Glyde and S.I. Herandi, in *Proceedings of the International Conference on Condensed Matter Theories*, edited by F.B. Malik (Plenum, New York, 1986), Vol. 1, p. 115 (1986), and references therein.

(7) C. Lhuillier and F. Laloë, J. Phys. (Paris) 43, 197, 225 (1982), C. Lhuillier, *ibid.* 44, 1 (1983); E.P. Bashkin and A.E. Meyerovich, Adv. Phys. 30, 1 (1981); W.J.

Mullin and K. Miyake, J. Low. Temp. Phys. 53, 313 (1983).

(8) D.E. Pritchard, Phys. Rev. Lett. 51, 1336 (1983); H.F. Hess, Phys. Rev. B 34, 3476 (1986); R.V.E, Lovelace, C. Mehanian, T.J. Tommila and D.M. Lee, Nature 318, 30 (1985); T.J. Tommila, Europhys. Lett. 2, 789 (1986).

(9) A.L. Migdall, J.V. Prodan, W.D. Phillips, T.H.Bergeman and H.J. Metcalf, Phys. Rev. Lett. 54, 2596 (1985).

(10) A. Lagendijk, I.F. Silvera and B.J. Verhaar, Phys. Rev. B 33, 626 (1986); H.T.C. Stoof, J.M.V.A. Koelman and B.J. Verhaar, Phys. Rev. B 38, 4688 (1988).

(11) B.J. Verhaar, J.M.V.A. Koelman, H.T.C. Stoof, O.J. Luiten and S.B. Crampton, Phys. Rev. A 35, 3825 (1987).

(12) J.P.H.W. van den Eijnde, Ph.D. Thesis, Eindhoven University of Technology, The Netherlands, 1984 (unpublished).

(13) A.J. Leggett, J. Phys. (Paris) C7, 19 (1980).

(14) J. Vigué, Phys.Rev. A 34, 4476 (1986).

Section 2.3
Spin-exchange decay of magnetically trapped deuterium atoms

In the previous section it was shown that under certain conditions fast spin-exchange processes lead to the purification of magnetically trapped D↑ gas into potentially ultrastable D↑↑ gas. In this section we examine this purification process in a more accurate and more realistic way. First, we relax some of the approximations made in the calculation of the spin-exchange rates: here it is no longer assumed that temperatures are sufficiently low to make the zero-temperature limit applicable, and also the low B-field restriction is somewhat relaxed. Secondly, we take into account the trap filling in the description of the D↑↑ purification process.

Spin–exchange decay rates

As discussed in the previous section the hyperfine population dynamics of magnetically trapped gaseous mixtures of δ-, ϵ-, and ζ-state atoms (D↑) is dominated by spin-exchange processes. As a result of the low values of the relevant collision energies and Fermi-Dirac statistics, only s-wave scattering between atoms in antisymmetrical spin states occurs. Here we derive closed expressions describing the low temperature and low magnetic field dependence of all rate constants corresponding to the 18 allowed spin-exchange transitions between the 15 antisymmetrized two-body spin states.

In order to do this we make use of the fact that for not too high B values the hyperfine energy-level separations have a very small influence on a collision quantity which has a finite value in the limit of vanishing initial and final kinetic energies (see previous section and section 4.3). For s-wave spin-exchange scattering the T-matrix provides us with such quantities. Neglecting the influence of the energy-level separations by calculating the s-wave spin-exchange T-matrix elements for common initial and final kinetic energies chosen halfway[1] between their exact values, we find that the rate constants $G_{i\to f}$ split up in a magnetic field dependent spin-matrix element and a "universal" rate constant G_0 depending on the specific transition and the magnetic field strength only via a dependence on $\epsilon_i-\epsilon_f$, the spin energy released in the transition (Cf. Eq. 49, section 3.3):

$$G_{i\to f}(B,T) = |\langle f|P_T-P_S|i\rangle|^2\, G_0(\epsilon_i-\epsilon_f,T)\,. \qquad (1)$$

Here, $|i\rangle$ and $|f\rangle$ are normalized antisymmetric spin states ($|(\alpha\beta-\beta\alpha)/\sqrt{2}\rangle$, ... , $|(\epsilon\zeta-\zeta\epsilon)/\sqrt{2}\rangle$), and $P_T(P_S)$ is the projection operator on the triplet (singlet) spin subspace. The reduced rate constant G_0 can be written as a thermal average over a cross section σ_0 times the relative velocity in the final spin-state (for a derivation see

section 4.3):

$$G_0(\Delta,T) = \langle \sqrt{2(E+\Delta)/\mu}\ \sigma_0(E+\tfrac{1}{2}\Delta) \rangle_E , \qquad (2)$$

in which μ denotes the reduced mass of the colliding D atoms, while the thermal (Boltzmann) average $\langle\ \rangle_E$ is given by

$$\langle f(E) \rangle_E \equiv (2/\sqrt{\pi}) \int_0^\infty dx\, e^{-x} x^{\frac{1}{2}} f(xk_BT) . \qquad (3)$$

Equation (2) only applies for positive Δ (downward hyperfine transitions). The reduced rate for upward transitions is related to that for downward ones via a simple Boltzmann factor:

$$G_0(-\Delta,T) = e^{-\Delta/k_BT}\, G_0(\Delta,T) . \qquad (4)$$

The cross section σ_0 is determined by

$$\sigma_0(\tfrac{\hbar^2k^2}{2\mu}) \equiv \tfrac{\pi}{k^2} \sin^2(\delta_T^0(k)-\delta_S^0(k)) , \qquad (5)$$

in which δ_T^0 (δ_S^0) is the s-wave scattering phase shift for triplet (singlet) potential scattering. In this way we have reduced the problem of calculating the spin-exchange rate constants to a standard phase-shifts calculation.

In order to arrive at closed expressions for the rate constants we apply another approximation. Making use of the smooth behavior of the quantity which is to be thermally averaged [the term between averaging brackets on the right-hand side of (2)] as a function of collision energy, we may apply a one-point generalized Gauss-integration based on the weight function $w(x) = x^{1/2}\exp(x)$ in Eq.(3) on the interval $[0,\infty)$:

$$\langle f(E) \rangle_E \simeq f(\tfrac{3}{2}k_BT) \qquad (6)$$

to the right-hand side of Eq.(2), yielding:

$$G_0(\Delta,T) = \sqrt{2(\Delta + \tfrac{3}{2}k_BT)/\mu}\ \sigma_0(\tfrac{1}{2}\Delta + \tfrac{3}{2}k_BT) . \qquad (7)$$

Taken together, Eqs.(1), (4), (5), and (7) provide us with closed expressions for the

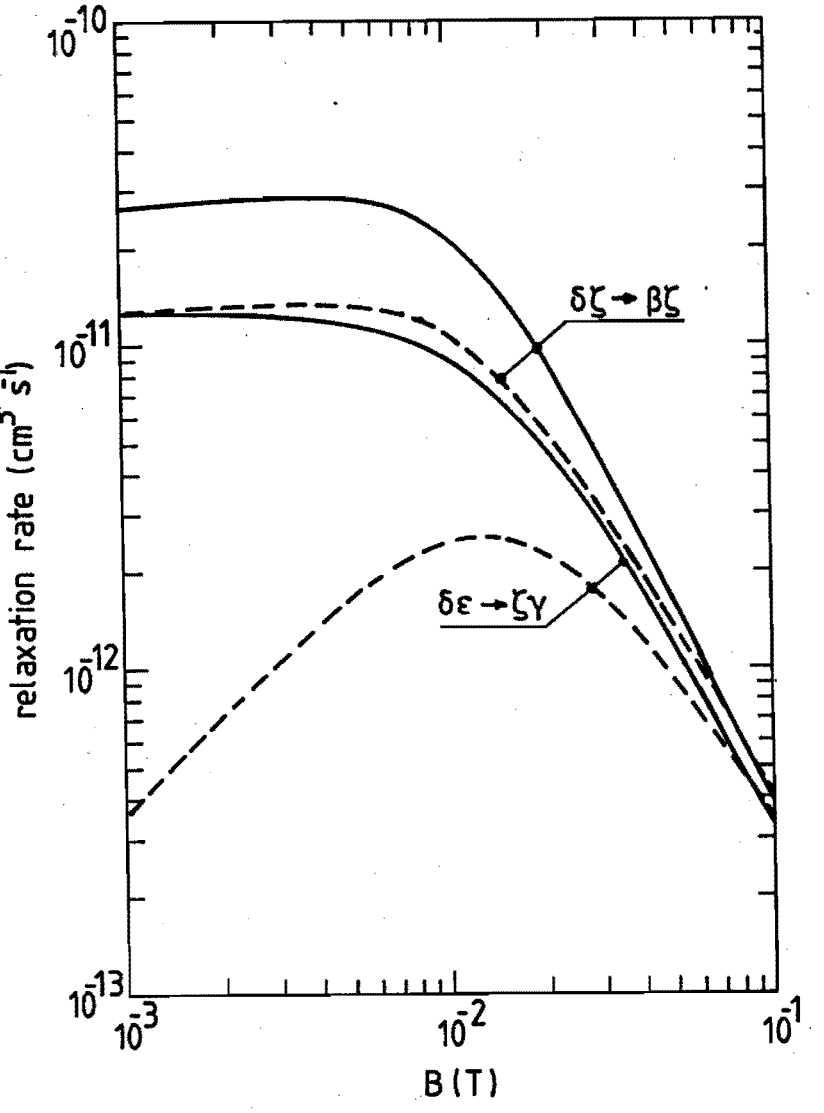

Fig.1. The spin-exchange relaxation rates $G_{\delta\zeta\rightarrow\beta\zeta}$ and $G_{\delta\varepsilon\rightarrow\zeta\gamma}$ as functions of magnetic field strength for T=0.3K (full curves) and T=0K (broken curves).

rate constants in terms of the triplet and singlet phase shifts. At low magnetic fields and low temperatures the resulting rate constants are fairly accurate. When applied to the case of spin-exchange relaxation in atomic hydrogen, we reproduce the values of

the H+H spin-exchange relaxation rates obtained with a computationally elaborate coupled-channels calculation within 1% for B<0.1T and T<50mK. At higher B-field strengths and higher temperatures the above expressions become less accurate. For B≈1.5T and T≈0.3K we find a 13% accuracy. For D+D spin-exchange relaxation we expect approximately the same degree of accuracy.

In the zero temperature limit and for small Δ values Eq.(7) reduces to the expression used in the previous section for the description of the D↑‡ purification process:

$$G_0(\Delta,0) = \sqrt{2\Delta/\mu}\ \pi(a_T-a_S)^2\,, \qquad (8)$$

in which $a_T(a_S)$ is the triplet(singlet) scattering length. Note furthermore that a complete neglect of the hyperfine energy-level separations in the calculation of the relaxation rates (Δ=0) yields very bad approximations as it leads to vanishing rates in the zero-temperature limit: $G_0(0,T) \sim T^{1/2}$. This is probably the reason why a neglect of the splitting between internal states is often thought to be a typical high-energy approximation. As may be clear from the above this is not the case: if the separation of the internal levels is neglected in a suitable way, the resulting expressions are accurate down to zero collision energy.

In order to facilitate the analysis of experiments with magnetically trapped deuterium, we parameterized the σ_0 cross section as a function of collision energy:

$$\sigma_0(E) \simeq 3.46\times10^{-18}\ \mathrm{m}^2\,(1 + 3.6\ E)^{-1}, \qquad (9)$$

with E in temperature units. The errors introduced in using this parameterization do not affect the above mentioned accuracy levels.

To illustrate the B-field and temperature dependence of the relaxation rates calculated according to the above scheme, two of the rates involved in the hyperfine population dynamics of trapped D↑ are shown in Fig.1 as functions of magnetic field strength for a temperature of 0.3 K (drawn curves) and in the zero-temperature limit (dashed curves). This figure clearly shows that the rates can have a considerable dependence on temperature, especially when the internal energy released in the transition is small (as for the transition $\delta\epsilon\rightarrow\zeta\gamma$ at low B fields).

Purification into D↑‡

We now consider the creation of D↑‡ by spin-exchange processes. In the previous section we assumed the trap to be filled with δ-, ϵ- and ζ-state atoms (D↑) and considered the subsequent evolution to a ζ-state atom gas (D↑‡). In actual

experimental situations it is more likely that the trap is filled with D↑ until a steady state is reached between filling flux and the flux of atoms escaping from the trap after spin relaxation events. We take this into account by including filling flux terms in the rate equations. Furthermore, by using the spin-exchange rate constants derived in the present section, we no longer work in the zero temperature limit but at typical trap-filling temperatures of a few hundreds of milli-kelvins.

Assuming the "high-field-seeking" atoms (D↓) formed in spin-relaxation events to escape to a perfect adsorber outside the trapping region, the population dynamics of the trapped hyperfine states is described by

$$\dot{n}_\delta = \tfrac{1}{3}\Phi/V - (G_{\delta\epsilon\to\zeta\gamma}+G_{\delta\epsilon\to\beta\epsilon}+G_{\delta\epsilon\to\beta\alpha})n_\delta n_\epsilon - (G_{\delta\zeta\to\alpha\epsilon}+G_{\delta\zeta\to\beta\zeta})n_\delta n_\zeta,$$

$$\dot{n}_\epsilon = \tfrac{1}{3}\Phi/V - (G_{\delta\epsilon\to\zeta\gamma}+G_{\delta\epsilon\to\delta\alpha}+G_{\delta\epsilon\to\beta\alpha})n_\delta n_\epsilon + G_{\delta\zeta\to\alpha\epsilon}n_\delta n_\zeta - G_{\zeta\epsilon\to\zeta\alpha}n_\epsilon n_\zeta,$$

$$\dot{n}_\zeta = \tfrac{1}{3}\Phi/V + G_{\delta\epsilon\to\zeta\gamma}n_\delta n_\epsilon - G_{\delta\zeta\to\alpha\epsilon}n_\delta n_\zeta . \qquad (10)$$

In these equations n_i is the density of atoms in hyperfine state i, Φ is the trap filling flux (atoms/s) assumed to be equally divided over the three "low-field-seeking" states, and V is the effective trap volume. Evaporative losses of atoms are not included in the above equations as they may be avoided during the filling stage by proper design of the experimental setup.[2] Note furthermore that only downward (exothermic) transitions enter in the rate equations due to the absence of upward (endothermic) spin-exchange transitions with an initial s-wave state consisting of two "low-field-seeking" atoms.

The time-evolution equations for n_ζ and n_δ can be combined to give

$$\dot{n}_\zeta \geq \frac{1}{1+r}\tfrac{1}{3}\Phi/V + \frac{r}{1+r}\dot{n}_\delta , \qquad (11)$$

with $r \equiv G_{\delta\zeta\to\alpha\epsilon}/G_{\delta\zeta\to\beta\zeta}$. So, even when the δ-atom density saturates ($\dot{n}_\delta=0$), the ζ-atom density still grows without limit. Such an unlimited growth of n_ζ is possible only if the δ- and ϵ-atom densities decay away. In the long-time limit the above rate equations yield that n_ζ grows at a rate $\frac{1}{3}(\Phi/V)/(1+r)$, while n_δ and n_ϵ decay away via an inverse proportionality to n_ζ. Notice that the resulting D↑↑ purification is independent of the actual values of the spin-exchange rate constants. Only the effective ζ-atom filling rate depends on the values of the spin-exchange rate constants via the proportionality factor $(1+r)^{-1}$, representing the fraction of ζ atoms which, after being loaded in the trap, survive the spin-exchange decay and stay trapped. In Fig.2 this dimensionless factor is shown as a function of magnetic field for a temperature of

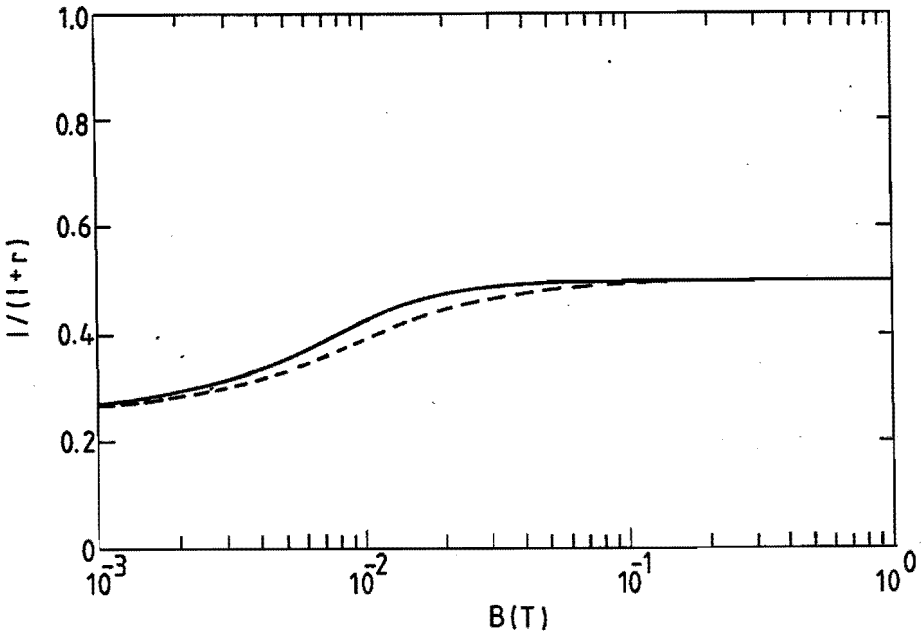

Fig.2. The proportionality factor $1/(1+r)$ *entering the effective* ζ*–atom filling rate as a function of magnetic field strength for* T=0.3K (*full curve*) *and T=0K* (*broken curve*).

0.3 K (drawn curve) and in the zero-temperature limit (dashed curve). As is evident from this figure, this ratio has only a weak B-field dependence and an almost negligible temperature dependence.

Of course, a real unlimited grow of n_ζ is unphysical. As high ζ-atom densities are built up, decay processes due to magnetic dipolar spin relaxation occurring in collisions between ζ-state atoms (predominantly $\zeta\zeta\rightarrow\zeta\alpha$ and $\zeta\zeta\rightarrow\alpha\alpha$, see next section) become important and ultimately limit the ζ-atom density. We included this effect by adding a dipolar relaxation term $-(G_{\zeta\zeta\rightarrow\zeta\alpha}+2G_{\zeta\zeta\rightarrow\alpha\alpha})n_\zeta^2$ on the right hand side of the time-evolution equation for n_ζ. Dipolar relaxation is relatively very slow. Having rates of the order of $10^{-14}cm^3s^{-1}$ for temperatures of a few hundreds of millikelvins (see next section), the dipolar processes affecting the ζ-atom density are three orders of magnitude slower than typical spin-exchange processes affecting the trapped atom densities. Solving the rate equations including the dipolar relaxation term to lowest order in the ratio of dipolar relaxation rates over spin-exchange relaxation rates, we

find a steady state with atom densities

$$n_\zeta = \left[\frac{1}{1+r} \frac{\frac{1}{8}\Phi/V}{G_{\zeta\zeta\to\zeta\alpha}+2G_{\zeta\zeta\to\alpha\alpha}} \right]^{\frac{1}{2}},$$

$$n_\epsilon = \frac{G_{\zeta\zeta\to\zeta\alpha}+2G_{\zeta\zeta\to\alpha\alpha}}{G_{\zeta\epsilon\to\zeta\alpha}} (2r+1)\, n_\zeta,$$

$$n_\delta = \frac{G_{\zeta\zeta\to\zeta\alpha}+2G_{\zeta\zeta\to\alpha\alpha}}{G_{\delta\zeta\to\beta\zeta}} n_\zeta. \qquad (12)$$

We conclude that the steady state δ- and ϵ-atom densities are about three orders of magnitude smaller than the ζ-atom density. After turning off the filling flux the δ and ϵ atoms decay away rapidly in spin-exchange collisions with ζ atoms, leaving the ζ-atom density relatively unaffected. In this way D↑↑ gas with density of the order of 10^{13}atoms/cm^3 (assuming Φ/V to be of the order 10^{13}atoms/s) is obtained.

References

(1) Section 3.3 [Phys. Rev. A 38, (Oct.1988)]; A.M. Schulte and B.J. Verhaar, Nucl. Phys. A232, 215 (1974); H.T.C. Stoof, J.M.V.A. Koelman, and B.J. Verhaar, Phys. Rev. B 38, 4688 (1988).

(2) R. van Roijen, J.J. Berkhout, S. Jaakkola and J.T.M. Walraven, Phys. Rev. Lett. 61, 931 (1988).

Section 2.4

Lifetime of magnetically trapped ultracold atomic deuterium gas

J.M.V.A. Koelman, H.T.C. Stoof, B.J. Verhaar, and J.T.M. Walraven*

Department of Physics, Eindhoven University of Technology,
5600 MB Eindhoven, The Netherlands
**Natuurkundig Laboratorium, Universiteit van Amsterdam,*
1018 XE Amsterdam, The Netherlands

[Published in Phys. Rev. B 38 (Nov. 1988)]

We have calculated the magnetic dipolar spin-relaxation rates of magnetically trapped doubly-spin-polarized atomic deuterium gas. The results are expressed in a simple closed formula describing the dipolar-relaxation-limited stability in the Boltzmann ($T>>T_f$), the degeneracy ($T<<T_f$), and the crossover ($T\simeq T_f$) regimes. In the degeneracy regime we typically find lifetimes of some hours. We also discuss the dipolar decay of magnetically trapped spin-polarized fermionic alkali-metal atoms.

Introduction

In the past decade dramatic progress has been made in the stabilization of spin-polarized atomic hydrogen. The observation of several exceptional properties in a large number of experiments on this new quantum gas[1] strongly overshadowed the few experimental results[2] on its fermionic counterpart: spin-polarized deuterium. The reason that deuterium has come into prominence to a much lesser amount is that the standard scheme to stabilize hydrogen,[1] i.e., confinement at high magnetic field in a cell with liquid-helium covered walls, is rather inefficient when applied to deuterium: even on superfluid-helium surfaces deuterium atoms undergo a strong adsorption and subsequent recombination.

Recently, we made an analysis[3] of the hyperfine population dynamics of surface-free confined deuterium atoms in a trap similar to those used for confining laser-cooled spin-polarized alkali-metal atoms[4] and spin-polarized hydrogen atoms[5]. It appears that fast two-body spin-exchange processes acting on the trapped electron spin "up" deuterium atoms ($D\uparrow$) lead to the formation of a gas of atoms in one single hyperfine state in which also the nuclear spins are polarized. This gas of doubly-spin-polarized deuterium atoms ($D\uparrow\ddagger$) is extremely stable at low temperatures. Not only are surface recombination processes eliminated but also collision processes leading to a decay of the deuterium atom gas are strongly suppressed thanks to the Pauli exclusion principle. In contrast to the case of the magnetically trapped boson gas $H\uparrow\ddagger$ where two-body dipolar relaxation is predicted to be very fast and, to lowest order,

independent of temperature,[6] the stability of the fermion gas D↑‡ against dipolar relaxation is expected to grow with decreasing temperature.[3] Applying an evaporative cooling scheme similar to that proposed for H↑‡,[7] will ultimately lead to an ultrastable low temperature D↑‡ gas. The dipolar relaxation limited stability of D↑‡ was estimated in Ref.3 for temperatures well above the Fermi temperature T_F.

Here we describe a more general theory for the dipolar relaxation of the D↑‡ gas which also applies to the degeneracy regime ($T<<T_F$) and the crossover regime ($T\simeq T_F$). The results are given in the form of a simple closed expression which, in the relevant regimes, describes the temperature and magnetic-field dependence of the effective decay rates within a few percent. This expression also determines the dipolar decay rates of magnetically trapped fermionic alkali-metal atoms. For a degenerate ($T<<T_F$) D↑‡ gas with density 10^{14} atoms/cm^3 at magnetic field B = 0.1 T we find a lifetime as large as 5×10^3 s. This figure even grows with increasing magnetic field. Therefore, magnetically trapped D↑‡ offers a unique possibility for the experimental observation of gas-phase degenerate quantum behavior.

Decay rates

In principle, a wealth of processes may cause a gas of doubly-spin-polarized magnetically trapped atoms to flip an electronic or nuclear spin. Such spin-depolarization processes lead to a decay of the gas as atoms are formed which are directly ejected out of the trap (because they acquire the released energy in the form of kinetic energy and also because they are formed in hyperfine states which are repelled from the minimum-B-field trap) or because atoms are formed in hyperfine states which disappear out of the trap due to a subsequent strong two-body spin-exchange process. In view of the extreme diluteness of trapped atom gases [highest density achieved up to now: $\sim 3\times10^{14}$ atoms/cm^3 with H↑‡ Ref.5)] the first type of spin-depolarization processes to discuss are single-atom processes. These are commonly considered to be negligible or at least to be made so by judicious selection of the experimental parameters. For instance, the lifetime due to spontaneous emission at hyperfine frequencies is enormous, and nonadiabatic spin-flips (Majorana transitions) can be reduced below any desired rate by a careful trap design.

Under these circumstances, two-atom processes determine the lifetime of doubly-spin-polarized trapped atom gases. As in the doubly-spin-polarized state the electronic spins of two colliding atoms are parallel, spin-exchange plays no role in the decay of the gas. Precession of the spins in the dipolar magnetic fields of other atoms, however, does lead to spin flipping, which results in a decay of the sample. Spin depolarization due to the magnetic dipole-dipole interaction is the dominant loss mechanism for trapped H↑‡[6] and D↑‡[3] gases. For magnetically trapped doubly-spin-polarized

alkali-metal atoms other decay processes such as resonance recombination are important.[8] At very low temperatures, however, also for trapped alkali-metal atoms dipolar relaxation may be the dominant decay process.

From now on we restrict ourselves to the case of dipolar relaxation in doubly-spin-polarized gases of deuterium atoms and assume the relevant collision energies to be small compared to the splittings between the various hyperfine energy levels. We denote the one-atom hyperfine states α, β, γ, δ, ϵ, and ζ in order of increasing energy (see inset Fig.1), so that the trapped doubly-polarized state is denoted by ζ. Assuming all atoms formed in dipolar relaxation events either to be in a hyperfine state with predominantly electron spin-down and hence to be ejected from the minimum-B-field trap, or to have acquired enough energy to escape from the trap and stick to a wall outside the trap region, we find for the decay of the ζ-atom gas

$$\frac{d}{dt} n_\zeta = -2 n_\zeta^2 \sum_{\{xy\}}' G_{\zeta\zeta\to xy} , \tag{1}$$

with n_ζ denoting the ζ-atom density, and the summation $\Sigma'_{\{xy\}}$ running over all distinct pairs of hyperfine states not equal to $\zeta\zeta$. Starting from the quantum-mechanical Bogoliubov-Born-Green-Kirkwood-Yvon (BBGKY) hierarchy we find that the relaxation rate $G_{\zeta\zeta\to xy}$ can be expressed as an ensemble average of the relative velocity $2\hbar k/m$ times an effective cross section $\sigma_{\zeta\zeta\to xy}$:

$$G_{\zeta\zeta\to xy} = (2\pi)^{-3} \int_0^\infty 4\pi k^2 dk \, F_{\zeta\zeta}(k) \frac{\hbar k}{m/2} \sigma_{\zeta\zeta\to xy}(k) . \tag{2}$$

In this equation $F_{\zeta\zeta}(k)$ is the distribution function for the relative wave number k defined as

$$F_{\zeta\zeta}(k) \equiv (2\pi)^{-3} \int d^3K \, f_\zeta(|\tfrac{1}{2}\underline{K} + \underline{k}|) \, f_\zeta(|\tfrac{1}{2}\underline{K} - \underline{k}|) , \tag{3}$$

in which $f_\zeta(k)$, the distribution function for the single atom wave numbers, is assumed to be isotropic and normalized as $(2\pi)^{-3} \int d^3k \, f_\zeta(k) = 1$. In Eq. (2) no Pauli blocking terms of the form $(1-f_x)(1-f_y)$ appear because the atoms in hyperfine state x and y formed in a dipolar relaxation event undergo no blocking effects as the internal states x and y are unequal to ζ or otherwise because they have acquired enough kinetic energy to prevent any blocking effect to occur.

In a dilute gas of identical fermions in one single internal state the antisymmetrization requirement prevents the fermions to approach one another at

distances much smaller than the thermal wavelength. As the thermal wavelength scales with the inverse square root of the temperature it follows that at low temperatures fermions experience only the long-range parts of their mutual interactions. Therefore, in our calculation the short-ranged triplet interaction is neglected and the dipolar interaction, of which only the very weak long-range part contributes, is taken into account to lowest order. We find

$$\sigma_{\zeta\zeta\to xy}(k) = \frac{\pi^3 m^2 k'}{\hbar^4 k} \int_{4\pi} d\hat{k} \int_{4\pi} d\hat{k}' \, |V_{\zeta\zeta,\{xy\}}(\underline{k},\underline{k}')|^2 . \qquad (4)$$

In this equation $\underline{k}'=k'\hat{k}'$ denotes the final-state wave vector, and the V matrix element is the antisymmetrized momentum representation of the dipolar interaction

$$V_{\zeta\zeta,\{xy\}}(\underline{k},\underline{k}') \equiv \int d\underline{r} \, \tfrac{1}{2}\{\exp[i(\underline{k}-\underline{k}').\underline{r}]-\exp[i(\underline{k}+\underline{k}').\underline{r}]\} V_{\zeta\zeta,\{xy\}}(\underline{r}) \qquad (5)$$

with $\{xy\}$ denoting a symmetrized and normalized spin state $(xy+yx)/\,[2(1+\delta_{xy})]^{1/2}$. Using the fact that the hyperfine energy splittings are much larger than typical kinetic energies so that $\hbar k << \hbar k' \simeq [m(2\epsilon_\zeta-\epsilon_x-\epsilon_y)]^{1/2}$ with ϵ_x the hyperfine energy of x-state atoms, and taking into account only the electron-electron part of the dipolar interaction, which by far dominates over the electron-deuteron and deuteron-deuteron contributions, we find

$$\sigma_{\zeta\zeta\to xy}(k) = \frac{a_{ee}^2}{90\pi} \frac{k}{k'} \, |\langle\zeta\zeta|\Sigma^{ee}|\{xy\}\rangle|^2 . \qquad (6)$$

In this equation the electronic-dipolar length scale

$$a_{ee} \equiv m\mu_0\mu_e^2/\hbar^2 , \qquad (7)$$

which when the deuterium atom mass is substituted for m takes the value $a_{ee} = 3.26\times10^{-11}$m, and the spin-matrix element $\langle\zeta\zeta|\Sigma^{ee}|\{xy\}\rangle$ describes the coupling of the electron spin-operators to a spin-operator of rank two. This matrix has nonvanishing off-diagonal elements for $xy = \zeta\epsilon$, $\epsilon\epsilon$, $\zeta\alpha$, $\epsilon\alpha$, and $\alpha\alpha$, with absolute values $2\sqrt{3}\sin(\theta_+)$, $2\sqrt{6}\sin^2(\theta_+)$, $2\sqrt{3}\cos(\theta_+)$, $2\sqrt{3}\sin(2\theta_+)$, and $2\sqrt{6}\cos^2(\theta_+)$, respectively. Here, the mixing angle θ_+ is determined by the relation $\sqrt{2}\cot(2\theta_+)=(\mu_e+\mu_n)B/a_{hf}+\frac{1}{2}$, in which μ_e (μ_n) is the electronic (nuclear) magnetic moment, and a_{hf} is the hyperfine constant (for deuterium: $a_{hf}= 1.446\times10^{-25}$ J).

Using the identity $(2\pi)^{-3}\int 4\pi k^2 dk \, (\hbar^2k^2/m)F_{\zeta\zeta}(k) = (2\pi)^{-3}\int 4\pi k^2 dk \, (\hbar^2k^2/2m)f_\zeta(k)$ in the right-hand side of which we recognize $\langle E_{kin}\rangle$, the average kinetic energy per

atom, we find

$$G_{\zeta\zeta\to xy} = g_{\zeta\zeta\to xy} \langle E_{kin} \rangle , \tag{8}$$

with the reduced relaxation rate depending only on the magnetic-field strength B given by

$$g_{\zeta\zeta\to xy} = \frac{1}{45\pi} \frac{a_{ee}^2}{\hbar k'} |\langle \zeta\zeta | \Sigma^{ee} | \{xy\} \rangle|^2 . \tag{9}$$

The average kinetic energy per atom depends on the precise form of the distribution function f_ζ. At low kinetic energies the dipolar interaction is much more effective for elastic collisions ($\zeta\zeta\to\zeta\zeta$) than for inelastic ones ($\zeta\zeta\to xy$), as the energy released in a hyperfine transition reduces the overlap between initial and final states. As a result, the translational degrees of freedom may be assumed to be in thermal equilibrium so that $f_\zeta(k)$ is given by the Fermi-Dirac distribution which depends on temperature and density. For practical purposes the mean free particle energy for a Fermi-Dirac distribution can be parameterized as

$$\langle E_{kin}(n_\zeta, T) \rangle \simeq \left[(\tfrac{3}{5} k_B T_F)^{1.7} + (\tfrac{3}{2} k_B T)^{1.7} \right]^{1/1.7} , \tag{10}$$

with k_B the Boltzmann constant and $T_F \equiv \hbar^2 (6\pi^2 n_\zeta)^{2/3} / (2mk_B)$ the Fermi temperature. This parameterization reduces to the well-known expressions in the Boltzmann limit ($T >> T_F$) and in the degeneracy limit ($T << T_F$), and is accurate within 2% over the whole range of T/T_F values.

Equation (8) together with the expression (9) for the reduced relaxation rate and the parameterization (10) for the mean kinetic energy per atom constitute a simple closed expression for the relaxation rates in a deuterium atom gas.

Implications for magnetically trapped D↑↑

An important feature of the above results is that the fermionic character of the deuterium atoms manifests itself in the relaxation rates as a proportionality to the mean kinetic energy of the atoms [Eq.(8)] so that the stability grows with decreasing temperature. This is not so for hydrogen atoms which behave like bosons. The same analysis applied to bosons in essence yields an equation similar to Eq.(8) but with $\langle E_{kin} \rangle$ replaced by the final-state energy $\hbar^2 k'^2/m$, yielding relaxation rates independent of temperature. Hence, we expect the fermion D↑↑ to be much more stable than the boson H↑↑ at temperatures which are small compared to their

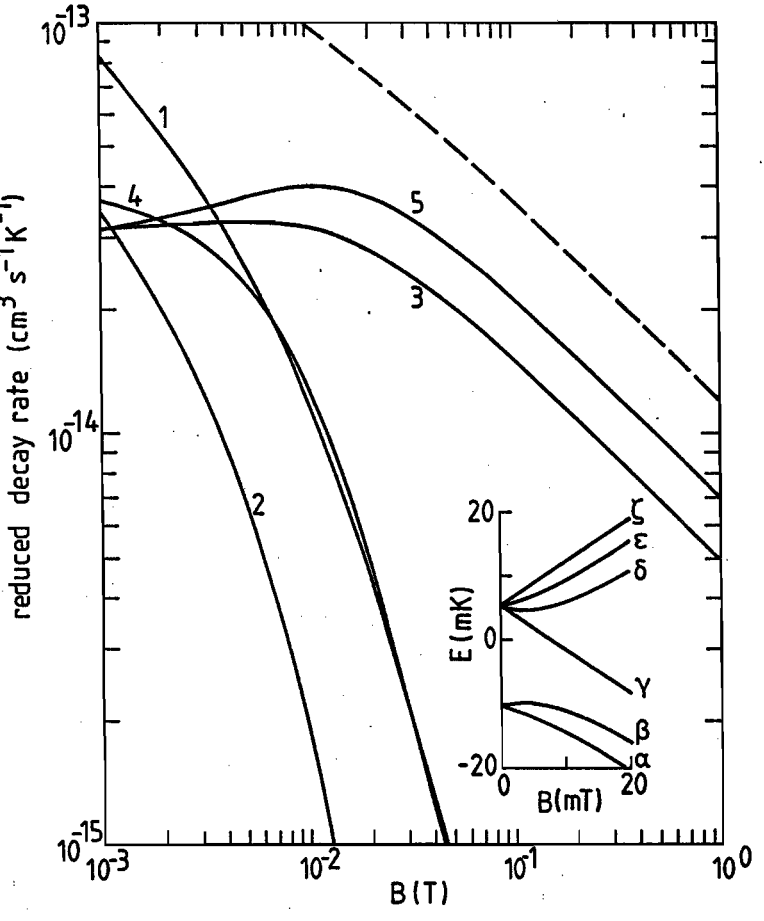

Fig.1. The reduced dipolar relaxation rates $g_{\zeta\zeta\to xy}$ *as functions of magnetic field. The curves correspond to* xy = *1:* $\zeta\epsilon$, *2:* $\epsilon\epsilon$, *3:* $\zeta\alpha$, *4:* $\epsilon\alpha$, *5:* $\alpha\alpha$. *The dashed curve represents the sum of the five rates. Inset: the ground-state hyperfine energy levels of atomic deuterium.*

hyperfine level splittings.

Another aspect worth mentioning here is that, with exception of the Boltzmann ($T>>T_F$) regime, the relaxation rates $G_{\zeta\zeta\to xy}$ not only depend on the magnetic field strength and temperature but via a dependence on T_F also on atom density. For instance, in the degeneracy limit ($T<<T_F$), the relaxation rates are proportional to $n_\zeta^{2/3}$ yielding a decay $\dot{n}_\zeta \sim n_\zeta^{5/3}$. This behavior makes it possible to determine the

trapped gas temperature, and more specifically to signal degeneracy, simply by monitoring the trapped atom density.

Using Eq.(9) we have calculated the various reduced dipolar-relaxation rates $g_{\zeta\zeta\to xy}$ and the sum rate $\Sigma'_{\{xy\}} g_{\zeta\zeta\to xy}$ for deuterium as functions of magnetic field. The results are displayed in Fig.1. A prominent feature of this figure is the rapid decrease with increasing magnetic field of the rates having an ϵ-atom in the final state. This is because these rates have Σ^{ee} matrix elements which vanish at high magnetic fields. The rates $\zeta\zeta\to\zeta\alpha$ and $\zeta\zeta\to\alpha\alpha$ diminish much more slowly as they are not reduced by their Σ^{ee} matrix elements which go to a constant for $B\to\infty$, but only by their inverse proportionality to the final-state momentum $\hbar k'$. For not too low magnetic fields, the sum rate is proportional to the inverse square root of the magnetic field. For $B \gtrsim 0.02$T we find $\Sigma'_{\{xy\}} g_{\zeta\zeta\to xy} \simeq g_0 B^{-1/2}$ with a relative error not exceeding a few percent for $g_0 = 1.16\times10^{-14}$ cm^{3}s^{-1}T$^{1/2}$K^{-1}. Using this expression and the parameterization (10) we find for the characteristic decay rate $\Gamma_{dip} \equiv -\dot{n}_\zeta/n_\zeta$:

$$\Gamma_{dip} \simeq 2g_0 n_\zeta B^{-1/2} \frac{3}{5} T_F \left[1 + (\tfrac{5}{2} T/T_F)^{1.7}\right]^{1/1.7}. \qquad (11)$$

For $n_\zeta = 10^{14}$cm^{-3} and B= 0.1 T kinetic energies are small compared to the relevant hyperfine level separations up to temperatures of a few tens of millikelvins. At T= 10 mK we find $\Gamma_{dip}\simeq 0.1$s^{-1}. At the same density and magnetic field but for $T=T_F\simeq 39\mu$K, Eq.(11) yields $\Gamma_{dip}\simeq 5\times10^{-4}$s^{-1}, while for $T\ll T_F$ the decay rate reaches its minimum value $\Gamma_{dip}\simeq 2\times10^{-4}$s^{-1}.

Equations (8) and (9) not only apply to the case of D↑‡, but also to any doubly-spin-polarized fermionic alkali-metal atom gas, provided the relevant kinetic energies are small in comparison with the hyperfine energy-levels separation. As the reduced relaxation rates depend on the atomic mass m as $\sim m^{3/2}$, we expect the alkali-metal atoms to be more unstable against dipolar relaxation than deuterium. Using the above expressions we find doubly-spin-polarized ^{6}Li to be most stable of all fermionic alkali-metal atoms with a total reduced dipolar-relaxation rate $g_0 \simeq 6.2\times10^{-14}$ cm^{3}s^{-1}T$^{1/2}$K^{-1} for magnetic fields $B \gtrsim 0.02$T. Hence, even without taking into account decay due to resonance recombination, which is absent in D↑‡[3] but effective in magnetically trapped doubly-spin-polarized alkali-metal atoms[8], deuterium is more stable than the alkali-metal atoms.

References

(1) T.J. Greytak and D. Kleppner, in *New Trends in Atomic Physics, Proceedings of the Les Houches Summer School, 1982,* edited by G. Grynberg and R. Stora (North-Holland, Amsterdam, 1984), p. 1125; I.F. Silvera and J.T.M. Walraven,

in *Progress in Low Temperature Physics*, edited by D. Brewer (North-Holland, Amsterdam, 1986), Vol. 10, p. 139.

(2) I.F. Silvera and J.T.M. Walraven, Phys. Rev. Lett. **45**, 1268 (1980); I.Shinkoda, M.W. Reynolds, R.W. Cline, and W.N. Hardy, *ibid.* **57**, 1243 (1986).

(3) J.M.V.A. Koelman, H.T.C. Stoof, B.J. Verhaar, and J.T.M. Walraven, Phys. Rev. Lett. **59**, 676 (1987).

(4) A.L. Migdall, J.V. Prodan, W.D. Phillips, T.H. Bergeman, and H.J. Metcalf, Phys. Rev. Lett. **54**, 2596 (1985); V.S. Bagnato, G.P. Lafyatis, A.G. Martin, E.L. Raab, R.N. Ahmad-Bitar, and D. Pritchard, *ibid.* **58**, 2194 (1987).

(5) H.F. Hess, G.P. Kochanski, J.M. Doyle, N. Masuhara, D. Kleppner, and T.J. Greytak, Phys. Rev. Lett. **59**, 672 (1987); R. van Roijen, J.J. Berkhout, S. Jaakkola, and J.T.M. Walraven, *ibid.* **61**, 931 (1988).

(6) A. Lagendijk, I.F. Silvera, and B.J. Verhaar, Phys. Rev. B **33**, 626 (1986); H.T.C. Stoof, J.M.V.A. Koelman, and B.J. Verhaar, Phys. Rev. B **38**, 4688 (1988).

(7) H.F. Hess, Phys. Rev. B **34**, 3476 (1986); T.J. Tommila, Europhys. Lett. **2**, 789 (1986).

(8) J. Vigué, Phys. Rev. A **34**, 4476 (1986).

Section 2.5
Evaporative cooling limit and Cooper pairing in D↑↑ gas.

In section 2.2 we discussed the temperature dependence of the decay rate and the thermalization rate of magnetically trapped deuterium atoms in the Boltzmann regime. We found that both decrease with decreasing temperature: the decay rate and thermalization rate being proportional to temperature and the square root of temperature, respectively. A parameter of utmost importance is the ratio of thermalization rate over decay rate: as long as this parameter is well above unity the gas remains in thermal equilibrium during decay. Furthermore, by forcing the most energetic particles to escape from the trap at a rate faster than the decay rate, but slower than the thermalization rate, the trapped gas can be cooled (forced evaporative cooling[1]). As the ratio of thermalization rate over decay rate increases as $T^{-1/2}$ with lowering temperature, we concluded that evaporative cooling is an effective means for cooling the trapped gas down to the degeneracy regime.

However, in the derivation of these results it is assumed that the temperature is well above the Fermi temperature. In the previous section we saw that the decay rate for temperatures $T<T_F$ is no longer proportional to temperature. In this section we investigate the thermalization rate in the degeneracy regime $T<<T_F$. As a result we are able to show that trapped D gas can be cooled by forced evaporation to unheard-of low temperatures considerably below the Fermi temperature and far below temperatures achievable with trapped H.

This result puts into focus the question: 'Can Cooper pairing occur in magnetically trapped deuterium gas, and if so, what is the critical temperature?'. This is the second subject of the present section.

Evaporative cooling limit

Below a few tens of millikelvins the dominant thermalization process of the trapped D gas is elastic scattering due to the long-ranged interatomic magnetic dipolar interaction. Using plane-wave Born expressions[2] we find for the thermalization rate in the non-degenerate regime[3]:

$$G_{th} \sim a_{ee}^2 \sqrt{k_B T/m} \ , \qquad (1)$$

with a_{ee} as defined in the previous section (Eq.7). Combined with the Boltzmann-regime decay rate (see previous section)

$$G_{rel} \sim a_{ee}^2 \frac{k_B T}{\sqrt{m \mu_e B}}, \qquad (2)$$

we find

$$\gamma \equiv \frac{G_{th}}{G_{rel}} \sim \sqrt{\mu_e B \,/\, k_B T}\,. \qquad (3)$$

For thermal kinetic energies far below the Zeeman splitting ($\mu_e B$ is typically of the order 0.1 K) the atoms undergo many thermalizing elastic collisions before they get involved in an inelastic spin-flipping collision.

As we saw in the previous section in the degeneracy regime ($T \ll T_F$) the decay rate is no longer proportional to temperature:

$$G_{rel} \sim a_{ee}^2 \frac{k_B T_F}{\sqrt{m \mu_e B}}. \qquad (4)$$

Also the thermalization rate is in the degeneracy regime no longer described by the Boltzmann expression. At ($T \ll T_F$) due to Pauli blocking elastic scattering is restricted to the vicinity of the Fermi surface. A simple phase-space argument shows that in the degeneracy regime the thermal velocity distribution in the neighborhood of the Fermi surface is restored at a rate which is essentially the Boltzmann thermalization rate (1) multiplied by the cube of the ratio of thermal wavenumber over Fermi wavenumber. This yields a thermalization rate proportional to the temperature squared:

$$G_{th} \sim a_{ee}^2 (T/T_F)^2 \sqrt{k_B T_F / m}\,. \qquad (5)$$

Using the theory of Vogel *et al.*[4] this result can be derived in a more rigorous way. Combining Eqs.(4) and (5) we find that in the degeneracy regime the average number of elastic collisions per spin-flipping collision is given by

$$\gamma \sim (T/T_F)^2 \sqrt{\mu_e B \,/\, k_B T_F}\,. \qquad (6)$$

When γ is close to unity, forced evaporative cooling is no longer effective in reducing the temperature. The evaporative cooling limit T_{min} is therefore

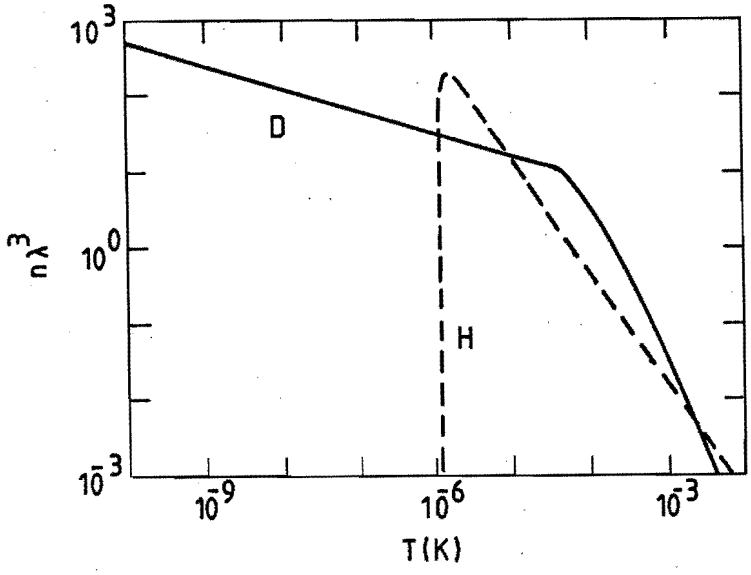

Fig.1. Degree of degeneracy $n\lambda^3$ ($\lambda^2=2\pi\hbar^2/mk_BT$) *versus temperature. The regions in which magnetically trapped D and H stay in thermal equilibrium and at the same time have a lifetime longer than several seconds are located below the full and the dashed curve, respectively.*

$$T_{min} \sim \left[\frac{k_B T_F}{\mu_e B}\right]^{1/4} T_F \,. \tag{7}$$

For $n \simeq 10^{11}$ cm^{-3} and $B \simeq 0.1$ T we have $T_F \simeq 0.39$ μK and a very low cooling limit $T_{min} \sim 0.05\ T_F \simeq 20$ nK. As T_{min} is proportional to $n^{5/6}$ we find even lower limiting temperatures at lower densities. The minimum atom density is set by the detection limit. This minimum density can be very low: using optical (Lyman-α) techniques 10^7 atoms can easily be detected.[5]

The above derived evaporative cooling limit should be compared to that for magnetically trapped H. In that case we have

$$G_{rel} \sim a_{ee}^2 \sqrt{\mu_e B/m}\,, \tag{8}$$

and a thermalization rate which is dominated by elastic s-wave triplet potential scattering:

$$G_{th} \sim \sigma_{trip} \sqrt{k_B T/m}\,, \tag{9}$$

with the elastic triplet scattering cross section $\sigma_{trip} = 6.3\times10^{-20}m^2$. In the same way as above we now find for the evaporative cooling limit of magnetically trapped H:

$$T_{min} \sim \left[\frac{a_{ee}^2}{\sigma_{trip}}\right]^2 \mu_e B/k_B\,, \tag{10}$$

which typically is of the order of $1\mu K$ and independent of atom density. The in some sense opposite behavior of trapped H and D gases is visualized in Fig.1 which shows the achievable degree of degeneracy $n\lambda^3$ (λ is the thermal wavelength) for H$\uparrow$ and D$\uparrow$ as a function of temperature. As is evident from this figure, a much larger experimental 'window' to observe degeneracy effects is available for D$\uparrow$.

Cooper pairing

Cooper pairing is a phenomenon which occurs in degenerate Fermi fluids. It manifests itself as a phase transition at some critical temperature T_c below which an energy gap exists between the ground state and the first exited states. Roughly speaking, the gap arises as the particles profit from an attractive part of their mutual interaction by forming correlated pairs (Cooper pairs) with zero total momentum. Associated with Cooper pairing is the phenomenon of flow without resistance as in superfluid ^{3}He and superconducting materials. The scattering which gives rise to resistance in a normal Fermi fluid is absent in a Cooper-paired Fermi fluid due to the gap energy required to excite the system.

In general, it is very difficult to predict the critical temperature T_c at which a Fermi fluid undergoes a phase transition to the Cooper-paired state. This is because the critical temperature depends exponentially on the effective interparticle-interaction strength which as a rule is not well-known. An illustrative example is formed by the large scatter of the predicted values of T_c for liquid ^{3}He before it was experimentally shown to be 2.7 mK [6]: these values ranged from 2 mK to 1 K [7]. In one case the critical temperature can be predicted. That is for a dilute gas of fermions interacting via a central two-body interaction for which the low-energy scattering phase shifts are accurately known. In such a system Cooper pairing into pair states with an angular momentum quantum number ℓ is possible if the phase shift $\delta^{\ell}(k)$ at

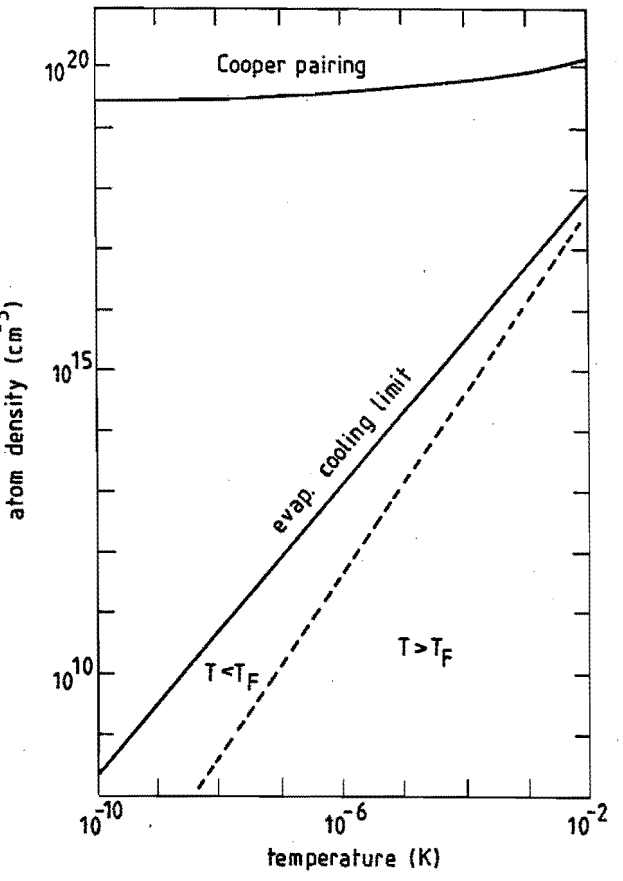

Fig.2. The region below the evaporative cooling limit line indicates the density-temperature region which is in principle accessible with magnetically trapped deuterium. The region where Cooper pairing should occur is way out of reach.

relative wave number $k=k_F$ is positive. In that case the critical temperature is given by[7,8]

$$T_c \sim T_F \exp\{-\tfrac{\pi}{2}\cot[\delta^{\ell}(k_F)]\}\,. \qquad (11)$$

Doubly-spin-polarized deuterium atoms interact via the central triplet interaction. For low atom densities k_F is very small and the largest $\delta^{\ell}(k_F)$, and hence the largest T_c, occurs for the lowest ℓ-value allowed: $\ell=1$. The low energy $\ell=1$ phase shifts can be expressed in terms of the scattering length a_1 for $\ell=1$ D+D triplet scattering[9],

$$\cot \delta^1(k) = -3/(a_1 k)^3. \qquad (12)$$

The scattering length a_1 is numerically determined to be -5.1×10^{-10} m. Substituting Eq.(12) and the expression for the Fermi wavenumber $k_F = (6\pi^2 n)^{1/3}$ in Eq.(11) leads to

$$T_c \sim T_F \exp\{1/(4\pi a_1^3 n)\} \sim T_F \exp\{-6\times10^{20}\text{cm}^{-3}/n)\}. \qquad (13)$$

An analogous equation for $\ell=0$ pairing in non–nuclear spin-polarized D↓ was considered by Leggett.[10] Due to the exponential dependence on $-1/n$ the value for T_c drops dramatically when the atom density is lowered. This is shown very clearly in Fig.2: Cooper pairing is only possible for atom densities not too far below 10^{20}cm^{-3}. As is evident from this figure Cooper pairing is way out of reach in experiments with trapped D↑↑ since in the regime where Cooper pairing should occur the atoms cannot be held in thermal equilibrium.

One could argue that the above-derived values of T_c are too pessimistic. As discussed in section 3.2 in cold dilute D↑↑ gas the atoms experience only the long-range part of their mutual interactions. For large interatomic separations the magnetic dipolar interaction dominates over the triplet interaction, so one might expect the attractive part of the dipolar interaction to give rise to larger values for T_c. We investigated this possibility by calculating what is likely to be an upper limit for the dipolar induced T_c. To this end we calculated T_c for a gas of atoms with an isotropic r^{-3} attraction and a short-ranged hard core repulsion. The strength of the r^{-3} attraction was chosen to be equal to the magnetic dipolar interaction for deuterium atoms with their magnetic moments in line, and the range of the hard core was chosen to be comparable to that of the repulsive part of the triplet interaction. The results of this calculation confirmed the above expectations. We find an expression for T_c which does not contain the inverse of the density in the exponent, but instead the inverse cube root of the density. Hence, this r^{-3} attraction induced T_c dominates at low density over the triplet induced T_c. However, this dominance occurs only for atom densities below approximately 10^{17} cm^{-3} at which T_c is unobservably low anyway.

We conclude that for systems of fermions with interactions falling off with r^{-3} or faster Cooper pairing is a high density phenomenon, which therefore is unobservable in magnetically trapped D↑↑ gases.

References.

(1) H.F. Hess, Phys. Rev. B 34, 3476 (1986); T.J. Tommila, Europhys. Lett. 2, 789 (1986).

(2) J.P.H.W. van den Eijnde, Ph.D. thesis, Eindhoven University of Technology, the Netherlands (1984).

(3) As the discussion is very strongly facilitated if we forget about mathematical factors of order unity, we leave them out in the following in order to keep the physics as transparent as possible.

(4) J. Vogel, E. Vogel, and C. Toepffer, Ann. Phys. 164, 463 (1985).

(5) T.W. Hijmans, O.J. Luiten, I.D. Setija, and J.T.M. Walraven, Proc. third Conf. on Spin-Polarized Quantum Systems, Torino 1988, World-Scientific.

(6) D.D. Osherhoff, R.C. Richardson and D.M. Lee, Phys. Rev. Lett. 28, 885 (1972); D.D. Osherhoff, W.J. Gully, R.C. Richardson and D.M. Lee, *ibid.* 29, 920 (1972).

(7) V.J. Emery, A.M. Sessler, Phys. Rev. 119, 43 (1960).

(8) V.J. Emery, Nucl. Phys. 19, 154 (1960).

(9) B.J. Verhaar, L.P.H. de Goey, J.P.H.W. van den Eijnde, and E.J.D. Vredenbregt, Phys. Rev. A 32, 1424 (1985).

(10) A.J. Leggett, J. Phys. (Paris), C7, 19 (1980)

CHAPTER 3

HYDROGEN MASERS: INSTABILITY DUE TO SPIN-EXCHANGE COLLISIONS

Section 3.1

Potential advantages of low-temperature hydrogen masers

Almost thirty years after its first realization by Goldenberg, Kleppner, and Ramsey,[1] the hydrogen maser continues to be the most stable of all atomic frequency standards. For measuring times of about one hour the relative frequency instability is observed to be below one part in 10^{15} (Fig.1). This extreme stability makes the hydrogen maser a very valuable research tool in fields as diverse as physics, astronomy, geodesy, and metrology.

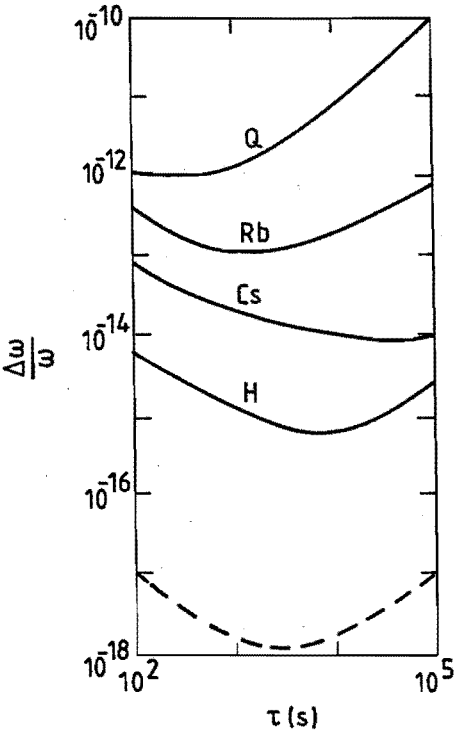

Fig.1. Predicted relative frequency stability[6] *of the cryogenic hydrogen maser (dashed curve) versus averaging time compared to that of a high-performance quartz crystal oscillator*[12] *(curve* Q*) and other atomic frequency standards (curve* Rb: *commercial rubidium gas-cell standard*[8], *curve* Cs: *state-of-the-art cesium beam standard*[8], *curve* H: *state-of-the-art room temperature hydrogen maser*[3]*).*

The principle of hydrogen maser operation is shown in Fig.2. Molecular hydrogen is dissociated into atomic form in an rf discharge. The H beam which is formed at the output of the dissociator, is state-selected by an axially symmetric multipole magnet. This magnet focuses the atoms in the upper hyperfine states (the "low-field-seekers") on a small entrance hole in a teflon coated quartz storage bulb, while it defocuses the atoms in the lower hyperfine states (the "high-field-seekers"). As a consequence, a beam of atoms with an inverted hyperfine population enters the storage bulb. This bulb is situated in a microwave cavity tuned to the low-field $\Delta m_F=0$ (c→a) transition, with a frequency of about 1420 MHz. When the intensity of the atomic beam entering the bulb is large enough, a selfsustained oscillation develops in which the atoms are stimulated to radiate at the $\Delta m_F=0$ transition. Some of the microwave power is coupled out of the cavity by an electrical coupling loop.

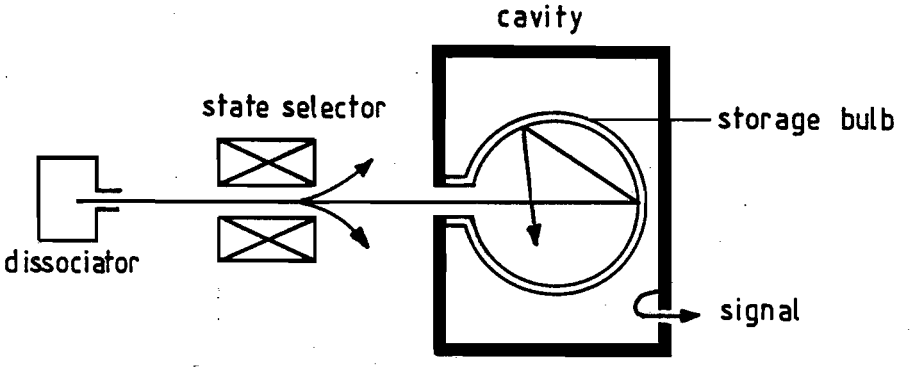

Fig.2. *Basic set-up of a conventional hydrogen maser.*

The extreme frequency stability of the H maser is mainly due to the fact that the hydrogen atoms are confined in the storage bulb for times as long as one second, leading to a very small observation time limited atomic linewidth. This is essential for achieving high frequency stabilities, particularly because a small atomic linewidth reduces cavity pulling effects. Cavity pulling (Fig.3) originates from a competition between the atomic hyperfine frequency and the cavity resonance frequency in determining the maser oscillation frequency. Under conditions of selfsustained maser oscillation the resulting frequency is not equal to the atomic frequency, but is rather a

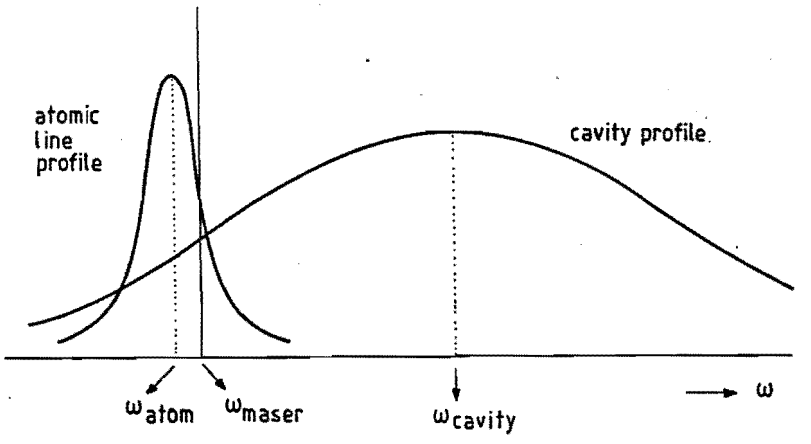

Fig.3. Cavity pulling: the maser oscillation frequency is shifted from the atomic transition frequency by a pulling of the cavity resonance frequency. Using the fact that the atomic and the cavity line profiles have a similar (Lorentzian) shape it follows that, if both profiles are drawn so as to be normalized to the same height, the maser oscillation frequency is located at the frequency at which these profiles intersect. The atomic linewidth is usually orders of magnitude smaller than the cavity resonance width. In the absence of noise the maser signal has zero bandwidth.

trade-off between atomic frequency and cavity frequency, in that the difference between oscillation frequency and atomic frequency measured in units of the atomic linewidth equals the difference between maser frequency and cavity frequency measured in units of the cavity linewidth (Fig.3). Evidently, a small atomic linewidth reduces the dependence of the oscillation frequency on the relatively unstable cavity resonance frequency.

A small atomic linewidth also suppresses the frequency instability due to the various sources of noise. This is because the fractional frequency stability due to noise is given by the fractional atomic linewidth divided by the signal-to-noise ratio. As the signal-to-noise ratio $S_n=(\tau P/k_B T)^{1/2}$ increases as a function of measuring time τ and oscillation power P, the long-term frequency stability is, for large enough power, not limited by instabilities due to noise but rather by instabilities in the atomic linewidth and cavity frequency which couple to the maser frequency via the cavity pulling effect.

Collisions of the atoms with the storage bulb walls perturb the hydrogen atom and thereby shift the hyperfine transition frequency (Fig.4). Although this wall shift very

strongly limits the accuracy of the hydrogen maser, it does not seriously limit the stability as this shift is sufficiently stable at temperature stabilities under which hydrogen masers are typically operated.

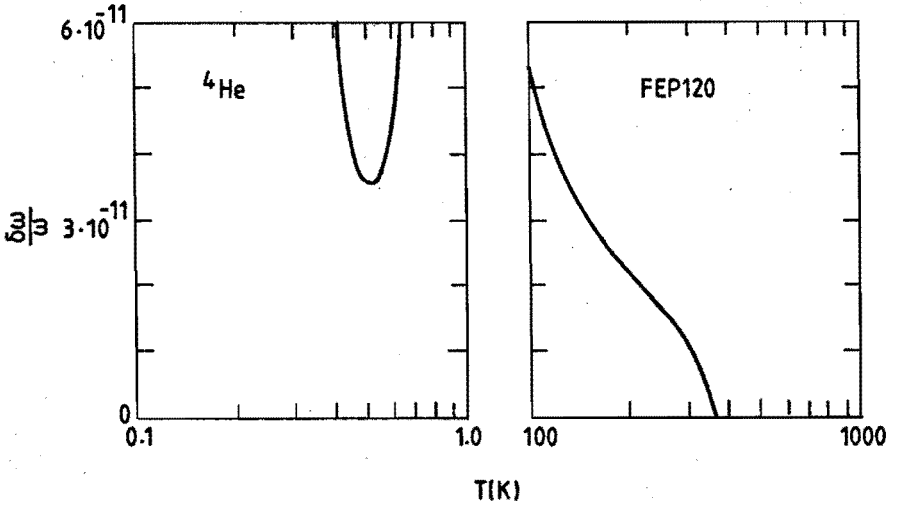

Fig.4. Temperature dependence of the fractional maser frequency shift due to collisions of the hydrogen atoms with the wall atoms. Right part: observed shift with a 15 cm diameter teflon (FEP120) coated bulb[13], *left part: predicted for a 15 cm diameter helium coated bulb*[5].

As pointed out a decade ago,[2,3] a hydrogen maser operating at liquid helium temperatures would have a much higher intrinsic frequency stability than a conventional (room-temperature) hydrogen maser. This is mainly due to the much smaller collisional H-atom line broadening at lower temperatures, allowing for a larger radiating atom density, and hence for a larger power P without increasing the atomic linewidth above the room-temperature value. Furthermore, lower temperatures increase the signal-to-noise ratio by decreasing k_BT, and help to get a better control over the cavity resonance frequency. At that time, the lack of a wall coating suitable for confining cold hydrogen atoms prevented the realization of a cryogenic hydrogen maser. A conventional maser, with Teflon-coated walls can be operated down to approximately 80 K, but only at the expense of introducing a large wall shift (Fig.4) and a large atomic line broadening. Wall coatings of solid neon and solid molecular hydrogen surfaces can be used down to lower temperatures, but they also introduce severe wall shifts and line broadenings. An important breakthrough was the success of

the spin-polarized hydrogen stabilization experiment of Silvera and Walraven,[4] which showed that H atoms do not enter a superfluid helium film. Of decisive importance for the feasibility of low-temperature hydrogen masers with increased stability was the discovery[5] that the frequency shift due to collisions of the hydrogen atoms with the He-coated walls and the He-vapor goes through a minimum as a function of temperature (Fig.4). Operation at this temperature of about 0.5 K, should produce a very high thermal stability. Berlinsky and Hardy predicted[6] that with such types of cryogenic hydrogen masers an improvement in frequency stability of about three orders of magnitude over that of a room-temperature hydrogen maser should be realizable.

Up till now we did not include the frequency shifts due to collisions between hydrogen atoms in our discussion. Analyses of the effect of spin-exchange collisions[7] showed that it shifts the maser frequency in the same way as the cavity pulling does: via a proportionality to the atomic linewidth. Therefore, in some sense, the spin-exchange frequency shift introduces no new difficulties. In this chapter we will show that this is definitely not true in case of low temperature hydrogen masers. The above mentioned papers discussing the spin-exchange frequency shift all ignore the effect of the hyperfine energy levels separation during the spin-exchange collisions. This is an essential omission in the case of cryogenic H-masers where, as we will show, the effect of the hyperfine interaction during collisions introduces large maser frequency shifts which strongly limit the achievable stability.

The following two sections both deal with this hyperfine-induced spin-exchange frequency shift. Section 3.2 gives a short account of the consequences of this shift on the operation of the cryogenic H maser. Section 3.3 is much more detailed. It gives a complete discussion of the combined effects of the spin-exchange and hyperfine interactions on frequency shift, line broadening and hyperfine relaxation effects in an oscillating H maser. It also discusses these effects for a room-temperature hydrogen maser.

For background information on atomic frequency standards the reader is referred to the review papers by Audoin and Vanier,[8] and Hellwig[9]. A recent review on the conventional hydrogen maser can be found in Ref.10. A detailed discussion on experiments with a cryogenic hydrogen maser is given in Ref.11.

References

(1) H.M. Goldenberg, D. Kleppner, and N.F. Ramsey, Phys. Rev. Lett. 5, 361 (1960).

(2) S.B. Crampton, W.D. Phillips, and D. Kleppner, Bull. Am. Phys. Soc. 23, 86 (1978).

(3) R.F.C. Vessot, M.W. Levine, and E.M. Mattison, in Proc. of the 9th Annual

Precise Time and Time Interval Conference, 1978 [NASA Techn. Memorandum No.78104, 1978(unpublished)] p.549.

(4) I.F. Silvera, and J.T.M. Walraven, Phys. Rev. Lett. 44, 164 (1980).

(5) M. Morrow, R. Jochemsen, A.J. Berlinsky, and W.N. Hardy, Phys. Rev. Lett. 46, 195 (1981).

(6) A.J. Berlinsky and W.N. Hardy, Proceedings of the Thirteenth Annual Precise Time and Time Interval (PTTI) Applications and Planning Meeting, Naval Research Laboratory, Washington, D.C. 1982 [NASA Conference Publication No. 2220, 1982 (unpublished)], p. 547.

(7) L.C. Balling, R.J. Hanson, and F.M. Pipkin, Phys. Rev. 133, A607 (1964); 135, AB1 (1964); P.L. Bender, Phys. Rev. 132, 2154 (1963); A.C. Allison, Phys. Rev. A 5, 2695 (1972); A.J. Berlinsky and B. Shizgal, Can. J. Phys. 58, 881 (1980).

(8) C. Audoin and J. Vanier, J. Phys. E 9, 697 (1976)

(9) H. Hellwig, in *Precision Frequency Control Vol.2*, edited by E.A. Gerber and A. Ballato (Academic Press Inc., 1985), p.113.

(10) J. Vanier, Metrologia 18, 173 (1982).

(11) W.N. Hardy, M.D. Hürlimann, and R.W. Cline, Jpn. J. Appl. Phys. 26, 2065 (1987) Suppl. 26–3 (Proc. Int. Conf. on Low Temp. Physics, Kyoto, 1987).

(12) W.L. Smith, in *Precision Frequency Control Vol.2*, edited by E.A. Gerber and A. Ballato (Academic Press Inc., 1985), p.79.

(13) M. Desaintfuscien, J. Viennet, and C. Audoin, Metrologia 13, 125 (1977).

Section 3.2

Hyperfine Contribution to Spin-exchange Frequency Shifts in the Hydrogen Maser

B.J.Verhaar, J.M.V.A.Koelman, H.T.C.Stoof, O.J.Luiten, and S.B.Crampton*

Department of Physics, Eindhoven University of Technology,
5600 MB Eindhoven, The Netherlands
**Department of Physics and Astronomy, Williams College,*
Williamstown, Massachusetts 01267

[Published in Phys. Rev. A 35, 3825 (1987)]

We have rigorously included hyperfine interactions during electron-spin-exchange collisions between ground-state hydrogen atoms and find additional frequency shifts which are significant for low-temperature atomic hydrogen maser oscillators.

Introduction

Electron-spin-exchange collisions between ground-state paramagnetic atoms are usually treated in a degenerate-internal-states approximation, which ignores hyperfine interactions relative to electron-exchange interactions during collisions.[1-5] Such calculations predict small shifts of the $\Delta m_F=0$ hyperfine transition frequency in ground-state atomic hydrogen proportional to the rate of collisions with other hydrogen atoms and to the difference between the two $\Delta m_F=0$ level populations.[4,5] Because of the proportionality to the level population difference, such shifts can be eliminated from the frequency of an atomic hydrogen maser oscillating in weak magnetic field on the $\Delta m_F=0$ transition by tuning the maser microwave cavity so that there is no change of oscillation frequency with collision rate.[6] A semiclassical treatment by one of us of hyperfine effects during collisions to first order revealed a small additional shift of the $\Delta m_F = 0$ hydrogen maser oscillation frequency not compensated for by cavity mistuning.[7] Both the degenerate-internal-states shift and the additional hyperfine-induced shift have been confirmed near room temperature,[7,8] and the degenerate-internal-states shift down to liquid-nitrogen temperatures.[9]

Recently, hydrogen maser oscillation has been achieved at 9 to 10.5 K using solid-neon storage surfaces,[10,11] and at 0.3 to 0.6 K using superfluid-helium storage surfaces.[12-14] For cryogenic masers operating with reduced thermal noise and potentially greater radiated power, the instability due to thermal noise may be[15-17] as low as two parts in 10^{18}. The actual instability minimum will be determined by mechanisms which couple the maser frequency to instabilities of other maser parameters. Understanding the magnitudes and level population dependencies of any

uncompensated hyperfine-induced spin-exchange-collision frequency shifts is therefore potentially important to using cryogenic hydrogen masers as frequency standards and spectroscopic tools. At cryogenic temperatures the effects of atom identity and quantization of collision angular momenta are significant, so that it is essential that calculations be fully quantum mechanical. Berlinsky and Shizgal have extended the quantum-mechanical degenerate-internal-states calculations to 10 K and below.[18] We report here a quantum-mechanical treatment of frequency shifts and broadening due to H-H spin-exchange collisions at low temperatures, including hyperfine-induced effects. We find effects which are large compared to the potential thermal instabilities of cryogenic hydrogen masers, but may also provide a sensitive probe of nonadiabatic contributions in hydrogen-hydrogen atom-atom interactions at low collision energies.

Method

Our starting point is the evolution equation for the spin density matrix,

$$\frac{d\rho_{\kappa\kappa'}}{dt} = -\frac{i}{\hbar}(E_\kappa - E_{\kappa'})\rho_{\kappa\kappa'} - \frac{i}{\hbar}[H_1(t),\rho]_{\kappa\kappa'}$$

$$+ n \sum_{\lambda,\mu,\nu,\mu',\nu'} \sum_{\ell,m,\ell',m'} \rho_{\mu\mu'}\rho_{\nu\nu'}[(1+\delta_{\kappa\lambda})(1+\delta_{\kappa'\lambda})(1+\delta_{\mu\nu})(1+\delta_{\mu'\nu'})]^{1/2}$$

$$\times \left\langle \frac{\pi\hbar}{m_a k} (S_{\{\kappa\lambda\}\ell m,\{\mu\nu\}\ell' m'} S^*_{\{\kappa'\lambda\}\ell m,\{\mu'\nu'\}\ell' m'} - \delta_{\{\kappa\lambda\},\{\mu\nu\}}\delta_{\{\kappa'\lambda\},\{\mu'\nu'\}}\delta_{\ell\ell'}\delta_{mm'}) \right\rangle$$

$$+ \left.\frac{d\rho_{\kappa\kappa'}}{dt}\right|_{rel}, \qquad (1)$$

the quantum-mechanical Boltzmann equation for a homogeneous system, which we have derived from the fundamental Bogoliubov-Born-Green-Kirkwood-Yvon (BBGKY) hierarchy for the distribution matrices. In this equation Greek subscripts take values a,b,c,d, the 1s hyperfine states in order of increasing energy E_α (Fig 1). The operator $H_1(t)$ represents any (time-dependent but position-independent) magnetic field operating on the atoms. The last term represents all relaxation terms except for the relaxation due to the two-body collisions taken into account in the previous term. The hydrogen atom density is denoted by n, the atomic mass by m_a, and the wave number in the entrance channels of the S-matrix elements by k. The notation $\{\alpha\beta\}$ implies normalized symmetrization (antisymmetrization) of two-body spin states for relative orbital angular momentum ℓ even (odd) having z component m. The brackets $\langle\ \rangle$ denote thermal averaging with the same velocity distribution for each of the spin states, assuming dominance of thermalizing elastic collisions with the

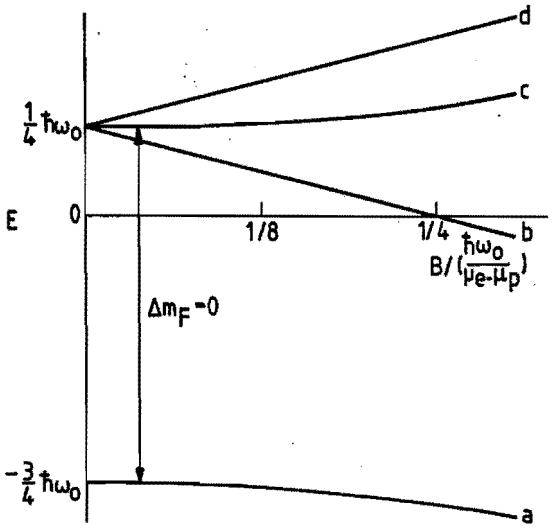

Fig.1. Atomic hydrogen ground-state energy levels vs applied magnetic field strength in units $(\hbar\omega_0)/(\mu_e-\mu_p)$ *(=0.102 T).*

walls or between atoms relative to inelastic collisions between atoms.

Considering situations with coherence only between the a and c levels, we have a 4x4 spin density matrix with only one pair of nonvanishing off-diagonal elements $\rho_{ac} = \rho_{ca}^*$. The collision terms in Eq.(1) contributing to the time development of ρ_{ac} have the form

$$\left.\frac{d\rho_{ac}}{dt}\right|_{coll} = n\,\rho_{ac}\sum_{\nu} G_\nu\,\rho_{\nu\nu} \tag{2}$$

with rate-constant-like[19] coefficients G_ν.

Let us now look more closely at the nature of these coefficients on the basis of some symmetry considerations. The S-matrix elements follow from the Schrödinger equation for two-body scattering. This contains a central interaction V^c consisting of singlet and triplet potentials

$$V^c = P_S V_S(r) + P_T V_T(r), \tag{3}$$

$P_S(P_T)$ standing for a projection on singlet (triplet) subspaces. In addition, it contains the intra-atomic hyperfine interactions,

$$V^{hf} = \hbar\omega_0(\underline{S}_1\cdot\underline{I}_1+\underline{S}_2\cdot\underline{I}_2), \tag{4}$$

in which ω_0 is the hyperfine frequency, while $\underline{S}_{1,2}$ and $\underline{I}_{1,2}$ are the electron and proton spins of the two colliding atoms. We consider only the case of very weak external magnetic fields and so leave out Zeeman terms in calculating the S-matrix elements. Although these terms, the interatomic hyperfine interactions, and the spin dipolar interactions can be included in our coupled-channel calculations,[20] their effects are negligible compared to the exchange and intra-atomic hyperfine interactions. We leave them out both in the discussion of symmetries and in the later first-order treatment so as to keep the physics as transparent as possible.

Each of the coefficients G_ν then contains a sum of products $S_{\{a\alpha\}\ell,\{a\nu\}\ell}$ $S^*_{\{c\alpha\}\ell,\{c\nu\}\ell}$, independent of m. It turns out that only elastic S-matrix elements contribute. For odd ℓ this follows from the selection rule $\Delta m_F = 0$, taking into account that antisymmetric spin states $\{a\nu\}$ and $\{c\nu\}$ can be formed simultaneously only for ν = b or d. For even ℓ it is due to assuming zero magnetic field: All five symmetric spin states consisting of two different hyperfine states, at least one of which is a or c, have unmixed S=1, so that no coupling by V^c (or V^{hf}) occurs within this set or to aa and cc. The five S=1 spin states having elastic S-matrix elements $\exp(2i\delta_T^\ell)$, with δ_T^ℓ the triplet phase shift, the S-matrix products within G_ν are canceled by the corresponding products of Kronecker deltas for ν = b or d. Therefore, in Eq.(2) the ν = b and d terms have contributions from odd ℓ only, the ν = a and c terms from even ℓ only.

The collision problem shows symmetry under a 180° combined rotation of the two electron spins and two proton spins about an axis perpendicular to the weak magnetic field. This rotation exchanges b and d while leaving a and c alone. We conclude that the S-matrix elements for the ab and ad spin states are equal, as are those for the spin states cb and cd. The result is finally that $G_\nu = \langle v\lambda_\nu\rangle = \langle v\rangle\overline{\lambda}_\nu$ with $\langle v\rangle$ the thermal average collision speed and $\overline{\lambda}_\nu$ the thermal average of the λ_ν "cross section" defined in simplified notation as

$$\lambda_a = \frac{2\pi}{k^2}\sum_{\ell\,\mathrm{even}}(2\ell+1)[S^\ell_{aa,aa}(S^\ell_{\{ac\},\{ac\}})^* - 1],$$

$$\lambda_c = \frac{2\pi}{k^2}\sum_{\ell\,\mathrm{even}}(2\ell+1)[S^\ell_{\{ac\},\{ac\}}(S^\ell_{cc,cc})^* - 1], \tag{5}$$

$$\lambda_b = \lambda_d = \frac{\pi}{k^2}\sum_{\ell\,\mathrm{odd}}(2\ell+1)[S^\ell_{\{a\nu\},\{a\nu\}}(S^\ell_{\{c\nu\},\{c\nu\}})^* - 1], \quad \nu = \mathrm{b\ or\ d}.$$

We stress that all of the S-matrix elements in Eq.(5) are to be calculated for a common value of kinetic energy in the particular elastic channel.

Substituting

$$\rho_{ac}(t) = \rho_{ac}(0)\exp[i(\omega_0+\delta\omega+i/\tau_2)t]$$

and using $\sum_\nu \rho_{\nu\nu} = 1$, we find for the frequency shift

$$\delta\omega = n<v>[(\rho_{cc}-\rho_{aa})\bar{\lambda}_0+(\rho_{cc}+\rho_{aa})\bar{\lambda}_1+\bar{\lambda}_2], \tag{6}$$

in which

$$\lambda_0 = \mathrm{Im}[(\lambda_c-\lambda_a)/2],$$

$$\lambda_1 = \mathrm{Im}[(\lambda_c+\lambda_a)/2-\lambda_b], \tag{7}$$

$$\lambda_2 = \mathrm{Im}(\lambda_b).$$

At this point it is interesting to indicate how these results reduce to those of Balling *et al.* when the hyperfine splitting is turned off. The channels can then be decoupled by transforming to the triplet and singlet channels, leading to the expressions

$$S^{\ell(0)}_{\{\alpha\beta\},\{\alpha\beta\}} = <\{\alpha\beta\}|e^{2i\delta_S^\ell} P_S + e^{2i\delta_T^\ell} P_T|\{\alpha\beta\}> \tag{8}$$

for the S-matrix elements in the degenerate-internal-states approximation as expectation values in (anti)symmetric spin states depending on ℓ. Alternatively, we may note that without V^{hf} the Hamiltonian for the two-body problem no longer depend on the proton-spin degrees of freedom. A combined rotation of proton spins by 180° about the magnetic field direction as an additional symmetry operation now exchanges a and c while leaving b and d alone. We then find

$$\lambda_0^{(0)} = \frac{\pi}{2k^2}\sum_{\ell\ \mathrm{even}}(2\ell+1)\sin[2(\delta_T^\ell-\delta_S^\ell)],$$

$$\lambda_1^{(0)} = \lambda_2^{(0)} = 0. \tag{9}$$

The frequency shift $\delta\omega$ thus reduces to the well-known expression for the case of vanishing hyperfine splitting ($\lambda_0^{(0)} = -\lambda^+/4$ of Ref. 18).

To determine the various λ quantities without neglecting hyperfine splitting, we

have to calculate the elastic S-matrix elements in Eq.(5). This can be done by integrating the coupled radial equations describing the H-H scattering wave functions in the various channels: the so-called coupled-channels (CC) approach,[20,21] which in principle yields exact results. This is one of the methods we have used.

Calculating the frequency shift by the CC approach over the wide temperature interval needed for thermal averaging would be rather time consuming. Instead, it is attractive to use an approach which exploits the weakness of the hyperfine interaction ($\hbar\omega_0 \approx 0.068$ K) in the form of a calculation that takes into account the hyperfine interaction as a first-order correction to the degenerate-internal-states approximation. However, a simple Born-type approach for the hyperfine interaction yields volume integrals which do not converge. This difficulty stems from the fact that the hyperfine interaction does not fall off at large distances. Yet as pointed out in Ref. 22, a first-order treatment is possible and leads to a Born-type integral restricted to a finite volume beyond which the singlet and triplet potentials are negligible, accompanied by a Wronskian surface term which in a way accounts for the nonvanishing hyperfine interaction in the outer volume. We use this method to calculate the various elastic S-matrix elements including the finite energy separation of other hyperfine energy levels from the hyperfine energy level associated with the particular elastic channel under consideration. The first-order corrections then arise from back and forth transitions to other hyperfine levels during a collision, as in the semiclassical treatment.[7] We find that the corrections to the degenerate-internal-states S-matrix elements are given by

$$\Delta S^{\ell}_{\{\alpha\beta\},\{\alpha\beta\}} = \langle\{\alpha\beta\}|(P_T-P_S)(V^{hf}-E_\alpha-E_\beta)(P_T-P_S)|\{\alpha\beta\}\rangle\,\Delta^{\ell}, \qquad (10)$$

i.e., a simple spin-matrix element times a quantity Δ^{ℓ} given by

$$\Delta^{\ell} = \frac{i}{4}\frac{\frac{1}{2}m_a}{\hbar^2 k^2}\left[k\int_0^{r_0}[u_S^{\ell(0)}(k,r)-u_T^{\ell(0)}(k,r)]^2dr + \frac{1}{2}(S_S^{\ell(0)}-S_T^{\ell(0)})^2\, W[0^{\ell}(kr),\frac{\partial}{\partial k}0^{\ell}(kr)]_{r=r_0}\right], \qquad (11)$$

with the Wronskian W defined as $W[f,g] = f\partial g/\partial r - g\partial f/\partial r$. The radial wave functions $u^{\ell(0)}$ are normalized so as to have asymptotic behavior

$$e^{-i(kr-\frac{1}{2}\ell\pi)} - S^{\ell(0)}e^{i(kr-\frac{1}{2}\ell\pi)},$$

and $O^{\ell}(kr)$ is a Hankel-like free outgoing wave with asymptotic behavior $e^{i(kr-\frac{1}{2}\ell\pi)}$. Expression (11) is independent of r_0 under the condition that the triplet and singlet potentials are zero for $r > r_0$.

Substituting the S-matrix elements including the first-order corrections into (5), we find for the right-hand side of (7):

$$\lambda_0 = \lambda_0^{(0)} - \tfrac{1}{2}\Delta\lambda_+,$$

$$\lambda_1 = \Delta\lambda_+ - \Delta\lambda_-, \tag{12}$$

$$\lambda_2 = \Delta\lambda_-,$$

with the corrections to the degenerate-internal-states $\lambda_1^{(0)}$ values of Eq. (9) given by

$$\Delta\lambda_+ = \frac{\pi}{2k^2}\sum_{\ell\ \mathrm{even}}(2\ell+1)\mathrm{Im}(2\Delta^{\ell*}S_T^{\ell(0)}),$$

$$\Delta\lambda_- = \frac{\pi}{2k^2}\sum_{\ell\ \mathrm{odd}}(2\ell+1)\mathrm{Im}([\Delta^{\ell*}S_T^{\ell(0)} + S_S^{\ell(0)})]. \tag{13}$$

Equations (6), (7), and (5) represent our final formulation of the spin-exchange frequency shift including the hyperfine contributions. In the following section these equations form the basis of a coupled-channel calculation. Likewise, Eqs. (12), (13), and (11) are used for a first-order calculation.

Results

Both in the CC calculation and in the first-order approximation we have used "state-of-the-art" singlet and triplet potentials.[23,24] Details of the CC calculation are given in Refs. 20 and 21. With respect to nonadiabatic effects, two types of calculations have been carried out. The first incorporates the departure from the Born-Oppenheimer approximation together with relativistic and radiative effects only as first-order corrections to the singlet and triplet potentials, as in Ref. 24, Sec. III. This approach is commonly called the "adiabatic" approximation. Wolniewicz (Ref. 24, Sec. IV) has devised a method for including the departure from Born-Oppenheimer in the bound-state energies to second order (usually referred to as "nonadiabatic" corrections), but this method does not apply to the continuum. Our own calculations and those of Ref. 25 indicate that the second-order corrections to the bound-state energies nearest the continuum can be reproduced by simply replacing the reduced proton mass $\frac{1}{2}m_p$ by the reduced atomic mass $\frac{1}{2}m_a$ in the first-order calculation. In the second type of calculation we incorporate nonadiabatic effects into the continuum calculation by replacing the reduced mass $\mu = \frac{1}{2}m_p$ by $\mu = \frac{1}{2}m_a$ in the radial Schrödinger equation.

Results show a remarkable sensitivity to this introduction of nonadiabaticity, far greater than would be expected from the relative change of the reduced-mass parameter μ from $\frac{1}{2}m_p$ to $\frac{1}{2}m_a$. In view of the large collection of results involved, we restrict the following figures to results calculated using $\mu = \frac{1}{2}m_a$. In discussing these figures, the most important differences with the adiabatic results will be indicated.

In Fig.2 we give the contributions of the partial waves $\ell = 0,1,2,3$ to λ_1, and of the partial waves $\ell = 1,3$ to λ_2, as functions of energy. The hyperfine-induced correction to λ_0 is small and does not seem to be significant. Note that the low-energy behavior in Fig.2 is proportional to $E^{\ell-\frac{1}{2}}$, in accordance with expectations. This figure makes clear that the first-order treatment is indeed of considerable help in covering the large

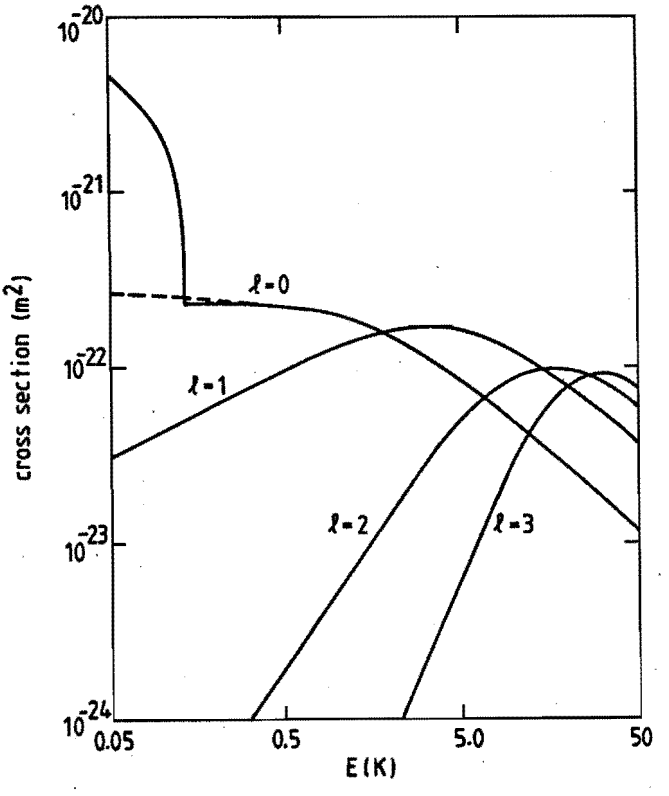

Fig.2. Partial contributions of the first four partial waves to the hyperfine-induced frequency shift cross sections as functions of energy: $-\lambda_1^\ell$ for even ℓ and $\lambda_1^\ell = -\lambda_2^\ell$ for odd ℓ. Solid lines, CC calculation; dotted line, first-order calculation where it differs significantly from the CC calculation.

energy range and the large number of partial waves needed to calculate Boltzmann-averaged values over the temperature range of interest: Comparing the CC results with the first-order results, the first-order calculation gives very accurate results except at low energies in the $\ell = 0$ partial wave. The deviation takes the form of a prominent cusp in the CC curve due to the threshold of the cc channel felt in the aa channel at $E = 2\hbar\omega_0$. This threshold behavior is easily understood by noting that each of the S-matrix elements involved is a regular analytic function[26] of the wave number in the channel opening up at the threshold. Purely imaginary values for this wave number below threshold, changing into real values above, explain the calculated result that the path which is followed by $S_{aa}^{\ell=0}$ in the complex plane shows a 90^0 kink. The latter gives rise to the cusp behavior in Fig. 2. It is understandable that it cannot be reproduced by a first-order treatment based on the idea that the hyperfine interaction has a small effect. However, it is clear that the hyperfine separation of the aa and cc thresholds is of primary importance at low energies. In a classical picture the hyperfine-precession angle of spins during a collision is no longer small for collisions with a longer duration at threshold.

From the same argument one might expect similarly large difference of CC and first-order results close to resonances, and that turns out to be the case. Calculations using reduced mass $\mu = \frac{1}{2}m_p$ show a pronounced resonance behavior of the λ quantities in the $\ell = 4$ partial wave due to the 14,4 vibration-rotation state in the continuum at 1.3 K. Close to resonance, the first-order treatment greatly overestimates the λ quantities, and Boltzmann averaging then leads to appreciable contributions by the resonance. The CC calculation shows two much weaker resonances with a $2\hbar\omega_0$ hyperfine separation, corresponding to the energies at which the aa and cc channels are resonant. Boltzmann averaging these leads to a much smaller contribution by the resonance. Using $\mu = \frac{1}{2}m_a$, the $\nu = 14$, $j = 4$ resonance shifts to lower energies in the continuum or even below the aa threshold,[27] depending on the radial extent of the 0.2 cm^{-1} "nonconvergence" correction of Ref. 24. In both cases the influence of the resonance is negligible.

Our earlier discussion of the $\ell = 0$ partial wave dealt only with the difference between the CC and first-order results. The $\ell=0$ curve shows a remarkable sensitivity to μ. Replacing $\mu = \frac{1}{2}m_a$ by the very nearly equal value $\frac{1}{2}m_p$ leads to changes of up to 50% in Fig.2. Even after Boltzmann averaging this difference is expected to be observable.

Figure 3 shows the temperature dependence of the thermally averaged quantities $\overline{\lambda}_1$ and $\overline{\lambda}_2$. For completeness we have also added $\overline{\lambda}_0$, $\overline{\sigma}_1 = \frac{1}{2}(\overline{\sigma}_+ - \overline{\sigma}_-)$, and $\overline{\sigma}_2 = \frac{1}{2}\overline{\sigma}_-$, with $\overline{\sigma}_+(\overline{\sigma}_-)$ the thermal average spin-exchange broadening cross section[18,28] for even (odd) ℓ. Our values for $\overline{\sigma}_1$, $\overline{\sigma}_2$, and $\overline{\lambda}_0$ differ significantly from those of Refs. 18 and 28. This is not due to hyperfine-induced contributions, which are negligible, but to differences

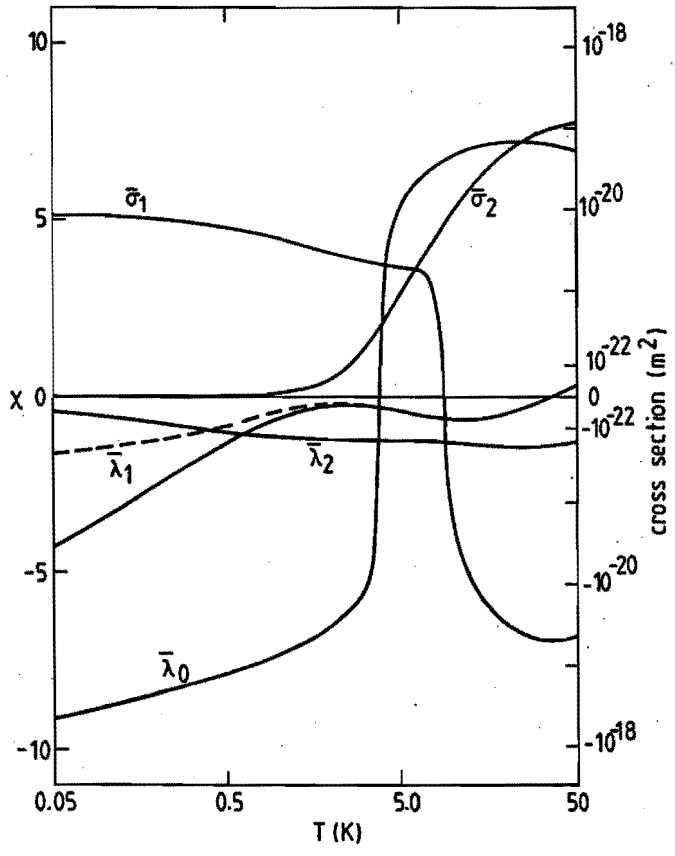

Fig.3. Thermally averaged values of the various frequency shift and broadening cross sections as functions of temperature. To combine the advantages of a logarithmic plot for larger values of the cross sections and a linear plot for small values, the vertical scale is taken to be linear in $x = \mathrm{arcsinh}(\bar{\sigma}_i/10^{-22}m^2)$ *and* $x = \mathrm{arcsinh}(\bar{\lambda}_i/10^{-22}m^2)$*, respectively. The horizontal scale is logarithmic. Solid lines, CC calculation; dotted line, first-order calculation where it differs significantly from the CC calculation.*

in the potentials used to calculate them. Note that the high CC values of λ_1 below the cusp result in significant deviations of the first-order values close to the important temperature 0.5K.

Significance for hydrogen masers

Although $\bar{\lambda}_1$ and $\bar{\lambda}_2$ are several orders of magnitude less than $\bar{\lambda}_0$ at the temperatures of interest to cryogenic hydrogen masers, they are significant because of the different

combinations of level populations $\rho_{\nu\nu}$ that accompany their contributions to $\Delta m_F=0$ transition frequency shifts. Under conditions of self-excited maser oscillation, $\rho_{cc}-\rho_{aa}$ is fixed by the requirement that the power radiated by the atoms be equal to that dissipated in the microwave cavity and other electronics. Assuming a single Lorentzian microwave cavity mode and using the methods of Ref. 6 we find

$$\rho_{cc}-\rho_{aa}=\frac{\hbar V_c(1+\Delta^2)}{\mu_0\mu_B{}^2\eta Q V_b n\tau_2}, \tag{14}$$

with $\Delta = Q(\omega_c/\omega-\omega/\omega_c)$ twice the ratio of cavity mistuning to cavity resonance width, μ_B the Bohr magneton, $\eta V_b/V_c$ a filling factor relating the rf energy density to the amplitude of rf field driving the $\Delta m_F=0$ transition,[29] and $1/\pi\tau_2$ the full frequency width (in Hz) of the $\Delta m_F=0$ transition. Substituting (14) into (6) and including the direct frequency pulling due to cavity mistuning,

$$\delta\omega=[\Delta+\alpha\bar{\lambda}_0(1+\Delta^2)]/\tau_2+n\langle v\rangle[\bar{\lambda}_1(\rho_{cc}+\rho_{aa})+\bar{\lambda}_2], \tag{15}$$

with $\alpha = (\langle v\rangle/\mu_0)(\hbar/\mu_B{}^2)(V_c/\eta Q V_b)$. The largest potential instability is due to cavity mistuning. Assuming linewidth $1/\pi\tau_2$ of order 1 Hz, cavity instabilities of parts in 10^5 of the cavity width would produce frequency instabilities of the order of parts in 10^{14} of the oscillation frequency, large compared to the 10^{-15} instabilities of room-temperature hydrogen maser standards[17] and very large compared to the potential thermal instabilities of cryogenic masers. In practice the cavity tuning must be reset by monitoring it either electronically, using external sources and detectors, or using variations of the oscillation frequency itself as some maser parameters are varied. Assuming linear dependence of the oscillation frequency on $1/\tau_2$, values of oscillation frequency measured for different values of $1/\tau_2$ and different values of Δ for $\Delta << 1$ can be used to correct the oscillation frequency to its "tuned" value: the value it would have if the cavity were tuned to produce no variation of oscillation frequency with $1/\tau_2$. Such methods[30] of setting the maser cavity are relatively insensitive to instabilities of coupling to external microwave sources and detectors. Moreover, in the absence of the frequency shifts proportional to $\bar{\lambda}_1$ and $\bar{\lambda}_2$, the tuned oscillation frequency would be unshifted by either cavity mistuning or collision effects. Because of the hyperfine-induced collision effects, such tuning methods may leave significant frequency offsets which can convert linewidth instabilities to instabilities of the tuned maser oscillation frequency.

To illustrate these effects we make use of

$$1/\tau_2=1/\tau_0+n\langle v\rangle[\bar{\sigma}_1(\rho_{cc}+\rho_{aa})+\bar{\sigma}_2], \tag{16}$$

the second term of which is obtained by a derivation[5] similar to that of (6), but ignoring hyperfine-induced effects which are negligible. Here $1/\tau_0$ includes all contributions to the linewidth not due to gas-phase spin-exchange collisions. Surface spin-exchange and recombination effects are small because the surface gas density is very low under cryogenic maser operating conditions, so that $1/\tau_0$ is dominated by the rate at which atoms flow in and out of the maser storage volume, plus any relaxation by motion through magnetic field gradients. Using (16) to eliminate n<v> from (15), we find

$$\delta\omega = [\Delta+\alpha\bar{\lambda}_0(1+\Delta^2)-\Omega]/\tau_2 + \Omega/\tau_0, \tag{17}$$

with

$$\Omega = -\frac{\bar{\lambda}_1(\rho_{cc}+\rho_{aa})+\bar{\lambda}_2}{\bar{\sigma}_1(\rho_{cc}+\rho_{aa})+\bar{\sigma}_2}. \tag{18}$$

The dimensionless quantity Ω generally depends on $1/\tau_2$ in a complicated way via a $1/\tau_2$ dependence of $\rho_{cc}+\rho_{aa}$. However, there are several important cases when the $1/\tau_2$ dependence of Ω can be neglected. At very low temperatures $\bar{\lambda}_2<<\bar{\lambda}_1$ and $\bar{\sigma}_2<<\bar{\sigma}_1$, yielding $\Omega = -\bar{\lambda}_1/\bar{\sigma}_1$ independent of $\rho_{cc}+\rho_{aa}$. If any single relaxation rate greatly exceeds all others, $\rho_{cc}+\rho_{aa}$ and Ω are approximately constant as relaxation processes vary. To get an impression of the likely instabilities of maser oscillation frequency due to hyperfine-induced collision effects, we therefore neglect the $1/\tau_2$ dependence of Ω. In this approximation $\delta\omega$ varies linearly with $1/\tau_2$ as the density is varied. Correcting the oscillation frequency to the value it would have with the cavity tuned for no variation of oscillation frequency as the density is varied then leaves the tuned oscillation frequency offset by the last term in (17). Figure 4 gives Ω as a function of temperature for the choices $\rho_{cc}+\rho_{aa}$= 0.5 and 1.0. We include values of $\alpha\bar{\lambda}_0$ calculated assuming $(\eta Q V_b/V_c)$=1000, a value intermediate between its value in the first cryogenic masers[10-13] and its likely value in actual cryogenic maser standards. The very large increase of Ω relative to $\alpha\bar{\lambda}_0$ as the temperature is lowered illustrates the much greater importance of hyperfine-induced frequency shifts at cryogenic temperatures, for example, at 0.5K and $\rho_{cc}+\rho_{aa}$=0.5, Ω=0.07. Even this small value puts severe limits on maser parameter stabilities required to achieve maser frequency instability as low as 2 parts in 10^{18}. For Ω = 0.07 the maximum allowed instability of $1/\tau_0$ would be $3 \times 10^{-7} s^{-1}$.

Note that measurements of changes of residual offset frequency with changes of $1/\tau_0$ could be used both to reduce the hyperfine-induced frequency offsets and to

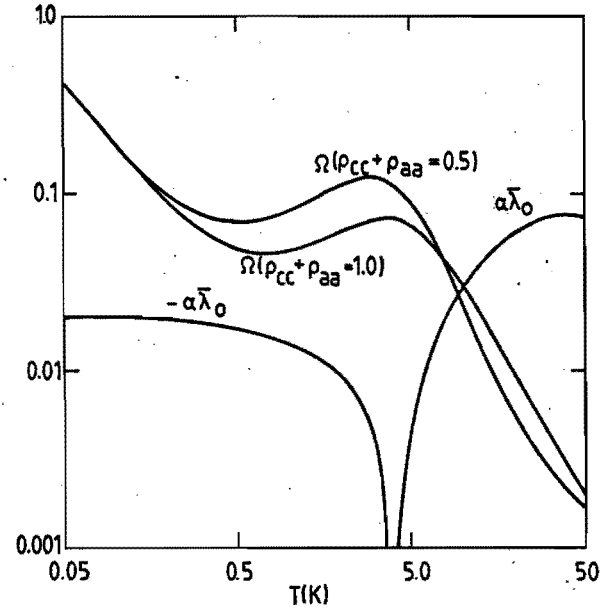

Fig.4. The dimensionless frequency offset parameters $\alpha\bar{\lambda}_0$ and Ω as functions of temperature. Ω is given for $\rho_{cc}+\rho_{aa}$ (total fraction of atoms in a or c states) equal to 0.5 and 1.0, and $\alpha\bar{\lambda}_0$ is given for $\eta Q V_b / V_c = 1000$.

measure $\bar{\lambda}_1$ and $\bar{\lambda}_2$, as in the high-temperature investigations of hyperfine-induced spin-exchange frequency shifts.[7] Considering the sensitivity of the low-temperature spin-exchange cross sections $\bar{\sigma}_{1,2}$ and $\bar{\lambda}_{0,1,2}$ to details of the H-H interaction, in particular to nonadiabatic effects, such experiments may yield interesting results.

Acknowledgement

We acknowledge support from the Stichting voor Fundamenteel Onderzoek der Materie and National Science Foundation Grant No. PHY–8406467.

References

(1) E.M. Purcell and G.B. Field, Astrophys. J. 124, 542 (1956).

(2) J.P. Wittke and R.H. Dicke, Phys. Rev. 103, 620 (1956).

(3) Dalgarno, Proc. R. Soc. London, Ser. A 262, 132 (1961).

(4) P.L. Bender, Phys. Rev. 132, 2154 (1963).

(5) L.C. Balling, R.J. Hanson, and F.M. Pipkin, Phys. Rev. 133, A607 (1964); 135,

AB1 (1964).

(6) S.B. Crampton, Phys. Rev. 158, 57 (1967).

(7) S.B. Crampton and H.T.M. Wang, Phys. Rev. A 12, 1305 (1975).

(8) S.B. Crampton, J.A. Duvivier, G.S. Read, and E.R. Williams, Phys. Rev. A 5, 1752 (1972).

(9) M. Desaintfuscien, J. Viennet, and C. Audoin, J. Phys. (Paris) Lett. 36, L–281 (1975).

(10) S.B. Crampton, Ann. Phys. (Paris) 10, 893 (1985).

(11) S.B. Crampton, K.M. Jones, G. Nunes, and S.P. Souza, Proceedings of the Sixteenth Annual Precise Time and Time Interval (PTTI) Applications and Planning Meeting, Greenbelt, Maryland, 1985 [NASA Technical Memorandum No. 8756, 1985 (unpublished)], p. 339.

(12) H.F. Hess, G.P. Kochanski, J.M. Doyle, T.J. Greytak, and D. Kleppner, Phys. Rev. A 34, 1602 (1986).

(13) M.D. Hürlimann, W.N. Hardy, A.J. Berlinsky, and R.W. Cline, Phys. Rev. A 34, 1605 (1986).

(14) R.L. Walsworth, I.F. Silvera, H.P. Godfried, C.C. Agosta, R.F.C. Vessot, and E.M. Mattison, Phys. Rev. A 34, 2550 (1986).

(15) W.D. Hardy and M. Morrow, J.Phys. (Paris) Colloq. 42, C8–171 (1981).

(16) A.J. Berlinsky and W.D. Hardy, Proceedings of the Thirteenth Annual Precise Time and Time Interval (PTTI) Applications and Planning Meeting, Naval Research Laboratory, Washington, D.C. 1982 [NASA Conference Publication No. 2220, 1982 (unpublished)], p. 547.

(17) R.F.C. Vessot, M.W. Levine, and E.M. Mattison, Proceedings of the Ninth Annual Precise Time and Time Interval (PTTI) Applications and Planning Meeting, Greenbelt, Maryland, 1977 [NASA Technical Memorandum No. 78104, 1978 (unpublished)], p. 549.

(18) A.J. Berlinsky and B. Shizgal, Cn. J. Phys. 58, 881 (977).

(19) A. Lagendijk, I.F. Silvera, and B.J. Verhaar, Phys. Rev. B 33, 626 (1986).

(20) R.M.C. Ahn, J.P.H.W. van den Eijnde, and B.J. Verhaar, Phys. Rev. B 27, 5424 (1983).

(21) J.P.H.W. van den Eijnde, Ph. D. Thesis, Eindhoven University of Technology, The Netherlands, 1984.

(22) A.M. Schulte and B.J. Verhaar, Nucl. Phys. A232, 215 (1974).

(23) W. Kolos and L. Wolniewicz, J. Chem. Phys. 43, 2429 (1965). W. Kolos and L. Wolniewicz, Chem. Phys. Lett. 24, 457 (1974); J.F. Bukta and W.J. Meath, Mol. Phys. 27, 1235 (1974).

(24) L. Wolniewicz, J. Chem. Phys. 78, 6173 (1983).

(25) P.R. Bunker, C.J. McLarnon, and R.E. Moss, Mol. Phys. 33, 425 (1977).

(26) L. Fonda, in *Fundamentals of Nuclear Theory*, edited by A. de-Salit and C. Villi (International Atomic Energy Agency, Vienna, 1967), p. 351.

(27) M.W. Reynolds, I. Shinkoda, R.W. Cline, and W.N. Hardy, Phys. Rev. B **34**, 4912 (1986).

(28) A.C. Allison, Phys. Rev. A **5**, 2695 (1972); A.C. Allison and F.J. Smith, At. Data **3**, 317 (1971).

(29) D. Kleppner, H.M. Goldenberg, and N.F. Ramsey, Phys. Rev. **126**, 603 (1962).

(30) D. Kleppner, H.C. Berg, S.B. Crampton, N.F. Ramsey, R.F.C. Vessot, H.E. Peters, and J. Vanier, Phys. Rev. **138**, A972 (1965).

Section 3.3
Spin-Exchange Frequency Shifts in Cryogenic and Room Temperature Hydrogen Masers

J.M.V.A.Koelman, S.B.Crampton*, H.T.C.Stoof, O.J.Luiten†, and B.J.Verhaar

Department of Physics, Eindhoven University of Technology,
Postbus 513, 5600 MB Eindhoven, The Netherlands,
**Department of Physics and Astronomy, Williams College*
Williamstown, Massachusetts 01267,
†Natuurkundig laboratorium, University of Amsterdam
Valckenierstraat 65, 1018 XE Amsterdam.

[Published in Phys. Rev. A 38 (Oct. 1988)]

We have calculated the spin-exchange shifts of the ground state $\Delta m_f=0$ transition of a gas of hydrogen atoms in zero magnetic field from zero temperature up to temperatures of 1000K. Taking into account the hyperfine interaction during spin-exchange collisions we find shifts nonlinear in the atomic linewidth and not compensated for by the usual methods of tuning the microwave cavities of oscillating hydrogen maser frequency standards. At room temperatures these shifts affect the H-maser stability at the level of $\delta\omega/\omega \simeq 10^{-15}$. At cryogenic temperatures these shifts are large compared to the potential thermal instabilities of liquid-helium-lined hydrogen masers. A detailed study of these nonlinear shifts reveals several ways to reduce these new sources of frequency instability.

Introduction

The unparalleled frequency stability of the hydrogen maser gives rise to numerous interesting scientific experiments and techniques. Important achievements such as submillisecond-of-arc angular resolutions in radio astronomy[1] and the detection of drifts of the earth's tectonic plates as small as a few centimeters per annum[2] are unthinkable without the very-long-baseline interferometry technique which is founded on the ultra high frequency stability of hydrogen masers. Also for physicists the hydrogen maser has developed into an important research tool. State-of-the-art hydrogen maser instabilities as low as one part in 10^{15} are essential in experiments such as the determination of the Stark shift of the hydrogen hyperfine splitting,[3] and accurate verifications of general relativity theory.[4]

Despite these impressive accomplishments, even more stable frequency standards would be extremely welcome, not only to improve upon the above-mentioned experiments and techniques, but also to open up new horizons in fields as diverse as metrology, physics, astronomy and geodesy. An illustrative example is the fact that

the best atomic clocks available are not sufficiently stable to determine any irregularities in the period of the fastest millisecond pulsar discovered.[5]

As pointed out a decade ago,[6] a cryogenic hydrogen maser might improve considerably upon the frequency stability of a conventional (room-temperature) hydrogen maser, thanks to the reduced thermal noise and cavity pulling at lower temperatures. In 1984 Crampton *et al.*[7] reported maser operation of a solid-Ne-coated hydrogen maser at 10 K. Two years ago Hess *et al.*, Hürlimann *et al.* and Walsworth *et al.* reported[8] the first observations of maser oscillation with liquid-^{4}He-coated walls at temperatures near 0.5 K. For this type of cryogenic hydrogen masers a frequency-instability limit due to thermal fluctuations as low as two parts in 10^{18} was anticipated by Berlinsky and Hardy,[9] leading to the exciting possibility for an improvement in the state-of-the-art of frequency stability with almost three orders of magnitude. However, as we pointed out already briefly in a previous publication,[10] one may cast doubt on the realization of that large stability improvement because of frequency instabilities associated with hydrogen atom spin-exchange collisions.

Spin-exchange collisions between the hydrogen atoms radiating in a hydrogen maser frequency standard affect the maser frequency in two distinct ways. They directly shift the transition frequency, and they broaden the atomic linewidth, which increases the frequency pulling due to cavity mistuning. The usual theoretical treatment of hydrogen atom spin-exchange collisions,[11] which treats the hyperfine energy levels during the collisions as degenerate, predicts that the direct spin-exchange frequency shifts are proportional to the atomic linewidth, as are frequency shifts due to cavity mistuning.[12] Tuning the cavity so that the oscillation frequency is independent of atomic linewidth ("spin-exchange tuning") is predicted by that treatment to cancel the direct spin-exchange shift against the cavity mistuning shift and hence to leave the oscillation frequency independent of collision rate.[13] As the collision rate is one of the most difficult parameters to stabilize, such "spin-exchange tuning" methods have been important to the development of hydrogen maser standards.

Including the hyperfine energy-level splitting to first order in a semi-classical spin-exchange collision calculation, predicts additional direct frequency shifts not proportional to the total atomic linewidth, but rather proportional to the collision part of the linewidth.[14] This leaves the spin-exchange tuned oscillation frequency independent of collision rate but offset by an amount proportional to that part of the atomic linewidth not caused by collisions.[14] Measurements of this offset in a room temperature hydrogen maser agreed within errors with the semiclassical estimate of the effect.[14] The offset predicted by that calculation does not adversely affect the stability of hydrogen maser standards unless something happens to affect that part of the linewidth not due to collisions, such as a change of relaxation by motion of the

atoms through magnetic field gradients or a change of relaxation due to interactions with the storage surface.

We have recently done a fully quantum-mechanical calculation of the direct shifts for cryogenic temperatures taking into account the nonzero hyperfine energy levels splitting.[10] We found new effects which are nonlinear in the collision rate and so produce not only an offset of the spin-exchange tuned oscillation frequency, but also a variation of the oscillation frequency with collision rate even after spin-exchange tuning.

In this paper we present a more complete description of the formalism. In addition, we extend the results for the additional direct shifts to a much larger temperature interval so that their implications for hydrogen maser frequency standards operating at room temperature can be investigated. Near room temperature these additional direct shifts are small, but in contrast to the semiclassical result, are highly nonlinear in the collision rate. We show that the semiclassical approximation used for the calculation of the direct shifts breaks down when the influence of the exchange interaction on the orbital degrees of freedom cannot be neglected. At collision energies large in comparison to the strength of the exchange interaction we show that the quantum-mechanical and semiclassical results agree, in which case both predict direct shifts linear in the collision rate.

A third aim of the present paper is to investigate in detail the variation of the spin-exchange tuned oscillation frequency with collision rate at cryogenic and room temperatures. Although near room temperature the additional direct shifts are small, the variations of the spin-exchange tuned oscillation frequency are large enough to affect the relative stability of the maser at the 10^{-15} level. At cryogenic temperatures variations of the spin-exchange tuned oscillation frequency are orders of magnitude larger than the potential thermal instabilities[9] of liquid-helium-temperature maser standards.

In examining the variation of the spin-exchange tuned frequency with collision rate we are able to propose various strategies to minimize these new sources of frequency instabilities. Several modifications of cryogenic hydrogen-maser designs potentially reduce the dependence of the spin-exchange tuned oscillation frequency on the atomic linewidth by some orders of magnitude, yielding the possibility of cryogenic hydrogen-maser frequency standards with long term frequency instabilities close to the potential thermal instability limit of 2 parts in 10^{18}.

Our starting point for the derivation of the direct frequency shifts is the evolution equation for the spin-density matrix

$$\frac{d}{dt}\rho_{\kappa\kappa'} + \frac{i}{\hbar}(\epsilon_\kappa - \epsilon_{\kappa'})\,\rho_{\kappa\kappa'} = \dot{\rho}_{\kappa\kappa'}|_{rad} + \dot{\rho}_{\kappa\kappa'}|_0 + \dot{\rho}_{\kappa\kappa'}|_c . \qquad (1)$$

In this equation ρ is the 4x4 one particle spin-density matrix in which the Greek subscripts take values a,b,c,d, the ground-state hyperfine levels in order of increasing energy ϵ_α (see Fig.1). The first term on the right-hand side of Eq.(1) is the radiation term resulting from the interaction of the atomic magnetic moments with the rf cavity magnetic field. The second term on the right-hand side represents all time-independent one-atom terms such as wall collisions, finite cavity residence time, and interactions with magnetic field inhomogeneities.

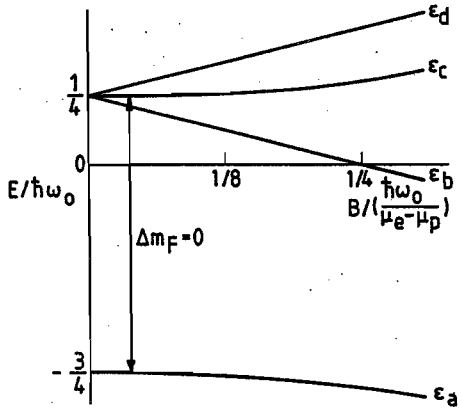

Fig.1. Atomic hydrogen ground-state energy levels.

The third term on the right-hand side of Eq.(1), the collision term, may be derived as follows. We start with a system of N ground state hydrogen atoms mutually interacting via a central spin-dependent (singlet or triplet) interaction enclosed in a large but finite volume L^3. At the end of this derivation we take the limit $L\to\infty$. The time evolution for the single-particle distribution matrix F' can be expressed in terms of the pair-distribution matrix F'' via the first equation of the quantum-mechanical Bogoliubov-Born-Kirkwood-Yvon (BBGKY) hierarchy[15], which in some suitable single-particle basis can be written

$$\frac{\partial}{\partial t}F'_{kk'} + \frac{i}{\hbar}\sum_p (H_{kp}F'_{pk'} - F'_{kp}H_{pk'}) = \frac{-i}{\hbar}\sum_{pmn}(V_{kp,mn}F''_{mn,k'p} - F''_{kp,mn}V_{mn,k'p}). \qquad (2)$$

Here H represents the single-particle hamiltonian and V the pair interaction. This equation may be converted to a closed equation for the single-particle distribution matrix by expressing the pair matrix at the right-hand side in terms of the single-particle distribution matrix. To first order in the hydrogen atom density and assuming at times long before a binary collision the absence of any correlation between the atoms not due to particle indistinguishability (molecular chaos assumption), the pair density matrix in Eq.(2) may be written

$$F''_{kl,mn} = \sum_{pqrs} \Omega^{(+)}_{kl,pq} \left(F'_{pr} F'_{qs} + \epsilon F'_{ps} F'_{qr}\right) \Omega^{(+)\dagger}_{rs,mn} \tag{3}$$

in which $\Omega^{(+)}$ is the causal two-body Møller wave operator,[16] while the statistics sign $\epsilon=+1$ for a gas of hydrogen atoms, being (composite) bosons ($\epsilon=-1$ applies to the case of fermions). To be more definite we work in a single-particle basis $\{|n>\}$ in which the single-particle Hamiltonian is diagonal ($H|n> = E^0_n|n>$). Furthermore, we restrict ourselves to spatially homogeneous systems so that these single-particle states are common eigenstates of the momentum operator and the hyperfine spin hamiltonian, $|n> = |\underline{k}_n,\nu>$. We have $E^0_n = \hbar^2\underline{k}_n^2/2m_a + \epsilon_\nu$, ($m_a$ is the atomic mass) and the single-particle density matrix is diagonal in the momentum indices. Transforming to the interaction representation: $F_{kn} = F'_{kn} \exp[i(E^0_k-E^0_n)t/\hbar]$, we find

$$\frac{\partial}{\partial t} F_{kk'} = \frac{-i}{\hbar} \sum_{mnpqrsl} \Big[V_{kl,mn}\Omega^{(+)}_{mn,pq}(F_{pr}F_{qs}+\epsilon F_{ps}F_{qr})\Omega^{(+)\dagger}_{rs,k'l} - \Omega^{(+)}_{kl,pq}(F_{pr}F_{qs}+\epsilon F_{ps}F_{qr})\Omega^{(+)\dagger}_{rs,mn}V_{mn,k'l}\Big] \exp(\tfrac{i}{\hbar}\Delta E t). \tag{4}$$

The "energy inelasticity" $\Delta E \equiv E^0_k - E^0_{k'} + E^0_r - E^0_p + E^0_s - E^0_q$ in the exponent on the right-hand side can only receive a contribution due to the hyperfine energy-level separations since F, being diagonal in momentum, does not couple between different kinetic energies. Terms with $\Delta E \neq 0$ average out on time scales long in comparison with the hyperfine precession time scale $\hbar/\Delta E$. So, in the long-time limit, we may restrict the summations on the right-hand side of Eq.(4) to values $E^0_k+E^0_r+E^0_s = E^0_{k'}+E^0_p+E^0_q$ and replace the exponent by unity. Assuming a dominance of either thermalizing collisions, with the walls or elastic collisions between the atoms relative to inelastic collisions, the translational degrees of freedom are Boltzmann distributed as

$$F_{mn} = F_{\underline{k}_m\mu,\underline{k}_n\nu} = N P_{m_a}(\underline{k}_m)\, \delta_{\underline{k}_m,\underline{k}_n}\, \rho_{\mu\nu} \exp[i(\epsilon_\mu-\epsilon_\nu)t/\hbar], \tag{5}$$

with the single-particle spin-density matrix ρ normalized to unity, $\sum_\alpha \rho_{\alpha\alpha} = 1$, and

$P_m(\underline{k})$ the Boltzmann distribution for free atoms with mass m also normalized to unity, $\Sigma_n P_m(\underline{k}_n) = 1$. Using the identity $P_m(\underline{k}) P_m(\underline{k}') = P_{2m}(\underline{k}+\underline{k}') P_{\frac{1}{2}m}(\frac{1}{2}(\underline{k}-\underline{k}'))$ and center of mass momentum conservation we may carry out the summation over the center of mass momenta. Taking the limit $N \to \infty$, $L \to \infty$, $N/L^3 = n$ = constant, and after performing the angular integrations, we finally arrive at

$$\dot{\rho}_{\kappa\kappa'}|_c = n \sum_{\lambda\mu\mu'\nu\nu'}{}' \rho_{\mu\mu'}\rho_{\nu\nu'}\left[(1+\delta_{\kappa\lambda})(1+\delta_{\kappa'\lambda})(1+\delta_{\mu\nu})(1+\delta_{\mu'\nu'})\right]^{1/2} \sum_{\ell} (2\ell+1)$$

$$\left\langle \frac{\pi\hbar}{m_a k}\left[S^{\ell}_{\{\kappa\lambda\}\{\mu\nu\}}(E_k) S^{\ell *}_{\{\kappa'\lambda\}\{\mu'\nu'\}}(E_k) - \delta_{\{\kappa\lambda\}\{\mu\nu\}}\delta_{\{\kappa'\lambda\}\{\mu'\nu'\}}\right]\right\rangle . \qquad (6)$$

In this equation the prime on the summation sign indicates the subsidiary condition $\epsilon_\kappa+\epsilon_{\mu'}+\epsilon_{\nu'} = \epsilon_{\kappa'}+\epsilon_\mu+\epsilon_\nu$, while Greek subscripts between brackets are a short-hand notation for normalized (anti)symmetric two-body spin states,

$$\{\alpha\beta\} \equiv \frac{\alpha\beta + \epsilon(-1)^{\ell}\beta\alpha}{\sqrt{2(1+\delta_{\alpha\beta})}}, \qquad (7)$$

which for a gas of hydrogen atoms (ϵ=+1) leads to (anti)symmetric spin states for (odd) even angular momentum numbers ℓ. The S-matrix elements, defined for the various angular momentum numbers so as to form a unitary matrix in spin space, are to be evaluated for a common kinetic energy $E_k=\hbar^2k^2/m_a$ in the entrance channels $\{\mu\nu\}$ and $\{\mu'\nu'\}$, and the brackets <...> denote thermal averaging over the wave number k. The final result, i.e., the collision contribution to the spin evolution [Eq.(6)], has already been presented in Ref.10.

We study situations in which the atoms are stimulated to radiate at one specific transition $\alpha \leftrightarrow \beta$. In that case the only nonvanishing off-diagonal elements of the spin-density matrix are $\rho_{\alpha\beta}$ and $\rho_{\alpha\beta}=\rho_{\alpha\beta}^*$. The one-particle and collision terms in Eq.(1) contributing to the time development of $\rho_{\alpha\beta}$ are of the form:

$$\dot{\rho}_{\alpha\beta}|_0 = -(\Gamma_0 - i\delta\omega_0)\,\rho_{\alpha\beta}, \qquad (8)$$

$$\dot{\rho}_{\alpha\beta}|_c = n\,\rho_{\alpha\beta}\sum_{\nu}\rho_{\nu\nu}\sum_{\lambda}\sqrt{(1+\delta_{\alpha\lambda})(1+\delta_{\beta\lambda})(1+\delta_{\alpha\nu})(1+\delta_{\beta\nu})}\,G_{\alpha\beta,\nu\to\lambda}, \qquad (9)$$

in which the complex coefficient $\Gamma_0 - i\delta\omega_0$ generally depends in a complicated way on the values of the diagonal spin-density matrix elements $\rho_{\nu\nu}$, but is independent of $\rho_{\alpha\beta}$.

The complex coefficients $G_{\alpha\beta,\nu\to\lambda}$ describe the contribution of collisions in which a ν-state atom makes a transition to the λ state in colliding with an atom which is in a coherent superposition of the α and β states. These ratelike coefficients may be expressed in terms of complex effective "cross sections" $\sigma_{\alpha\beta,\nu\to\lambda}$ using

$$G_{\alpha\beta,\nu\to\lambda} = \left\langle v\, \sigma_{\alpha\beta,\nu\to\lambda}(E_k) \right\rangle , \tag{10}$$

with $v=2\hbar k/m_a$ being the relative collision velocity. In turn these "cross sections" are given in terms of S-matrix elements via:

$$\sigma_{\alpha\beta,\nu\to\lambda}(E_k) = \frac{\pi}{k^2}\sum_{\ell}(2\ell+1)\left[S^{\ell}_{\{\alpha\lambda\}\{\alpha\nu\}}(E_k)\, S^{\ell *}_{\{\beta\lambda\}\{\beta\nu\}}(E_k) - \delta_{\lambda\nu}\right] . \tag{11}$$

Upon substituting

$$\rho_{\alpha\beta}(t) = \rho_{\alpha\beta}(0)\exp[i(\epsilon_\beta-\epsilon_\alpha)/\hbar + i\delta\omega - \Gamma]t \tag{12}$$

together with Eqs.(8) and (9) in Eq.(1) for $\kappa\kappa'=\alpha\beta$ and neglecting for a moment the radiation term, we find for the direct frequency shift $\delta\omega$ and the atomic linewidth Γ:

$$\delta\omega = \delta\omega_0 + \delta\omega_c , \tag{13}$$

$$\Gamma = \Gamma_0 + \Gamma_c , \tag{14}$$

in which the direct frequency shift $\delta\omega_c$ and line broadening Γ_c due to spin-exchange collisions are related to the "cross sections" $\sigma_{\alpha\beta,\nu\to\lambda}$ via:

$$i\delta\omega_c-\Gamma_c = n\langle v\rangle\sum_{\nu}\rho_{\nu\nu}\sum_{\lambda}\left[(1+\delta_{\alpha\lambda})(1+\delta_{\beta\lambda})(1+\delta_{\alpha\nu})(1+\delta_{\beta\nu})\right]^{1/2}\overline{\sigma}_{\alpha\beta,\nu\to\lambda}. \tag{15}$$

Here we have introduced the modified thermal averaging $\overline{\sigma} \equiv \langle v\sigma\rangle/\langle v\rangle$, with the thermally averaged collision velocity $\langle v\rangle=(16k_BT/\pi m_a)^{1/2}$.

In a hydrogen maser oscillating at low magnetic field on the $\Delta m_F=0$ transition with unperturbed atomic frequency $\omega_0=(\epsilon_c-\epsilon_a)/\hbar$ there is only coherence between the a and c states. Substituting $\alpha\beta$=ac in the preceding expressions we find at zero magnetic field $G_{ac,\nu\to\lambda} = \delta_{\nu\lambda}\, G_{ac,\lambda\to\lambda}$ (no contribution from inelastic processes) and $G_{ac,b\to b} = G_{ac,d\to d}$, yielding

$$\delta\omega_c = n\langle v\rangle [(\rho_{cc}-\rho_{aa})\overline{\lambda}_0 + (\rho_{cc}+\rho_{aa})\overline{\lambda}_1 + \overline{\lambda}_2] , \tag{16}$$

$$\Gamma_c = n\langle v\rangle [(\rho_{cc}-\rho_{aa})\overline{\sigma}_0 + (\rho_{cc}+\rho_{aa})\overline{\sigma}_1 + \overline{\sigma}_2] , \tag{17}$$

with the real spin-exchange shift and broadening "cross-sections" λ_i and σ_i defined in terms of the $\sigma_{ac,\nu\to\nu}$ coefficients by

$$i\lambda_0-\sigma_0 \equiv \sigma_{ac,c\to c} - \sigma_{ac,a\to a} , \tag{18}$$

$$i\lambda_1-\sigma_1 \equiv \sigma_{ac,c\to c} + \sigma_{ac,a\to a} - \sigma_{ac,d\to d} , \tag{19}$$

$$i\lambda_2-\sigma_2 \equiv \sigma_{ac,d\to d} . \tag{20}$$

The elastic S-matrix elements occurring in the expressions for $\sigma_{ac,\nu\to\nu}$ follow from the Schrödinger equation describing H+H scattering with an effective central two-body interaction consisting of singlet and triplet potentials,

$$\langle\{\alpha\beta\}|V^c(r)|\{\lambda\delta\}\rangle \equiv \sum_{S=0,1} \langle\{\alpha\beta\}|P_S|\{\lambda\delta\}\rangle V_S(r) , \tag{21}$$

with $V_0(V_1)$ being the singlet(triplet) potential and P_S standing for the projection operator on the subspace with total electron spin S. Since these projection operators are nondiagonal in the $|\{\alpha\beta\}\rangle$ basis we have to deal with sets of coupled radial equations describing the H+H scattering wave function in the various channels. Calculations of this kind are easily carried out[17] at the low temperature of 0.5 K, where the liquid-^{4}He-covered cryogenic hydrogen maser is to operate: S-matrix elements need to be calculated only at a relatively small number of energy values. For calculations at higher temperatures, such as those necessary to obtain thermally averaged frequency-shift cross sections for room temperature hydrogen masers, however, a coupled-channel approach becomes a tedious task. Fortunately, in this regime it is possible to circumvent this task by means of the degenerate-internal-states (DIS) approximation which neglects the internal energy-level separation and replaces the various internal energy levels ϵ_α by a common constant ϵ_0, in which case the equations can be decoupled in transforming to a basis in which the total electron spin S is a good quantum number. Splitting off factors containing the low energy behavior this leads to the result[18,17]

$$\frac{S^{\ell(DIS)}_{\{\gamma\delta\}\{\alpha\beta\}}(E-\epsilon_\alpha-\epsilon_\beta) - \delta_{\{\gamma\delta\}\{\alpha\beta\}}}{\left[\sqrt{E-\epsilon_\gamma-\epsilon_\delta}\ \sqrt{E-\epsilon_\alpha-\epsilon_\beta}\ \right]^{\ell+\frac{1}{2}}} = \sum_{S=0,1} \frac{e^{2i\,\delta^\ell_S(E-2\epsilon_0)}-1}{(E-2\epsilon_0)^{\ell+\frac{1}{2}}} <\{\gamma\delta\}|P_S|\{\alpha\beta\}>. \quad (22)$$

Notice that we have some freedom in choosing a value for ϵ_0. When dealing with elastic S-matrix elements $S_{\{\alpha\beta\}\{\alpha\beta\}}$ a suitable choice is to set $2\epsilon_0$ equal to the internal energy in the specific channel under consideration ($2\epsilon_0=\epsilon_\alpha+\epsilon_\beta$), which leads to the evaluation of singlet or triplet phaseshifts at an energy equal to the kinetic energy in the elastic channel considered. Substituting expression (22) with this choice of ϵ_0 for the elastic S-matrix elements in the $\sigma_{ac,\nu\to\nu}$ coefficients on the right-hand side of Eqs.(18)-(20) yields

$$\lambda_0^{(DIS)} = \frac{\pi}{2k^2} \sum_{\ell\ \text{even}} (2\ell+1)\sin(2\delta_1^\ell - 2\delta_0^\ell)\,, \quad (23)$$

$$\lambda_1^{(DIS)} = \lambda_2^{(DIS)} = 0\,, \quad (24)$$

$$\sigma_0^{(DIS)} = 0\,, \quad (25)$$

$$\sigma_1^{(DIS)} = \frac{\pi}{k^2} \sum_{\ell} (-1)^\ell (2\ell+1)\sin^2(\delta_0^\ell - \delta_1^\ell)\,, \quad (26)$$

$$\sigma_2^{(DIS)} = \frac{\pi}{k^2} \sum_{\ell\ \text{odd}} (2\ell+1)\sin^2(\delta_0^\ell - \delta_1^\ell)\,, \quad (27)$$

in which the phase shifts δ^ℓ_S are to be evaluated at a collision energy $E_k=\hbar^2k^2/m_a$. These equations are in agreement with the results obtained by Balling *et al.*

On the basis of previous experience[18,17] one might expect that treating the hyperfine energy levels during collisions as degenerate yields a very accurate description of hydrogen atom spin-exchange collision processes down to zero collision energy, so that the direct frequency shift due to spin-exchange collisions is accurately described by the well-known DIS result:

$$\delta\omega_c^{(DIS)} = n <v> \bar{\lambda}_0^{(DIS)}(\rho_{cc}-\rho_{aa})\,, \quad (28)$$

rendering the more complicated Eq.(16) of less interest. However, as pointed out previously,[10] although $\bar{\lambda}_1$ and $\bar{\lambda}_2$ are indeed small compared to $\bar{\lambda}_0$, in a H-maser $\bar{\lambda}_1(\rho_{cc}+\rho_{aa})$ and $\bar{\lambda}_2$ may be large compared to $\bar{\lambda}_0(\rho_{cc}-\rho_{aa})$. The reason for this is that

in having self-sustained maser oscillation $\rho_{cc}-\rho_{aa}$ is strongly reduced by transfer of energy to the cavity electromagnetic field, yielding a strongly suppressed DIS direct frequency shift. Moreover, retaining the radiation term in Eq.(1) for $\kappa\kappa'=ac$ shows $n(\rho_{cc}-\rho_{aa})$ to be proportional to the total atomic linewidth[12]

$$n(\rho_{cc}-\rho_{aa}) = \gamma(1+\Delta^2)\Gamma\,, \tag{29}$$

in which γ is a constant dependent on cavity parameters, and Δ is twice the ratio of cavity mistuning to cavity resonance linewidth. This yields the possibility to compensate the DIS direct shifts against shifts due to cavity mistuning.[13] These considerations make it necessary to take into account hyperfine-induced effects in the calculation of the direct frequency shifts. On the other hand, in the equation describing spin-exchange line broadening [Eq.(17)], only the terms having a nonvanishing DIS contribution have to be retained. This is because even when the hyperfine-induced cross section $\bar{\sigma}_0$ is comparable in magnitude to $\bar{\sigma}_1$, the quantity $(\rho_{cc}-\rho_{aa})\bar{\sigma}_0$ can still be neglected compared to $(\rho_{cc}+\rho_{aa})\bar{\sigma}_1$ because $|\rho_{cc}-\rho_{aa}|<<1$.

The shift $\Delta\omega$ in the maser frequency is the sum of the direct shift $\delta\omega$ and the shift $\Gamma\,\Delta$ due to cavity mistuning.[12] In view of the previous paragraph the direct shift due to spin-exchange collisions is calculated using expression (16) with the result (29) substituted and Eq.(17) with $\rho_{cc}-\rho_{aa}=0$ substituted. For later use it is convenient to split the oscillation frequency shift $\Delta\omega$ as a sum of a shift $\Delta\omega_0$ independent of collision rate and a shift $\Delta\omega_c$ vanishing at zero-collision rate,

$$\Delta\omega = \Delta\omega_0 + \Delta\omega_c = (\delta\omega_0 + \tilde{\Omega}\,\Gamma_0) + (\tilde{\Omega}-\Omega)\Gamma_c\,, \tag{30}$$

with the dimensionless parameters Ω and $\tilde{\Omega}$ defined as

$$\Omega \equiv -\frac{\bar{\lambda}_1(\rho_{cc}+\rho_{aa})+\bar{\lambda}_2}{\bar{\sigma}_1(\rho_{cc}+\rho_{aa})+\bar{\sigma}_2}\,, \tag{31}$$

$$\tilde{\Omega} \equiv \Delta + \gamma\langle v\rangle\bar{\lambda}_0(1+\Delta^2)\,. \tag{32}$$

Here $\delta\omega_0$ is the direct frequency shift due to one atom processes which in most cases is dominated by the shift due to wall collisions. The combined effect of the shift due to cavity pulling and the direct shift due to almost-pure spin-exchange collisions on the H-maser frequency is described by the parameter $\tilde{\Omega}$. The parameter Ω is a measure for the additional effects of hyperfine induced spinexchange shifts on the H-maser frequency. The DIS value for Ω vanishes ($\lambda_1=\lambda_2=0$), in which case spin-exchange tuning the cavity, i.e. setting Δ so as to make $\Delta\omega$ independent of collisional linewidth,

yields the frequency shift purely determined by the shifts due to one-atom processes such as wall collisions: $\Delta\omega=\delta\omega_0$. Taking into account the hyperfine level separation in a semi-classical picture[14] yields Ω to be nonzero but independent of $\rho_{cc}+\rho_{aa}$ ($\lambda_1=\sigma_1=0$). In this case the spin-exchange tuning procedure leads to an oscillation frequency shift being the sum of a shift due to one-atom processes and a shift proportional to the contribution of one-atom processes to the linewidth: $\Delta\omega=\delta\omega_0+\Omega\Gamma_0$. According to the preceding analysis Ω is nonzero and depends in a complicated way on collision rate via the collision rate dependence of the level population sum $\rho_{cc}+\rho_{aa}$, yielding the oscillation frequency shift to depend on the collision rate even after spin-exchange tuning.

Hyperfine-level population dynamics

As is evident from Eqs.(30)-(32), the evaluation of the frequency shift $\Delta\omega$ requires knowledge of the value of $\rho_{cc}+\rho_{aa}$. We determine this parameter starting from Eq.(1), but now for the time evolution of the diagonal spin-density matrix elements. We start by investigating the rate of change of $\rho_{cc}+\rho_{aa}$. Using Eq.(6) we find for the collision term on the right-hand side of Eq.(1) at zero magnetic field:

$$(\dot{\rho}_{cc}+\dot{\rho}_{aa})|_c/n = 2[(G_{bd\to ac}+G_{bd\to aa}+G_{bd\to cc})\rho_{bb}\rho_{dd} - G_{cc\to bd}\rho_{cc}^2 - G_{aa\to bd}\rho_{aa}^2 - G_{ac\to bd}(\rho_{aa}\rho_{cc}+|\rho_{ac}|^2)] . \quad (33)$$

Using the unitarity property of the S matrix, the downward spin-exchange relaxation rates are given by[17]

$$G_{\alpha\beta\to\gamma\delta} \equiv \left\langle \frac{2\pi\hbar^2}{m_a k} \sum_{\ell} (2\ell+1)|S^{\ell}_{\{\gamma\delta\}\{\alpha\beta\}}(E_k) - \delta_{\{\gamma\delta\}\{\alpha\beta\}}|^2 \right\rangle . \quad (34)$$

Again using the dominance of thermalizing elastic collisions over inelastic collisions, the upward relaxation rates $G_{\gamma\delta\to\alpha\beta}$ are related to the corresponding downward relaxation rates $G_{\alpha\beta\to\gamma\delta}$ via a Boltzmann factor

$$G_{\gamma\delta\to\alpha\beta} = e^{-(\epsilon_\gamma+\epsilon_\delta-\epsilon_\alpha-\epsilon_\beta)/k_BT} G_{\alpha\beta\to\gamma\delta} . \quad (35)$$

The level populations $\rho_{\alpha\alpha}$ on the right-hand side of Eq.(33) may be expressed in terms of $\rho_{cc}-\rho_{aa}$, $\rho_{cc}+\rho_{aa}$, and $\rho_{dd}-\rho_{bb}$. Furthermore we use the fact that in oscillating H masers $\gamma\Gamma/n$ is a small parameter (typically $\gamma\simeq 10^9 cm^{-3}s$) yielding $|\rho_{cc}-\rho_{aa}|<<1$ and

$|\rho_{ac}|^2 << 1$ so that Eq.(33) can be approximated by

$$(\dot{\rho}_{cc}+\dot{\rho}_{aa})|_c/n_H = \tfrac{1}{2}(G_{bd\to}-G_{\to bd})(\rho_{cc}+\rho_{aa})^2 + \tfrac{1}{2}G_{bd\to}[1-2(\rho_{cc}+\rho_{aa})-(\rho_{dd}-\rho_{bb})^2] \tag{36}$$

with

$$G_{bd\to} \equiv G_{bd\to ac} + G_{bd\to aa} + G_{bd\to cc}\,, \tag{37}$$

$$G_{\to bd} \equiv G_{ac\to bd} + G_{aa\to bd} + G_{cc\to bd}\,. \tag{38}$$

We now turn to the remaining terms in Eq.(1) contributing to the rate of change of the level population sum $\rho_{cc}+\rho_{aa}$. No contribution comes from the radiation term. The one-body term, however, does contribute. An important contribution to this term arises from atom flow in and out of the maser bulb. Of the many possible other one-body processes that may affect the level populations, we include transitions due to motion through magnetic field gradients both as an example of the complications introduced by additional hyperfine transition processes and as an example of the opportunities to use these processes to diagnose or even "tune out" frequency instabilities. We thus have[19]

$$\dot{\rho}_{dd}|_0 = -\Gamma_b\,(\rho_{dd}-\rho^0_{dd}) - \Gamma_m\,(\rho_{dd}-\rho_{cc})\,, \tag{39}$$

$$\dot{\rho}_{cc}|_0 = -\Gamma_b\,(\rho_{cc}-\rho^0_{cc}) - \Gamma_m\,(\rho_{cc}-\rho_{bb}) - \Gamma_m\,(\rho_{cc}-\rho_{dd})\,, \tag{40}$$

$$\dot{\rho}_{bb}|_0 = -\Gamma_b\,(\rho_{bb}-\rho^0_{bb}) - \Gamma_m\,(\rho_{bb}-\rho_{cc})\,, \tag{41}$$

$$\dot{\rho}_{aa}|_0 = -\Gamma_b\,(\rho_{aa}-\rho^0_{aa})\,, \tag{42}$$

in which Γ_b and Γ_m are the contributions of atom flow and magnetic field gradients to the atomic linewidth Γ and $\rho^0_{\nu\nu}$ are the fractional hyperfine level populations of atoms entering the maser bulb.

For stationary oscillation the total rate of change of $\rho_{cc}+\rho_{aa}$ must be zero, which again using $|\rho_{cc}-\rho_{aa}| << 1$ leads to

$$n\,(G_{bd\to}-G_{\to bd})(\rho_{cc}+\rho_{aa})^2 + n\,G_{bd\to}[1-2(\rho_{cc}+\rho_{aa})-(\rho_{dd}-\rho_{bb})^2]$$

$$-2\,\Gamma_b\,[(\rho_{cc}+\rho_{aa})-(\rho^0_{cc}+\rho^0_{aa})] - 2\,\Gamma_m\,[2(\rho_{cc}+\rho_{aa})-1] = 0\,. \tag{43}$$

Using the fact that the difference between the d- and b-level populations is only affected by relaxation due to atom flow and magnetic gradients (not by the interaction

with the rf cavity magnetic field nor by spin-exchange collisions), we have

$$\rho_{dd}-\rho_{bb} = (\rho^{o}_{dd}-\rho^{o}_{bb})\,\Gamma_b/(\Gamma_b+\Gamma_m). \tag{44}$$

Using this result, Eq.(43) reduces to a quadratic equation in the single unknown $\rho_{cc}+\rho_{aa}$. Eliminating n in favor of Γ_c using Eq.(17) with $(\rho_{cc}-\rho_{aa})\bar{\sigma}_0 \simeq 0$ leaves this equation quadratic in $\rho_{cc}+\rho_{aa}$ with the partial relaxation widths entering the coefficients only in the form of their ratios. We conclude that $\rho_{cc}+\rho_{aa}$ (and hence Ω) depends on Γ_b, Γ_m, and Γ_c only in the form of a dependence on two of their ratios, for instance, Γ_c/Γ_b and Γ_m/Γ_b.

The various spin-exchange relaxation rates contributing to $G_{\to bd}$ and $G_{bd\to}$ may be calculated using the DIS expression (22) in Eq.(34). A somewhat cruder approximation,[11] a high-energy version of the DIS approximation, consists of a complete neglect of the difference between the channel energies $\epsilon_\alpha+\epsilon_\beta$, $\epsilon_\gamma+\epsilon_\beta$, and $2\epsilon_0$ in Eq.(22) which, when substituted in Eq.(34), yields

$$G_{bd\to ac} = G_{ac\to bd} = \langle v\rangle\,\bar{\sigma}_2^{(DIS)}, \tag{45}$$

$$G_{bd\to aa} = G_{aa\to bd} = G_{bd\to cc} = G_{cc\to bd} = \langle v\rangle\,(\bar{\sigma}_1^{(DIS)}+\bar{\sigma}_2^{(DIS)})/2, \tag{46}$$

and

$$G_{bd\to} = G_{\to bd} = \langle v\rangle(\bar{\sigma}_1^{(DIS)}+2\bar{\sigma}_2^{(DIS)}), \tag{47}$$

leading to a vanishing quadratic term in Eq.(43), with the corresponding simple solution

$$\rho_{cc}+\rho_{aa} = \frac{1}{2}\,\frac{nG_{bd\to}[1-(\rho_{dd}-\rho_{bb})^2] + 2\Gamma_b(\rho^{o}_{cc}+\rho^{o}_{aa}) + 2\Gamma_m}{nG_{bd\to} + \Gamma_b + 2\Gamma_m} \tag{48}$$

This high-energy approximation is valid only at collision energies which are large in comparison with the internal energy-levels splittings. Since at the operating temperatures of liquid-helium-lined hydrogen masers (T≃0.5 K) typical collision energies are comparable in magnitude to the internal energy-level splittings $[(\epsilon_b+\epsilon_d-\epsilon_a-\epsilon_a)/k_B = 2\hbar\omega_0/k_B \simeq 0.14\ \mathrm{K}]$, the solution of the more complicated Eq.(43) rather than Eq.(48) must in general be used as a closed formula for $\rho_{cc}+\rho_{aa}$.

Methods of calculation

As is clear from the preceding sections, to determine the H-maser frequency shift (Eq.30), we have to calculate several spin-exchange collision cross sections and relaxation rates. We start with the inelastic processes. Substituting the DIS expression (22) in Eq.(34) we find[17]

$$G_{\alpha\beta\to\gamma\delta} = \sum_{\ell} (2\ell+1) \left\langle \frac{2\pi\hbar}{m_a k} \left[\frac{\sqrt{E_k}\,\sqrt{E_k+\epsilon_\alpha+\epsilon_\beta-\epsilon_\gamma-\epsilon_\delta}}{E'_k} \right]^{2\ell+1} \sin^2\left(\delta_1^\ell(E'_k)-\delta_0^\ell(E'_k)\right) \right\rangle$$

$$\times \left| \langle \{\alpha\beta\} | P_1 - P_0 | \{\gamma\delta\} \rangle \right|^2 \qquad (49)$$

with $E'_k = E_k+\epsilon_\alpha+\epsilon_\beta-2\epsilon_0$. As in Eq.(22), we have some freedom in choosing the value of $2\epsilon_0$. The evaluation of the relaxation rates amounts to a standard phase-shift calculation for singlet- and triplet-potential scattering. In these and all further calculations we use "state-of-the-art" singlet and triplet potentials,[20] including adiabatic, relativistic, and radiative corrections. Nonadiabatic corrections are taken into account simply by replacing the nuclear mass occurring in the adiabatic equations by the atomic mass m_a.[21,10] Choosing $2\epsilon_0$ in Eq.(49) halfway between the initial and final channel energies, i.e., $2\epsilon_0 = \frac{1}{2}(\epsilon_\alpha+\epsilon_\beta+\epsilon_\gamma+\epsilon_\delta)$, yields good agreement with coupled channel[17] results (typical deviations below 1%).

The calculation of elastic processes is somewhat more involved. In particular, the hyperfine-induced spin-exchange frequency shift and broadening "cross sections" (λ_1, λ_2, and σ_0) require the evaluation of elastic S-matrix elements taking into account the hyperfine energy-level separation. This can be done by taking the hyperfine energy-level separation into account as a first-order correction to the DIS approximation,[22, 10]

$$S^\ell_{\{\alpha\beta\}\{\alpha\beta\}} = S^{\ell(\mathrm{DIS})}_{\{\alpha\beta\}\{\alpha\beta\}} + \Delta S^\ell_{\{\alpha\beta\}\{\alpha\beta\}}. \qquad (50)$$

When choosing $2\epsilon_0=\epsilon_\alpha+\epsilon_\beta$ in Eq.(22) the DIS elastic S-matrix elements reduce to:

$$S^{\ell(\mathrm{DIS})}_{\{\alpha\beta\}\{\alpha\beta\}}(E_k) = \sum_{S=0,1} S^\ell_S(E_k) \langle \{\alpha\beta\} | P_S | \{\alpha\beta\} \rangle, \qquad (51)$$

with

$$S^\ell_S(E) \equiv e^{2i\delta^\ell_S(E)}, \qquad (52)$$

and the first-order correction takes the form

$$\Delta S^{\ell}_{\{\alpha\beta\}\{\alpha\beta\}}(E_k) = \Delta^{\ell}(E_k) \sum_{\{\gamma\delta\}} |\langle\{\alpha\beta\}|P_1-P_0|\{\gamma\delta\}\rangle|^2 \frac{\epsilon_\gamma+\epsilon_\delta-\epsilon_\alpha-\epsilon_\beta}{2\hbar\omega_0}, \quad (53)$$

with the dimensionless quantity Δ^{ℓ} defined by

$$\Delta^{\ell}(E_k) \equiv \frac{i}{4}\frac{\omega_0 m_a}{\hbar\, k^2}\left[k\int_0^{r_0}\left[u_0^{\ell}-u_1^{\ell}\right]^2 dr + \tfrac{1}{2}(S_0-S_1)^2\, W(O^{\ell},\frac{\partial}{\partial k}O^{\ell})_{r=r_0}\right]. \quad (54)$$

Here W(,) is a Wronskian, O^{ℓ} a Hankel-like free outgoing wave with asymptotic behavior $e^{i(kr-\frac{1}{2}\pi)}$, and the radial singlet(triplet) wave functions u_0^{ℓ} (u_1^{ℓ}) are normalized so as to have the outgoing part $-S_S^{\ell}\, O^{\ell}$. In a classical picture the first-order correction $\Delta S^{\ell}_{\{\alpha\beta\}\{\alpha\beta\}}$ arises due to the finite separation of other hyperfine energy levels ($\epsilon_\gamma+\epsilon_\delta$) from the total hyperfine energy $\epsilon_\alpha+\epsilon_\beta$ associated with the particular elastic channel under consideration, which is felt when making back and forth transitions to other hyperfine levels during the time that the exchange interaction is active.

Using Eqs.(50)-(53) we find for the hyperfine-induced frequency shift and broadening cross sections:

$$\lambda_0 = \lambda_0^{(DIS)} - \tfrac{1}{2}(\lambda_1+\lambda_2), \quad (55)$$

$$\lambda_1 = \frac{\pi}{2k^2}\sum_{\ell}(2\ell+1)\,\mathrm{Im}\left[\Delta^{\ell *}(S_1^{\ell}-S_0^{\ell})/2 + (-1)^{\ell}\Delta^{\ell *}(3S_1^{\ell}+S_0^{\ell})/2\right], \quad (56)$$

$$\lambda_2 = \frac{\pi}{2k^2}\sum_{\ell}(2\ell+1)\,[1+(-1)^{\ell+1}]\,\mathrm{Im}\left[\Delta^{\ell *}(S_1^{\ell}+S_0^{\ell})/2\right], \quad (57)$$

$$\sigma_0 = \frac{-\pi}{2k^2}\sum_{\ell}(2\ell+1)\,[1+(-1)^{\ell}]\,\mathrm{Re}\left[\Delta^{\ell *}S_1^{\ell}\right], \quad (58)$$

$$\sigma_1 = \sigma_1^{(DIS)} - \frac{1}{2}\sigma_0, \quad (59)$$

$$\sigma_2 = \sigma_2^{(DIS)}. \quad (60)$$

Classically speaking, this first-order treatment breaks down when the collision time

becomes large compared to the precession frequency associated with the internal energy-level splitting. The collision duration is large at low collision energies and at narrow resonances, occurring in the singlet channel at certain collision energies.[23] We were able to find out about the range of applicability of the first-order approach under various circumstances in comparing the first-order results with results obtained with the coupled-channel analysis. This comparison fully confirmed the preceding classical expectation: the agreement of the first-order approach with the coupled-channel method turned out to be excellent except for the dominating $\ell=0$ partial wave at the low energies relevant for the cryogenic H maser and at energies and ℓ values at which narrow resonances for singlet scattering occur.

The low-energy deviation for $\ell=0$ is most prominent at collision energies below $2\hbar\omega_0$, due to the fact that the path in the complex plane which is followed by the elastic S-matrix element $S^{\ell=0}_{a\,a,aa}$ when varying the energy shows a 90^0 kink at $E=2\epsilon_a+2\hbar\omega_0$ originating from the threshold in the cc channel felt in the aa channel at this energy. This behavior is absent in the first-order calculation which leads to S-matrix elements which all follow smooth paths in the complex plane.

The deviation at singlet resonances turned out to be most prominent for resonance widths roughly comparable to or smaller than the hyperfine energy-level splitting $2\hbar\omega_0$. The quantity $\Delta^{\ell}(E)$ characterizing the hyperfine-induced correction to the elastic S-matrix elements is then no longer small compared to unity, yielding a large overestimation of hyperfine-induced effects. Fortunately, we were able to avoid a time-consuming coupled-channel calculation at narrow resonances by devising a modified zeroth-order approach. This approach is based on the fact that we have some freedom in choosing a value for ϵ_0 in Eq.(22) so as to make the first-order contribution to the elastic S-matrix elements as small as possible. As is clear intuitively, a good choice for ϵ_0 at narrow singlet resonances appears to be one which gives the first-order correction to the two-body Hamiltonian

$$V' = \sum_{\{\gamma\delta\}} |\{\gamma\delta\}>(\epsilon_\gamma+\epsilon_\delta-2\epsilon_0)<\{\gamma\delta\}| \qquad (61)$$

a vanishing expectation value in singlet spin space. The calculation of the elastic S-matrix elements occurring in the expression for $\sigma_{ac,\nu\to\nu}$ in zeroth order using this choice for ϵ_0 leads to the evaluation of singlet or triplet phase shifts at energies shifted from the kinetic energy in the particular elastic channel under consideration [Eq.(22)]. In view of the result that all narrow resonances occur at energies which are large in comparison with the internal energy levels splitting (a typical narrow resonance being the v=11, ℓ=13 resonance at E $\simeq$ 276K), we may neglect the energy difference $\epsilon_\alpha+\epsilon_\beta-2\epsilon_0$ compared to typical kinetic energies in the denominators of Eq.(22). This

leads to an expression for the elastic S-matrix elements of the form of Eq.(51) but with the energy argument of the singlet or triplet S matrix on the right-hand side replaced by $E_k+\epsilon_\alpha+\epsilon_\beta-2\epsilon_0$. Using this expression for the elastic S-matrix elements in the $\sigma_{ac,\gamma\to\gamma}$ coefficients on the right-hand sides of Eqs.(18)-(20) gives rise to nonvanishing hyperfine-induced frequency shift and broadening cross-sections. Comparison with coupled-channels results reveals that at narrow resonances these modified zeroth-order results are almost indistinguishable from the exact results.

It is of interest to compare the semiclassical results for the hyperfine-induced frequency-shift cross sections of Ref.14 in some detail with our quantum-mechanical results. In the semiclassical straight-line calculation spin-exchange collisions are modeled as spin evolutions under the influence of time-dependent spin interactions originating from the triplet and singlet potentials as the particles move along the undeflected classical trajectories. Defining the singlet (triplet) spin propagators G_0 (G_1) as

$$G_S^{(t_+,t_-)}(b,E) \equiv \exp\left[\frac{-i}{\hbar}\int_{t_-}^{t_+} V_S(b,t)dt\right], \tag{62}$$

with b the impact parameter, and neglecting hyperfine-induced effects we find for the semiclassical (SC) elastic S-matrix elements

$$S^{(DIS,SC)}_{\{\alpha\beta\}\{\alpha\beta\}}(b,E) = \sum_{S=0,1} G^{(+\infty,-\infty)}(b,E) <\{\alpha\beta\}|P_S|\{\alpha\beta\}> \tag{63}$$

[cf. Eq.(51)]. The first-order corrections to the elastic S-matrix elements take the form of Eq.(53) with $\Delta'(E)$ replaced by

$$\Delta(b,E) \equiv \frac{-i}{2}\omega_0 \int_{-\infty}^{+\infty} \left[G_1^{(+\infty,t)}-G_0^{(+\infty,t)}\right]\left[G_1^{(t,-\infty)}-G_0^{(t,-\infty)}\right]dt, \tag{64}$$

leading to the semiclassical expression for the hyperfine induced frequency-shift cross section $\lambda_2(E)$,

$$\lambda_2^{(SC)}(E) = \frac{1}{4}\int_0^\infty Im\left[\Delta^*(b,E)[G_1^{(+\infty,-\infty)}(b,E)+G_0^{(+\infty,-\infty)}(b,E)]\right] 2\pi b\, db \tag{65}$$

[cf. Eq.(57)]. The analogous expression for $\lambda_1^{(SC)}(E)$ is identical to the right-hand side

of Eq.(65) except for the replacement of the plus sign by a minus sign. However, it can be shown that the imaginary part of $\Delta^* G_1^{(+\infty,-\infty)}$ is just equal to the imaginary part of $\Delta^* G_0^{(+\infty,-\infty)}$, so that $\lambda_1^{(SC)}$ vanishes. The origin of this cancellation can be traced back to the neglect of the influence of the exchange interaction on the orbital degrees of freedom: generalizing the preceding calculation scheme so as to take into account the difference between the classical singlet and triplet scattering trajectories would yield non-vanishing values for $\lambda_1^{(SC)}$.[14] This picture is confirmed by the numerical results presented in the following section.

Numerical results

We first consider the spin-exchange frequency shift and broadening cross sections. Although the cross sections λ_0, σ_1, and σ_2 have already been calculated by several authors,[24,25] we include them here because these previous values for σ_1 differ

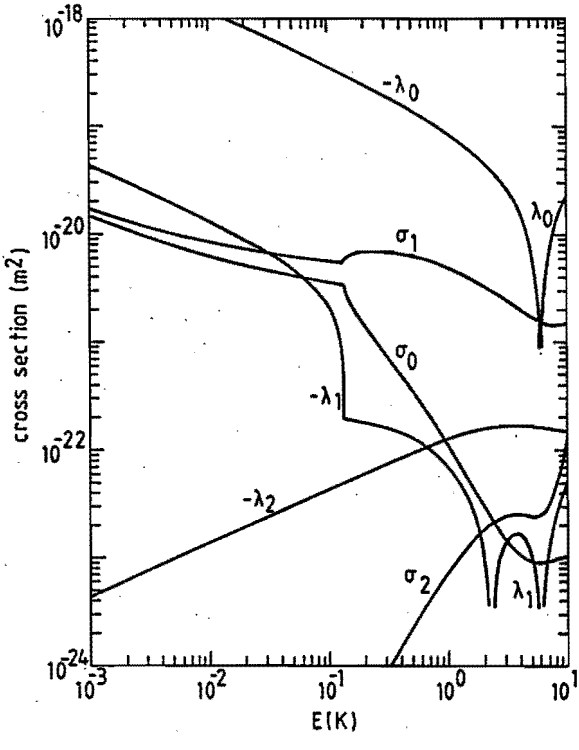

Fig.2. Spin-exchange frequency shift and broadening cross sections for low collision energies.

quantitatively and qualitatively from our values due to the neglect of hyperfine-induced effects at low collision energies. Also due to the use of improved potentials, our results for λ_0, σ_1, and σ_2 differ at low collision energies from previous results.

In Fig.2 the frequency and broadening cross sections are given as functions of relative collision energy. A prominent feature of Fig.2 is the occurrence of cusps in the λ_1, σ_0, and σ_1 cross sections at $E = 2\hbar\omega_0 = 0.14$ K. As discussed in the previous section, the origin of this behavior can be traced back to threshold effects in the $\ell=0$ partial wave. The corresponding cusp in the λ_0 cross section is invisible at the scale of this figure since the main contribution to this cross section comes from the DIS term which behaves smoothly as a function of energy. The λ_2 and σ_2 cross sections vanish at zero collision energy and show no cusp behavior as they have no $\ell=0$ contribution. All other cross sections diverge as $E^{-1/2}$ at low collision energy. For the σ_1 cross section this is in contrast to the finite value at zero collision energy, expected[25] on the basis of DIS considerations.

In Fig.3 the thermally averaged frequency-shift cross sections are shown as functions of temperature. The low-temperature behavior in this figure corresponds to the low-energy behavior in Fig.2. The cross section σ_1 is strongly reduced at high

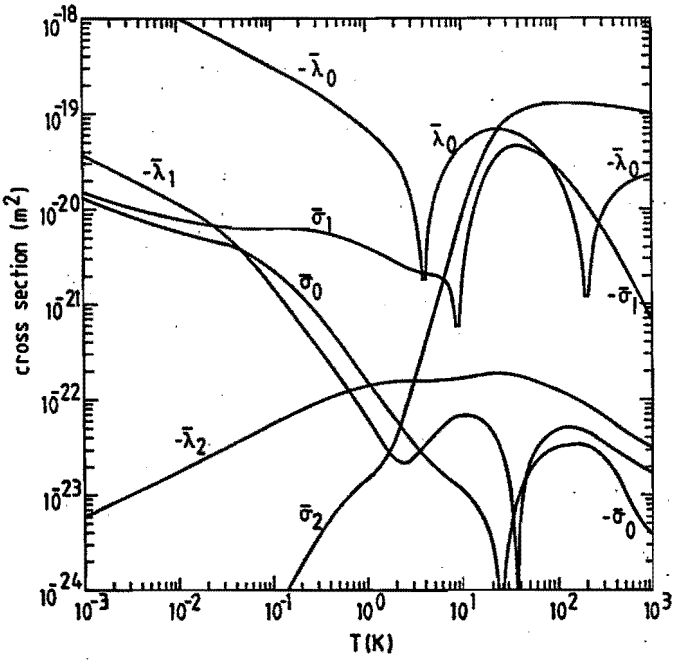

Fig.3. Thermally averaged values of the frequency shift and broadening cross sections.

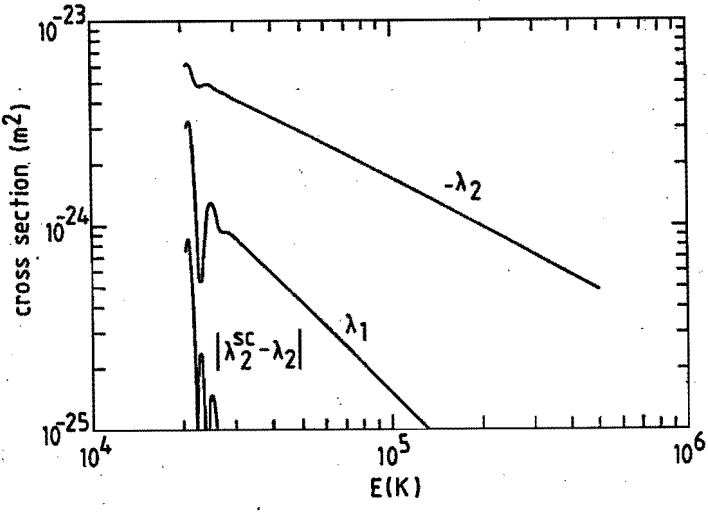

Fig.4. Values of λ_1 and λ_2 resulting from the quantum–mechanical calculation and the deviation of the semi-classical value for λ_2 with the quantum-mechanical value as functions of energy.

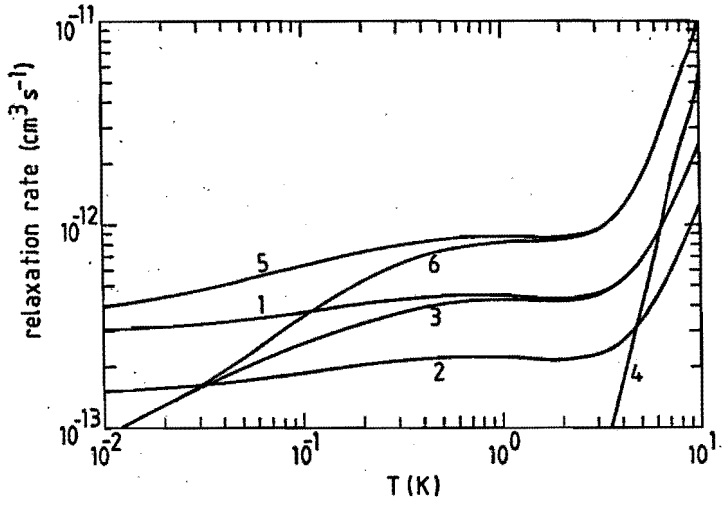

Fig.5. Degenerate-internal-state values of relaxation rates at B=0 for all allowed downward spin-exchange transitions as functions of temperature; 1, $G_{bd\to aa}$; 2, $G_{cc\to aa}$; 3, $G_{cc\to bd}$; 4, $G_{bd\to ac} = G_{cd\to ad} = G_{cb\to ab}$; and the sum rates 5, $G_{bd\to}$; 6, $G_{\to bd}$.

temperatures due to a cancellation of contributions from subsequent ℓ values [see Eq.(19)]. Although a semiclassical theory predicts $\overline{\lambda}_1$ to vanish,[14] we find $\overline{\lambda}_1$ to be comparable in magnitude to $\overline{\lambda}_2$, even at temperatures as high as 1000 K. This in contrast to $\overline{\sigma}_1$, which is negligible compared to $\overline{\sigma}_2$ at T= 1000 K, which by itself would suggest that the semiclassical theory predicting $\overline{\sigma}_1$ to vanish is applicable at this temperature. Calculating λ_1 and λ_2 fully quantummechanically as well as λ_2 semi-classically assuming straight-line trajectories, we find that λ_1 as well as the difference between the semiclassical and quantummechanical values for λ_2 both become small in comparison with λ_2 (Fig.4) when collision energies become large in comparison with the typical strength of the exchange interaction (a few eV), as may be expected from the picture described above. In this way we arrive at the conclusion that the applicability of the semi-classical straight-line calculation scheme is restricted to collision energies above a few eV (corresponding to temperatures $\simeq 10^5$ K).

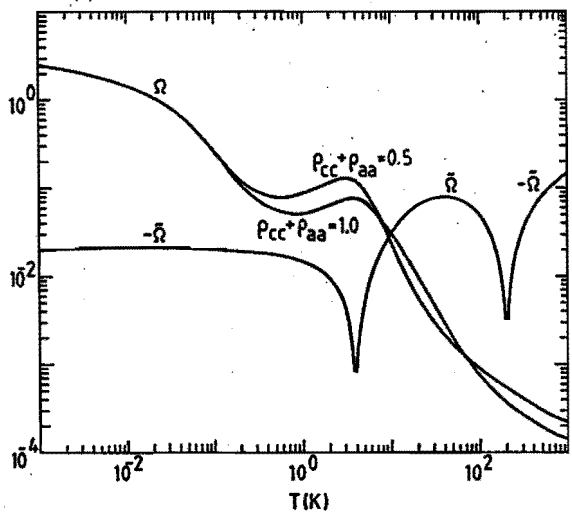

Fig.6. Dimensionless frequency-shift parameters $\tilde{\Omega}$ (for $\Delta=0$ and $\gamma=10^9 cm^{-3}s$) and Ω (for $\rho_{cc}+\rho_{aa}$= 0.5, 1.0) as functions of temperature.

To determine the effective spin-exchange relaxation rates $G_{bd\rightarrow}$ and $G_{\rightarrow bd}$ playing a role in the dependence of $\rho_{cc}+\rho_{aa}$ on H–atom density, we have to calculate the DIS values of several spin-exchange relaxation rates $G_{\alpha\beta\rightarrow\gamma\delta}$. In Fig.5 the rate constants corresponding to the allowed downward spin-exchange transitions at B=0 are presented as functions of temperature. Also, the effective rates $G_{bd\rightarrow}$ and $G_{\rightarrow bd}$ are shown. The figure clearly shows that the rate constants involving odd ℓ values only are completely negligible at sub-kelvin temperatures, but become increasingly important

at temperatures above 1 K. Note that the difference $G_{bd\to}-G_{\to bd}$, which vanishes in the high-energy approximation, is negligible compared to $G_{bd\to}$ only at temperatures well above 1 K.

Using the values of $\bar{\lambda}_1$, $\bar{\lambda}_2$, $\bar{\sigma}_1$, and $\bar{\sigma}_2$ displayed in Fig.3, we are able to determine the dimensionless frequency-offset parameter Ω [Eq.(31)]. Figure 6 shows Ω for two different values of $\rho_{cc}+\rho_{aa}$ as a function of temperature. In order to compare this hyperfine-induced frequency-offset parameter with the DIS frequency offset parameter $\tilde{\Omega}$ we also show the latter as a function of temperature for $\Delta=0$ and a typical value $\gamma=10^9$ cm^{-3}s. Figure 6 shows very clearly that hyperfine-induced spin-exchange frequency shifts become increasingly important at lower temperatures. Both frequency-offset parameters have a finite zero-temperature limit. We find $\Omega(T=0)=3.4$ and $\tilde{\Omega}(T=0,\Delta=0)$ well below unity but depending on the precise value for γ.

To get an idea whether hyperfine induced effects lead to important new sources of frequency instabilities we simulated the operation of hydrogen-maser frequency standards at various temperatures. To begin with, we restricted ourselves to the collision-rate-dependent oscillation frequency shift $\Delta\omega_c$ which potentially causes the largest instabilities since the collision rate is difficult to keep constant in an oscillating H maser. Using Eqs.(30)(32), (43), (44), and the calculated values of the various spin-exchange collision quantities we determined the variations of the oscillation frequency with varying collision rate for various cavity tunings. Since the dependence of Ω on Γ_b, Γ_m and Γ_c can be written as $\Omega(\Gamma_c/\Gamma_b,\Gamma_m/\Gamma_b)$, Eq.(30) shows that the offset $\Delta\omega_c$ of the oscillation frequency from its value at zero collision rate when expressed in units of Γ_b also depends on the various contributions to the hyperfine relaxation rates as $\Delta\omega_c(\Gamma_c/\Gamma_b,\Gamma_m/\Gamma_b)$. Figure 7 displays $\Delta\omega_c/\Gamma_b$ as a function of Γ_c/Γ_b for a maser operating at 0.5K with $\Gamma_m=0$ at various cavity frequency settings. As is evident from this figure, the oscillation frequency varies nonlinearly with Γ_c, because of the dependence of Ω on the level populations sum $\rho_{cc}+\rho_{aa}$, which is itself dependent on collision rate. Even when applying the usual "spin-exchange tuning" procedure, i.e., tuning the cavity so that the oscillation frequency is the same at the minimum collision rate at which self-sustained oscillation can be obtained and the maximum collision rate available, there remains an appreciable variation of oscillation frequency in between these two values. Because it is difficult to reproduce and keep constant the collision rate in a hydrogen maser, these variations of the "spin-exchange tuned" oscillation frequency with Γ_c pose severe problems to the realization of ultrastable cryogenic hydrogen microwave standards: due to the large slopes present in Fig.7 variations of the collisional linewidth Γ_c as small as 0.01 s^{-1} lead to variations of the fractional oscillation frequency offset $\Delta\omega/\omega$ of the order 10^{-15}, which is very large when compared to the potential thermal instabilities of cryogenic masers. Of course, when working at very low atom densities the collisional linewidth can be kept stable within a much smaller interval. However, this can only be done at the expense of increasing

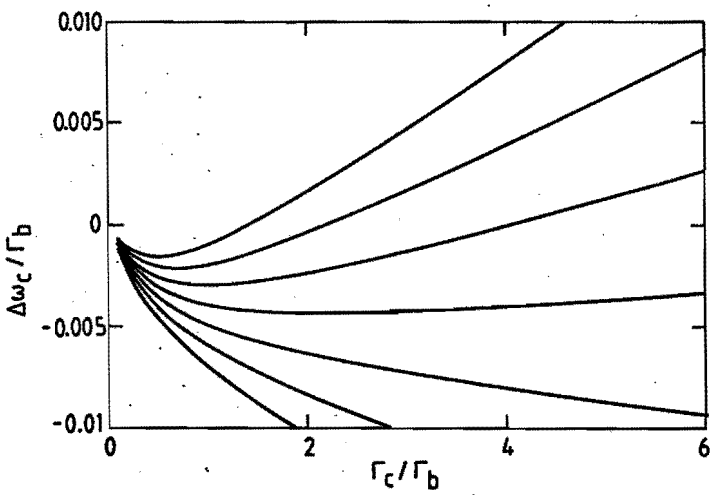

Fig.7. Variations of fractional frequency offset with collision rate at T=0.5 K and $\Gamma_m=0$ for different cavity frequency settings Δ corresponding to $\tilde{\Omega}$ increments of 0.001 between subsequent curves.

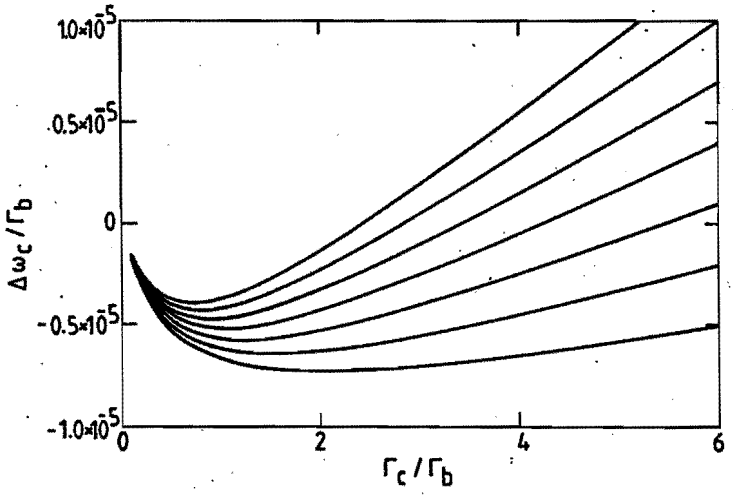

Fig.8. Variations of fractional frequency offset with collision rate at T=300 K and $\Gamma_m=0$ for different cavity frequency settings Δ corresponding to $\tilde{\Omega}$ increments of 0.5×10^{-6} between subsequent curves.

the oscillation frequency instabilities due to thermal noise.[6,9] In the next section we investigate strategies which reduce the frequency instability due to variations in the collisional linewidth while leaving the potential thermal instabilities at a level of 2 parts in 10^{18}.

At room temperatures these problems are much less serious. Figure 8 shows the oscillation frequency shifts for various cavity frequency settings as functions of the collisional linewidth for T = 300 K. The nonlinear variations of oscillation frequency are three orders of magnitude smaller in comparison with the cryogenic results, thanks to the much smaller value of Ω (Fig.6). When the cavity is tuned so that the oscillation frequency is the same at the minimum and maximum collision rates at which maser oscillation occurs, it leaves a fractional variation of frequency with collision rate typically of order 10^{-15} per Hz of collisional linewidth. In order to keep fractional variations of oscillation frequency due to the nonlinear dependence of linewidth safely below the 10^{-15} level, marking the state of the art of room temperature hydrogen-maser relative frequency instabilities, the variations in collision rate then need only to be kept below the 10% level.

Strategies for minimizing the nonlinear direct shifts

Since the instabilities in the maser frequency due to the nonlinear dependence of the oscillation frequency on collision rates seems to be prohibitive in improving substantially upon the stability of room temperature hydrogen masers using cryogenic hydrogen masers, it is necessary to develop techniques for minimizing this nonlinear dependence. We can distinguish three different approaches to accomplish this. First, we may reduce (or even remove) the slope of the cavity frequency as function of collision rate at ambient collision frequency by some refinement of the spin-exchange tuning procedure. Secondly, we can reduce the dependence of the frequency-offset parameter Ω on the level population sum $\rho_{cc}+\rho_{aa}$. As a third possibility we can reduce the dependence of the relative level population sum $\rho_{cc}+\rho_{aa}$ on collision rate.

The first strategy amounts to using a smaller range of Γ_c variations to set the cavity tuning. The optimum spin-exchange tuning procedure clearly would be the one which eliminates the slope of the collision frequency with collision rate at a certain collision rate. However, even the most refined spin-exchange tuning procedure cannot annihilate any nonlinear dependence on collision rate. Indeed, differentiating Eq.(30) twice with respect to the collisional linewidth Γ_c while keeping the linewidth not due to collisions Γ_0 constant yields

$$\frac{\partial^2 \Delta\omega}{\partial \Gamma_c{}^2} = -2\frac{\partial \Omega}{\partial \Gamma_c} - \frac{\partial^2 \Omega}{\partial \Gamma_c{}^2}\Gamma_c, \tag{66}$$

which can not be eliminated by any cavity frequency setting since it is independent of Δ. Using the fact that $\rho_{cc}+\rho_{aa}$, and hence Ω, depends only on the relative magnitudes of the various hyperfine relaxation contributions, it is easily seen that also the dimensionless quantity $\Gamma_c\partial^2\Delta\omega/\partial\Gamma_c^2$ depends only on the ratios of Γ_b, Γ_m, and Γ_c. Figure 9 shows the nonlinearity parameter $\Xi \equiv \Gamma_c|\partial^2\Delta\omega/\partial\Gamma_c^2|$ for $\Gamma_c=\Gamma_b$ at various temperatures with varying Γ_m/Γ_b. A very prominent feature of Fig.9 is the sharp decrease of the nonlinearity parameter with increasing temperature: at room temperature Ξ is typically 3 orders of magnitude smaller than at T=0.5K. At T=0.5K the parameter Ξ is of the order 2×10^{-3} for the linewidth due to collisions roughly equal

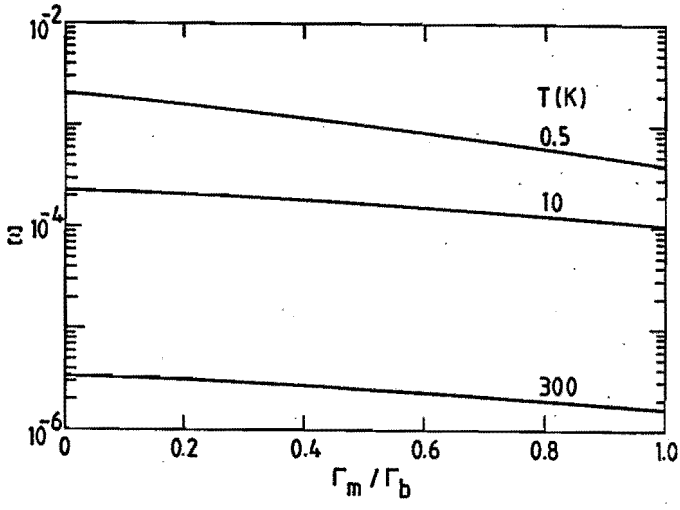

Fig.9. Nonlinearity parameter Ξ for $\Gamma_c/\Gamma_b=1$ and T= 0.5K, 10K, 300K as functions of Γ_m/Γ_b.

to the linewidth due to atom flow and a small contribution of magnetic field gradients to the radiative linewidth. Assuming $\Gamma_c\simeq 2s^{-1}$ variations of the collision rate of 1% lead to variations of the fractional oscillation frequency shift $\Delta\omega/\omega$ of approximately 2×10^{-17}, still an order of magnitude larger than the potential thermal instabilities of liquid-helium-lined hydrogen masers. Moreover, it seems unlikely that the optimum spin-exchange tuning procedure can be realized in practice, as such a tuning procedure requires small Γ_c variations to set the cavity tuning, which leads to a decrease in the accuracy of the cavity-tuning procedure. In the following we nevertheless make use of the nonlinearity parameter Ξ since it provides a fundamental lower bound to instabilities in the oscillation frequency due to variations in the collision rate

We have only the temperature as a single adjustable parameter available to reduce the nonlinear direct shifts by the second strategy, reducing the dependence of Ω on $\rho_{cc}+\rho_{aa}$. As is already clear from Fig.9, higher cryogenic temperatures of about 10 K reduce the nonlinearity parameter roughly by a factor of 10. In this respect neon-surface hydrogen masers operating near 10 K hold some promise although solid neon surfaces are harder to reproduce and maintain than superfluid helium surfaces. The dependence of Ω on $\rho_{cc}+\rho_{aa}$ can be completely eliminated at temperatures at which $\bar{\lambda}_1\bar{\sigma}_2-\bar{\sigma}_1\bar{\lambda}_2$ vanishes. This occurs at very low and very high temperatures, as well as at T= 7.6 K and T= 77 K (Fig.6). From these, the low-temperature limit and the 7.6 K temperature would in principle hold some promise for achieving an ultrastable hydrogen-maser standard because at these temperatures spin-exchange relaxation cross sections are low enough that collisions are not likely to limit the radiated power at achievable hydrogen atom fluxes. However, the operation temperature of 7.6 K is unsuitable for hydrogen-maser standards as it seems unlikely that any wall coating suitable for operation at this particular temperature exists. Also, the T→0 limit is unsuitable not only because of the problem of confining ultracold atoms without disturbing the hyperfine frequency, but also because in this limit the magnitude of Ω exceeds unity, yielding for the cavity mistuning parameter required by the spin-exchange tuning condition $\tilde{\Omega}=\Omega$ a value of order 1, which is unrealistic since the cavity mistuning Δ is limited to values $|\Delta|<<1$.

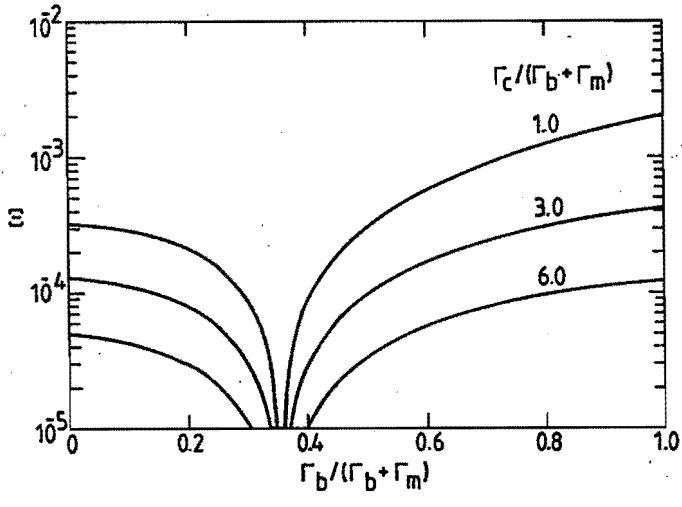

Fig.10. Nonlinearity parameter Ξ with varying $\Gamma_b/(\Gamma_b+\Gamma_m)$ for various values of $\Gamma_c/(\Gamma_b+\Gamma_m)$ at T=0.5 K.

There are several ways to reduce the dependence of the maser frequency on collision rate using the third strategy, reducing the dependence of $\rho_{cc}+\rho_{aa}$ on collision rate. For instance, when working at high atom densities so that $nG_{bd\to}>>\Gamma_b+\Gamma_m$, Eq.(43) yields a strongly reduced dependence of $\rho_{cc}+\rho_{aa}$ on collision rate. This can be seen clearly in Fig.10, which shows the nonlinearity parameter for various values of $\Gamma_c/(\Gamma_b+\Gamma_m)$ as functions of $\Gamma_b/(\Gamma_b+\Gamma_m)$: for fixed values of $\Gamma_b/(\Gamma_b+\Gamma_m)$ the nonlinearity parameter decreases sharply with increasing $\Gamma_c/(\Gamma_b+\Gamma_m)$. Another important feature of Fig.10 is the large dip in the nonlinearity parameter for $\Gamma_b/(\Gamma_b+\Gamma_m) = 0.35$. This dip results from the fact that at this value for $\Gamma_b/(\Gamma_b+\Gamma_m)$ for $\rho^o_{dd}-\rho^o_{bb}=1/2$ the level population difference $2(\rho_{dd}-\rho_{bb}) = 0.35$ [Eq.(44)] which is just equal to the value of

$$\sqrt{(G_{bd\to}-G_{\to bd})/G_{bd\to}}$$

at T=0.5 K. Substituting

$$2(\rho_{dd}-\rho_{bb}) = \sqrt{(G_{bd\to}-G_{\to bd})/G_{bd\to}}$$

together with $\rho^o_{cc}+\rho^o_{aa}= 1/2$ in Eq.(43) yields the level population sum $\rho_{cc}+\rho_{aa}= 1/2$ independent of collision rate. This gives rise to a modified tuning procedure which in principle annihilates the collision-rate-dependent oscillation frequency shift $\Delta\omega_c$ completely. The essence of this tuning procedure is first to set the magnetic field inhomogeneities so as to make $\tilde{\Omega}-\Omega$ [Eq.(30)] independent of collision rate before applying the usual spin-exchange tuning procedure. The dependence of $\tilde{\Omega}-\Omega$ on Γ_c can be monitored by determining the oscillation frequency and the total linewidth [which can be determined experimentally from variations $\Delta\omega$ of oscillation frequency with cavity mistuning Δ, as shown by Eqs.(30) and (32)] at three different collision rates: if the oscillation frequency depends nonlinearly on total linewidth at these three points, $\tilde{\Omega}-\Omega$ still has some dependence on collision rate. For $\tilde{\Omega}-\Omega$ independent of collision rate the usual spin-exchange tuning procedure yields $\tilde{\Omega}=\Omega$ and hence a vanishing collision rate dependent shift, $\Delta\omega_c=0$.

Even when $\Delta\omega_c$ is completely removed, we still have to deal with the collision-rate-independent shift $\Delta\omega_0 = \delta\omega_0 + \tilde{\Omega}\,\Gamma_0 = \delta\omega_0 + \Omega\,\Gamma_0$. For a ^{4}He-lined hydrogen maser operating at a temperature T=0.5K Berlinsky and Hardy predicted[9] that the shift $\delta\omega_0$ could be kept constant against thermal instabilities to within 1 part in 10^{18}. The second term contributing to $\Delta\omega_0$ seems more critical. For $\rho_{cc}+\rho_{aa}= 1/2$ and T = 0.5 K we have $\Omega = 0.07$ (Fig.6). This value implies a maximum allowed instability in the linewidth not due to collisions as low as $\delta\Gamma_0=3\times10^{-7}s^{-1}$ in order to achieve a frequency instability of 2 parts in 10^{18}. It seems unlikely that all line-broadening processes contributing to Γ_0 (atom flow, motion through magnetic field gradients, wall collisions, Doppler broadening, etc.) can be kept stable within this limit.

At room temperature $\Omega \simeq 0.0002$, more than two orders of magnitude smaller than

at T= 0.5 K. In order to achieve a frequency instability of 1 part in 10^{15} the linewidth not due to collisions must be kept stable within approximately 0.05 s^{-1}.

Acknowledgement

This work is supported by the National Science Foundation Grant No. PHY-840467, and is part of a research program of the Stichting voor Fundamenteel Onderzoek der Materie (FOM) which is financially supported by the Nederlandse Organisatie voor Wetenschappelijk Onderzoek (NWO).

References

(1) M.H. Cohen, Proc. IEEE 61, 1192 (1973).

(2) W.E. Carter, D.S. Robertson, and J.R. Mackay, J. Geophys. Res. 90, 4577 (1985).

(3) E.N. Fortson, D. Kleppner, and N.F. Ramsey, Phys. Rev. Lett. 13, 22 (1964).

(4) R.F.C. Vessot *et.al.*, Phys. Rev. Lett. 45, 2081 (1980).

(5) L.A. Rawley, J.H. Taylor, M.M. Davis, and D.W. Allan, Science 238, 761 (1987).

(6) S.B. Crampton, W.D. Phillips, and D. Kleppner, Bull. Am. Phys. Soc. 23, 86 (1978); R.F.C. Vessot, M.W. Levine, and E.M. Mattison, in Proceedings of the Ninth Annual Precise Time and Time Interval Conference, 1978 [NASA Techn. Memorandum No.78104, 1978 (unpublished)] p.549.

(7) S.B. Crampton, K.M. Jones, G. Nunes, and S.P. Souza, in Proceedings of the Sixteenth Annual Precise Time and Time Interval Conference, 1985 [NASA Techn. Memorandum No.8756, 1985 (unpublished)] p.339.

(8) H.F. Hess, G.P. Kochanski, J.M. Doyle, T.J. Greytak, and D. Kleppner, Phys. Rev. A 34, 1602 (1986); M.D. Hürlimann, W.N. Hardy, A.J. Berlinsky, and R.W. Cline, Phys. Rev. A 34, 1605 (1986); R.L. Walsworth, I.F. Silvera, H.P. Godfried, C.C. Agosta, R.F.C. Vessot, and E.M. Mattison, Phys. Rev. A 34, 2550 (1986).

(9) A.J. Berlinsky and W.N. Hardy, Proceedings of the Thirteenth Annual Precise Time and Time Interval (PTTI) Applications and Planning Meeting, Naval Research Laboratory, Washington, D.C. 1982 [NASA Conference Publication No. 2220, 1982 (unpublished)], p. 547.

(10) B.J. Verhaar, J.M.V.A. Koelman, H.T.C. Stoof, O.J. Luiten and S.B. Crampton, Phys. Rev. A 35, 3825 (1987).

(11) L.C. Balling, R.J. Hanson, and F.M. Pipkin, Phys.Rev. 133, A607 (1964); 135, AB1 (1964).

(12) S.B. Crampton, Phys.Rev. 158, 57 (1967).
(13) D. Kleppner, H.C. Berg, S.B. Crampton, N.F. Ramsey, R.F.C. Vessot, H.E. Peters, and J. Vanier, Phys.Rev. 138, A972 (1965).
(14) S.B. Crampton and H.T.M. Wang, Phys.Rev. A 12, 1305 (1975).
(15) S. Hess, Z. Naturforsch. 22a, 1871 (1967).
(16) W. Glöckle, *The Quantum Mechanical Few-Body Problem* (Springer-Verlag, Berlin, 1983).
(17) H.T.C. Stoof, J.M.V.A. Koelman, and B.J. Verhaar, Phys.Rev. B 38, 4688 (1988).
(18) J.M.V.A. Koelman, H.T.C. Stoof, B.J. Verhaar, and J.T.M. Walraven, Phys. Rev. Lett. 59, 676 (1987).
(19) D. Kleppner, H.M. Goldenberg, and N.F. Ramsey, Phys. Rev. 126, 603 (1962).
(20) W. Kolos and L. Wolniewicz, J. Chem. Phys. 43, 2429 (1965); W. Kolos and L. Wolniewicz, Chem. Phys. Lett. 24, 457 (1974); J.F. Bukta and W.J. Meath, Mol. Phys. 27, 1235 (1974); L. Wolniewicz, J. Chem. Phys. 78, 6173 (1983).
(21) P.R. Bunker, C.J. McLarnon, and R.E. Moss, Mol. Phys. 33, 425 (1977).
(22) A.M. Schulte and B.J. Verhaar, Nucl.Phys. A232, 215 (1974).
(23) T.G. Weach and R. Bernstein, J. Chem. Phys. 46, 4905 (1967).
(24) A.C. Allison, Phys. Rev. A 5, 2695 (1972).
(25) A.J. Berlinsky and B. Shizgal, Can. J. Phys. 58, 881 (1980).

CHAPTER 4
SPIN WAVES IN DILUTE H↓ GAS

Section 4.1
Spin waves in dilute gases

Among the many fascinating properties of spin-polarized hydrogen gas, the spin-wave phenomenon takes a prominent place. Of course, spin waves are rather commonplace in dense systems such as liquid ^{3}He and electrons in ferromagnetic metals. In dilute hydrogen atom gas however, the observation of spin waves[1] came as a surprise. Although the possibility of coherent spin oscillations in dilute non-degenerate gases was predicted by Bashkin[2] and independently in considerable detail by Lhuillier and Laloë,[3] workers in the field were rather skeptical about the observability of spin waves in such systems. It was believed that the exchange effects which are at the origin of the spin-wave phenomenon, to be effective, require a dense degenerate phase such as in the Fermi liquid ^{3}He.

The success of the Cornell spin-wave experiment for H gas,[1] and a related experiment with ^{3}He gas,[4] showed that this skepticism was too pessimistic. In fact, these experiments showed very convincingly that spin waves can propagate in any system of identical particles independent of particle statistics or particle density, as long as there is some degree of spin-polarization, and if temperature is low enough. This last requirement can be stated more precisely as follows: If the thermal De Broglie wavelength of the constituent particles is considerably longer than the range of the interparticle interaction.

The theoretical description of spin waves in dilute gases differs from that in dense systems, in that no adjustable phenomenological parameters are required. This nice feature, typical for theories on dilute systems, makes it possible to predict the spin-wave modes for any experimental geometry. Such modes, calculated for the Cornell experimental geometry by Lévy and Ruckenstein[5] agreed excellently with the experimental results.

The hydrogen gas in which the spin waves are observed is in a high magnetic field (B= 6-10 T), so that only the high-field-seeking a- and b-states are populated (sect.1.2, Fig.1). At high magnetic field these hyperfine states both have their electron spin antiparallel to the magnetic field, but differ in their nuclear spin orientations, which are parallel (state b) or antiparallel (state a) to the electron spin. In the Cornell experiment, starting from a doubly polarized gas, the nuclear spins were tilted by applying an NMR pulse at the a⟷b transition frequency. This gave rise to collective oscillations of the nuclear magnetization, although the gas was dilute and had no

significant nuclear-spin-dependent interactions. Essential for the occurrence of these spin waves is the large initial polarization of the nuclear spins, which originates from preferential recombination of the a-state atoms (sect. 1.2).

In the next section we give a simple model which makes plausible that spin waves can propagate in a dilute system with spin-independent interactions if the spins are polarized. The remaining two sections are devoted to the possibility of exciting spin waves in the two-dimensional H↓ gas adsorbed on a superfluid helium film. Section 2.3 gives a derivation of the spin wave equation from first principles, valid for any number of spatial dimensions $d \geq 2$. Using these results, we discuss the possibilities for observing spin waves in 2D H↓ gas.

References

(1) B.R. Johnson, J.S. Denker, N. Bigelow, L.P. Lévy, J.H. Freed, and D.M. Lee, Phys. Rev. Lett. 52, 1512 (1984).

(2) E.P. Bashkin, Pis'ma Zh. Eksp. Teor. Fiz. 33, 11 (1981) [JETP Lett. 33, 8 (1981)].

(3) C. Lhuillier and F. Laloë, J. Phys. (Paris) 43, 197 (1982); 43, 225 (1982).

(4) P.J. Nacher, G. Tastevin, M. Leduc, S.B. Crampton, and F. Laloë, J. Phys. (Paris) Lett. 45, L441 (1984).

(5) L.P. Lévy and A.E. Ruckenstein, Phys. Rev. Lett. 52, 1512 (1984).

Section 4.2
A simple microscopic picture

How can spin waves originate in a rarefied Boltzmann gas of particles with spin-independent interactions? Here, we want to give an answer to this question in the form of a simple microscopic model which, although it may have some tentative aspects (like any simple description of a complicated phenomenon), does give reasonable results and certainly has its merits in giving some physical insight into this subtle phenomenon.

We consider a gas of identical particles (bosons or fermions) with two degenerate[1] internal states (spin½ particles). In particular we study the spin evolution due to two-particle collisions occurring in the gas. Such collisions are described by a wavefunction which is a combined spin-spatial wave function. We choose the bisector of the spin-axes of the two colliding particles as the spin quantization axis (z-axis), φ as the angle of the x-axis with the plane spanned by the two spinvectors, and Θ as the angle between the spins and the z-axis (Fig.1). For gases in which the mean free path of the particles is much shorter than the length scale over which the spin-orientation varies appreciably, only scattering between particles with almost parallel spins ($|\Theta|<<1$) occurs. For small angle Θ, we may work out all expressions to first order in Θ, so that the spin functions of the particles take the form[2]

$$|\chi(1)> = e^{-\frac{1}{2}i\varphi}|\uparrow> - \tfrac{1}{2}\Theta\, e^{+\frac{1}{2}i\varphi}|\downarrow>,$$
$$|\chi(2)> = e^{-\frac{1}{2}i\varphi}|\uparrow> + \tfrac{1}{2}\Theta\, e^{+\frac{1}{2}i\varphi}|\downarrow>. \qquad (1)$$

The two-particle spinfunction consists of a symmetric (triplet) part and an antisymmetric (singlet) part:

$$|\chi(1,2)> = e^{-i\varphi}|\uparrow\uparrow> + \tfrac{1}{2}\Theta\ |\uparrow\downarrow - \downarrow\uparrow>. \qquad (2)$$

The magnitude and direction of the transverse spin component of a particle is given by the magnitude and phase, respectively, of the expectation value of the spin operator $\sigma_+ = \frac{1}{2}(\sigma_x + i\sigma_y)$, which satisfies the rules $\sigma_+|\uparrow> = 0$, and $\sigma_+|\downarrow> = |\uparrow>$.

Now, we take the spatial degrees of freedom into our consideration. Taking into account s-wave scattering (dominant at low temperatures) due to a central spin-independent interaction, some textbook scattering theory[3] gives for the asymptotic form of the symmetric (Φ_+) or antisymmetric (Φ_-) scattering wave function in relative

coordinates:

$$\Phi_{\pm}(\underline{k},\underline{r}) \overset{r\to\infty}{=} \left[\frac{m}{2\hbar k}\right]^{1/2}\left[e^{i\underline{k}.\underline{r}} \pm e^{-i\underline{k}.\underline{r}} + (1\pm1)f_0(k)\frac{e^{ikr}}{r}\right], \tag{3}$$

with the s-wave scattering amplitude $f_0(k)$ given in terms of the s-wave phaseshift $\delta^0(k)$ by

$$f_0(k) = \frac{1}{2ik}\left[e^{2i\delta^0(k)}-1\right]. \tag{4}$$

Notice that, consistent with the s-wave scattering assumption, according to Eq.(3) only the spatially symmetric component undergoes scattering. Depending on whether the particles obey Bose-statistics (ϵ=+1), or Fermi-statistics (ϵ=–1), the total wavefunction must be symmetric or antisymmetric, respectively, under permutation of the particles. For the total wavefunction we therefore write

$$\Psi_{\epsilon}(\underline{k},\underline{r}) = \Phi_{\epsilon}(\underline{k},\underline{r})\, e^{-i\varphi}|\uparrow\uparrow> + \Phi_{-\epsilon}(\underline{k},\underline{r})\, \tfrac{1}{2}\Theta\, |\uparrow\downarrow-\downarrow\uparrow>. \tag{5}$$

Using the expression for the asymptotic form of the plane wave[3]

$$e^{i\underline{k}.\underline{r}} \overset{r\to\infty}{=} \frac{2\pi}{ikr}\left\{e^{ikr}\,\delta(\hat{k}-\hat{r}) - e^{-ikr}\,\delta(\hat{k}+\hat{r})\right\}, \tag{6}$$

with $\delta(\hat{x})$ defined via the relation $\int_{4\pi} d\hat{x}\, \delta(\hat{x}-\hat{x}_0)\, f(\hat{x}) = f(\hat{x}_0)$, we can split up the wave functions $\Phi_{\pm}$ in incoming ($\Phi_{\pm}^{-}$) and outgoing ($\Phi_{\pm}^{+}$) parts:

$$\Phi_{\pm}(\underline{k},\underline{r}) \overset{r\to\infty}{=} \Phi_{\pm}^{-}(\underline{k},\underline{r}) + \Phi_{\pm}^{+}(\underline{k},\underline{r}), \tag{7}$$

with

$$\Phi_{j}^{n}(\underline{k},\underline{r}) \overset{r\to\infty}{=} \frac{2\pi m}{ikr}\left[\frac{m}{2\hbar k}\right]^{\frac{1}{2}}\left\{\delta(\hat{k}-n\hat{r}) + j\delta(\hat{k}+n\hat{r}) + \delta_{j,+}\delta_{n,+}\frac{e^{2i\delta^0(k)}-1}{2\pi}\right\}e^{nikr},\ (j,n=\pm) \tag{8}$$

In the same way the total wave function [Eq.(5)] can be split in an ingoing and an outgoing part:

$$\Psi_{\epsilon}(\underline{k},\underline{r}) \overset{r\to\infty}{=} \Psi_{\epsilon}^{-}(\underline{k},\underline{r}) + \Psi_{\epsilon}^{+}(\underline{k},\underline{r}), \tag{9}$$

with

$$\Psi^{\pm}_{\epsilon}(\underline{k},\underline{r}) \overset{r\to\infty}{=} \Phi^{\pm}_{\epsilon}(\underline{k},\underline{r})\, e^{-i\varphi}|\uparrow\uparrow> + \Phi^{\pm}_{-\epsilon}(\underline{k},\underline{r})\, \tfrac{1}{2}\Theta\, |\uparrow\downarrow - \downarrow\uparrow>. \tag{10}$$

We define the expectation value

$$\underline{J}(1)_{rad}\{\Psi\} \equiv \frac{\hbar}{2im}\left[\Psi^{*}\sigma_{+}(1)\left(\frac{\partial}{\partial r}\Psi\right) - \left(\frac{\partial}{\partial r}\Psi^{*}\right)\sigma_{+}(1)\Psi\right]\hat{r} \tag{11}$$

which gives the radial flux of the transverse spin component (radial spin current) of particle 1 for a wavefunction Ψ. By changing $\sigma_{+}(1)$ into $\sigma_{+}(2)$ and $\hat{r}$ into $-\hat{r}$ the right-hand side of (11) changes into the definition of the radial spin flux of particle 2. For the total radial spin flux of both particles we have

$$\underline{J}_{rad}\{\Psi\} \equiv \underline{J}(1)_{rad}\{\Psi\} + \underline{J}(2)_{rad}\{\Psi\}$$

$$= \frac{\hbar}{2im}\left[\Psi^{*}[\sigma_{+}(1)-\sigma_{+}(2)]\left(\frac{\partial}{\partial r}\Psi\right) - \left(\frac{\partial}{\partial r}\Psi^{*}\right)[\sigma_{+}(1)-\sigma_{+}(2)]\Psi\right]\hat{r} \tag{12}$$

Calculating the radial spin current for the ingoing (Ψ^{-}_{ϵ}) and the outgoing (Ψ^{+}_{ϵ}) wavefunctions by combining Eqs.(8–10,12), we find them to differ for asymptotic r-values by a term $\Delta\underline{J}_{rad}$:

$$\underline{J}_{rad}\{\Psi^{+}_{\epsilon}\} \overset{r\to\infty}{=} \underline{J}_{rad}\{\Psi^{-}_{\epsilon}\} + \Delta\underline{J}_{rad}. \tag{13}$$

The $\Delta\underline{J}_{rad}$ term can be interpreted as the net radial spin current at location $\underline{r}$ due to the scattering. It receives a non-vanishing contribution only from the interference term between the transmitted waves [proportional to $\delta(\hat{k}\pm\hat{r})$], and the spherically scattered wave:

$$\Delta\underline{J}_{rad}(\underline{r}) \overset{r\to\infty}{=} \frac{2\pi\hat{r}}{k^2r^2}\left[e^{-2i\epsilon\delta^{0}}-1\right]\left[\delta(\hat{r}-\hat{k})-\delta(\hat{r}+\hat{k})\right]\Theta e^{i\varphi}. \tag{14}$$

Integrating over the surface of a sphere with radius r, we find for the difference between the total outgoing spin current and the total ingoing spin current:

$$\int_{4\pi} r^2 d\hat{r}\; \Delta\underline{J}_{rad}(\underline{r}) = \frac{4\pi}{k^2}\left[\Theta e^{i[\varphi-2\epsilon\delta^{0}(k)]} - \Theta e^{i\varphi}\right]\hat{k}. \tag{15}$$

This result can be interpreted as follows. It describes a change in the spin current

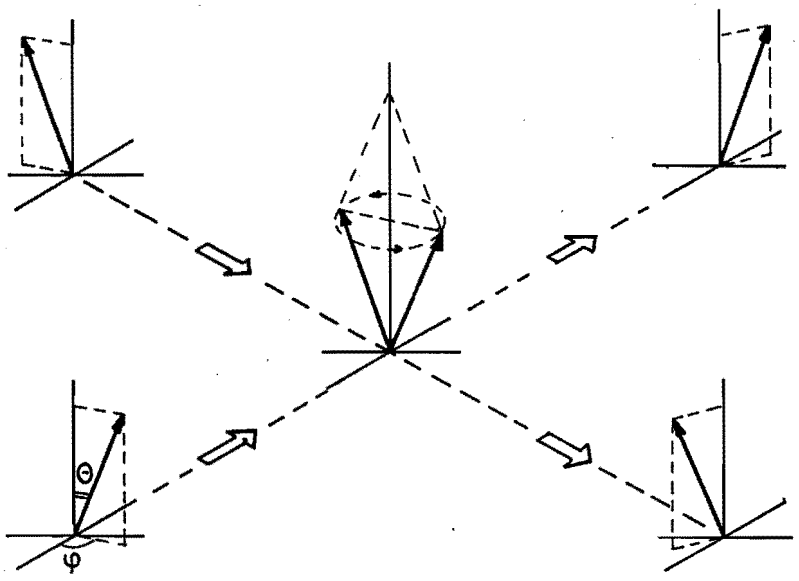

Fig.1. Visualization of the spin-rotation effect in low-energy collisions between identical particles.

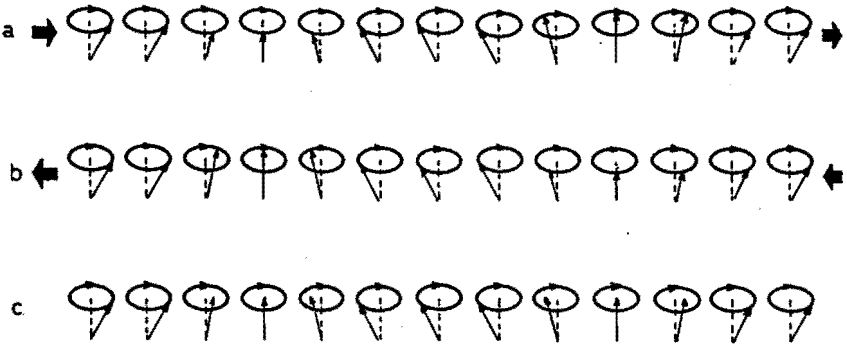

Fig.2. Spin wave modes, a: right traveling spin wave, b: left traveling spin wave, and c: standing spin wave (superposition of a and b).

given by a rotation of the plane in which the spinvectors are located around the vector of the total spin over an angle $-2\epsilon\delta^0(k)$ [Fig.(1)]. Due to the factor $\hat{k}$ this total spin current is only in the direction of the transmitted wave. The factor $4\pi/k^2$ is the effective cross section for this "spin-rotation" process. At low temperatures, $|\delta^0(k)| << 1$ for all relevant k-values. In that case, the spin rotations are in the same direction. It thus becomes clear intuitively that, although collisions occur at random times, subsequent spin rotations add up and form, at a macroscopic scale, a coherent oscillation of the spin magnetization (Fig.2). A formalism for the discussion of such coherent oscillations is considered in the following section.

References

(1) The assumption that the internal energy levels are degenerate is not essential. The problem with finite internal energy level separation can be reduced to the degenerate problem when we transform to the spin-coordinate system rotating with the average Larmor frequency associated with the energy level splitting.

(2) U. Fano, Rev. Mod. Phys. **29**, 74 (1957).

(3) A. Messiah, *Quantum Mechanics* (North-Holland, Amsterdam, 1961).

Section 4.3
Spin waves in 2D and 3D gases

Derivation of the spin wave equation

Our starting point for the derivation of the spin diffusion equation is the quantum mechanical BBGKY hierarchy for a system of N identical particles in a large but finite volume L^d (d is the number of physical dimensions) with periodic boundary conditions. The lowest equation of this hierarchy describes the time evolution of the single particle distribution matrix F′ (normalized as Tr[F′]=N) in terms of the pair distribution matrix F″ (normalized as Tr[F″]=N(N–1)):

$$\frac{\partial}{\partial t} F'_{kk'} + \frac{i}{\hbar}\sum_{p}(H_{kp}F'_{pk'} - F'_{kp}H_{pk'}) = \frac{-i}{\hbar}\sum_{pmn}(V_{kp,mn}F''_{mn,k'p} - F''_{kp,mn}V_{mn,k'p}). \quad (1)$$

Here H represents the single-particle Hamiltonian and V the pair interaction. This equation may be converted to a closed equation for the single particle distribution matrix by expressing the pair matrix at the right hand side in terms of the single-particle distribution matrix. To first order in the hydrogen atom density and assuming at times long before a binary collision the absence of any correlation between the atoms not due to particle indistinguishability (molecular chaos assumption), the pair density matrix in Eq.(1) may be written[1]

$$F''_{kl,mn} = \sum_{pqrs}\Omega^{(+)}_{kl,pq}(F'_{pr}F'_{qs} + \epsilon F'_{ps}F'_{qr})\Omega^{(+)\dagger}_{rs,mn} \quad (2)$$

in which $\Omega^{(+)}$ is the causal two-body Møller wave operator,[2] while the statistics sign ϵ=+1 for a gas of bosonic hydrogen atoms (ϵ=–1 applies to the case of fermions). To be more definite we work from now on in a single-particle basis $\{|n>\}$ in which the single-particle hamiltonian is diagonal ($H|n> = E_n|n>$). Defining the T-operator as $T \equiv V\Omega^{(+)}$, and using some relations for the Møller wave operator from scattering theory,[2] we find

$$\frac{\partial}{\partial t} F'_{kk'} + \frac{i}{\hbar}(E_k - E_{k'})F'_{kk'} =$$

$$\frac{-i}{\hbar}\sum_{pql}T_{kl,pq}(F'_{pk'}F'_{ql} + \epsilon F'_{pl}F'_{qk'}) + \frac{i}{\hbar}\sum_{rsl}(F'_{kr}F'_{ls} + \epsilon F'_{ks}F'_{lr})T^{\dagger}_{rs,k'l}$$

$$-\frac{i}{\hbar}\sum_{pqrsl}T_{kl,pq}(F'_{pr}F'_{qs} + \epsilon F'_{ps}F'_{qr})T^{\dagger}_{rs,k'l}\left[\frac{1}{E_{rs} - E_{k'l} - i\eta} - \frac{1}{E_{pq} - E_{kl} + i\eta}\right] \quad (3)$$

in which η is a small positive constant. We will take the limit $\eta \to 0$ after going to the limit $L \to \infty$. At this point in the derivation the limit $\eta \to 0$ cannot be taken as for finite L the value for η is bounded from below by the requirement[3] $\eta >> \hbar\omega_t$ with ω_t the mean traversal frequency for motion through the volume L^d.

Using the fact that inhomogeneities of the system show up only over macroscopic distances of order L we can write out the indices labelling the single-particle states in terms of wave vectors (underlined characters) and internal-state labels (Greek subscripts):

$$E_k \to E(\underline{k}) + E_\alpha,$$
$$F'_{kk'} \to F_{\alpha\alpha'}(\underline{k},\underline{k}'),$$

with $E(\underline{k}) \equiv \hbar^2k^2/2m$. For spin-independent interactions and splitting off the center of mass momentum we find for the T-matrix:

$$T_{kp,lq} \to T_{\underline{k}\alpha\underline{p}\gamma,\underline{l}\beta\underline{q}\nu} = T(\underline{k}-\underline{p},\underline{l}-\underline{q})\,\delta_{\underline{k}+\underline{p},\underline{l}+\underline{q}}\,\delta_{\alpha,\beta}\,\delta_{\gamma,\nu}.$$

After working out the resulting expression we take the thermodynamic limit: $N \to \infty$, $L \to \infty$, $N/L^d = n$ = constant, so that summations over wavevectors change into integrations. Taking also the limit $\eta \to 0$, and applying the Wigner transformation

$$f_{\alpha\beta}(\underline{k},\underline{r}) \equiv (2\pi)^{-d}\int d\underline{k}'\, e^{-i\underline{k}'.\underline{r}}\, F_{\alpha\beta}(\underline{k}+\tfrac{1}{2}\underline{k}',\underline{k}-\tfrac{1}{2}\underline{k}'), \tag{4}$$

while using the fact that the gas is only slightly inhomogeneous, we find:

$$\frac{\partial}{\partial t} f_{\alpha\beta}(\underline{k},\underline{r}) + \frac{\hbar}{m}\underline{k}.\underline{\nabla}_{\underline{r}} f_{\alpha\beta}(\underline{k},\underline{r}) + \frac{i}{\hbar}[E_\alpha(\underline{r})-E_\beta(\underline{r})]\, f_{\alpha\beta}(\underline{k},\underline{r}) =$$

$$-\frac{i}{\hbar}\sum_\gamma (2\pi)^{-d}\int d\underline{l}\,\Big[T(\underline{k}-\underline{l},\underline{k}-\underline{l}) f_{\alpha\beta}(\underline{k},\underline{r}) f_{\gamma\gamma}(\underline{l},\underline{r}) - T^\dagger(\underline{k}-\underline{l},\underline{k}-\underline{l}) F_{\alpha\beta}(\underline{k},\underline{r}) F_{\gamma\gamma}(\underline{l},\underline{r})$$

$$+ \epsilon\, T(\underline{k}-\underline{l},\underline{l}-\underline{k}) F_{\alpha\gamma}(\underline{l},\underline{r}) F_{\gamma\beta}(\underline{k},\underline{r}) - \epsilon\, T^\dagger(\underline{k}-\underline{l},\underline{l}-\underline{k}) F_{\alpha\gamma}(\underline{k},\underline{r}) F_{\gamma\beta}(\underline{l},\underline{r})\Big]$$

$$+ \frac{2\pi}{\hbar}\sum_\gamma (2\pi)^{-3d}\int d\underline{l}\int d\underline{p}\int d\underline{q}\,\Big[T(\underline{k}-\underline{l},\underline{p}-\underline{q}) T^\dagger(\underline{p}-\underline{q},\underline{k}-\underline{l}) F_{\alpha\beta}(\underline{p},\underline{r}) F_{\gamma\gamma}(\underline{q},\underline{r})$$

$$+ \epsilon\, T(\underline{k}-\underline{l},\underline{p}-\underline{q}) T^\dagger(\underline{p}-\underline{q},\underline{l}-\underline{k}) F_{\alpha\gamma}(\underline{p},\underline{r}) F_{\gamma\beta}(\underline{q},\underline{r})\Big]\, \delta(\underline{p}+\underline{q}-\underline{k}-\underline{l})\, \delta(E(\underline{p})+E(\underline{q})-E(\underline{k})-E(\underline{l})). \tag{5}$$

Using the optical theorem[2] this may be re-written as

$$\frac{\partial}{\partial t} f_{\alpha\beta}(\underline{k},\underline{r}) + \frac{\hbar}{m}\underline{k}.\underline{\nabla}_{\underline{r}} f_{\alpha\beta}(\underline{k},\underline{r}) + \frac{i}{\hbar}[E_\alpha(\underline{r})-E_\beta(\underline{r})]\, f_{\alpha\beta}(\underline{k},\underline{r}) =$$

$$+\frac{i\epsilon}{\hbar}(2\pi)^{-d}\int d\underline{l}\ \mathrm{Re}\{T(\underline{k}-\underline{l},\underline{k}-\underline{l})\}\sum_\gamma\left[F_{\alpha\gamma}(\underline{k},\underline{r})F_{\gamma\beta}(\underline{l},\underline{r})-F_{\alpha\gamma}(\underline{l},\underline{r})F_{\gamma\beta}(\underline{k},\underline{r})\right]$$

$$-\frac{2\pi}{\hbar}(2\pi)^{-3d}\int d\underline{l}\int d\underline{p}\int d\underline{q}\Bigg[|T(\underline{k}-\underline{l},\underline{p}-\underline{q})|^2\sum_\gamma\left[F_{\alpha\beta}(\underline{k},\underline{r})F_{\gamma\gamma}(\underline{l},\underline{r})-F_{\alpha\beta}(\underline{p},\underline{r})F_{\gamma\gamma}(\underline{q},\underline{r})\right]$$

$$-\epsilon T(\underline{k}-\underline{l},\underline{p}-\underline{q})T^\dagger(\underline{p}-\underline{q},\underline{l}-\underline{k})\sum_\gamma\Big[F_{\alpha\gamma}(\underline{p},\underline{r})F_{\gamma\beta}(\underline{q},\underline{r}) - \tfrac{1}{2}F_{\alpha\gamma}(\underline{k},\underline{r})F_{\gamma\beta}(\underline{l},\underline{r})$$

$$-\tfrac{1}{2}F_{\alpha\gamma}(\underline{l},\underline{r})F_{\gamma\beta}(\underline{k},\underline{r})\Big]\Bigg]\ \delta(\underline{p}+\underline{q}-\underline{k}-\underline{l})\ \delta(E(\underline{p})+E(\underline{q})-E(\underline{k})-E(\underline{l})). \qquad (6)$$

We define the spin density as the zeroth-order moment of the distribution function with respect to $\underline{k}$:

$$\sigma_{\alpha\beta}(\underline{r}) \equiv (2\pi)^{-d}\int d\underline{k}\ F_{\alpha\beta}(\underline{k},\underline{r}). \qquad (7)$$

From Eq.(6) a spin density conservation equation can be derived:

$$\frac{\partial}{\partial t}\sigma_{\alpha\beta} + \underline{\nabla}_{\underline{r}}.\underline{J}_{\alpha\beta} + \frac{i}{\hbar}(E_\alpha - E_\beta)\sigma_{\alpha\beta} = 0, \qquad (8)$$

with the spin current defined as the first-order moment of the distribution function with respect to $\underline{k}$:

$$\underline{J}_{\alpha\beta} \equiv (2\pi)^{-d}\int d\underline{k}\ \hbar\underline{k}/m\ F_{\alpha\beta}(\underline{k},\underline{r}). \qquad (9)$$

Equation (8) has precisely the form one should expect for a system with spin-independent interactions. However, it is not a closed equation as it contains the spin current. Just as for the spin density we may derive from Eq.(6) an evolution equation for the spin current. However, this equation would contain a second order $\underline{k}$-moment of the distribution function f. In this way a hierarchy of equations describing the time evolution of the $\underline{k}$-moments of the distribution function arises. We may cut off this hierarchy using the Chapman-Enskog scheme.[4] Physically this means that we suppose, as a first approximation, local thermal equilibrium, i.e. that in each separate region of the gas thermal equilibrium is reached, whereas the gas as a whole is out of

equilibrium. Mathematically this amounts to treating the drift term at the left hand side of Eq.(6) as a small perturbation compared to the collision term at the right hand side. Neglecting for a moment the drift term, Eq.(6) describes a rapid relaxation to a local equilibrium situation:

$$f_{\alpha\beta}(\underline{k},\underline{r}) = f_{eq}(\underline{k})\,\sigma_{\alpha\beta}(\underline{r}), \tag{10}$$

with $f_{eq}(\underline{k})$ the Boltzmann distribution function satisfying the detailed balance condition $f_{eq}(k)f_{eq}(l)=f_{eq}(p)f_{eq}(q)$ for $\underline{k}+\underline{l}=\underline{p}+\underline{q}$, and $E(\underline{k})+E(\underline{l})=E(\underline{p})+E(\underline{q})$. Linearizing around local equilibrium, i.e., writing

$$f_{\alpha\beta}(\underline{k},\underline{r},t) = f_{eq}(\underline{k})[\sigma_{\alpha\beta}(\underline{r},t)+g_{\alpha\beta}(\underline{k},\underline{r},t)], \tag{11}$$

and working out all terms in Eq.(6) to first order in $g_{\alpha\beta}$, except for the drift term which is worked out to zeroth order in $g_{\alpha\beta}$, we find that the first order correction to the distribution function is given by $g_{\alpha\beta}(\underline{k},\underline{r},t) = (\hbar/k_BT)(\underline{k}.\underline{J}_{\alpha\beta})$. For the spin-current evolution equation we find

$$\frac{\partial}{\partial t}\underline{J}_{\alpha\beta} + \frac{k_BT}{m}\underline{\nabla}_r\sigma_{\alpha\beta} + \frac{i}{\hbar}(E_\alpha - E_\beta)\underline{J}_{\alpha\beta} + \frac{\underline{\nabla}_r(E_\alpha - E_\beta)}{2m}\sigma_{\alpha\beta} =$$

$$+\frac{i\epsilon\Omega}{n}\sum_\gamma(\sigma_{\alpha\gamma}\underline{J}_{\gamma\beta}-\underline{J}_{\alpha\gamma}\sigma_{\gamma\beta}) - \frac{K}{n}\sum_\gamma\sigma_{\gamma\gamma}\underline{J}_{\alpha\beta} \tag{12}$$

To derive this result, we applied the s-wave approximation to the T-matrix in which case the T-matrix depends only on the magnitude of the wavenumbers: $T(\underline{k},\underline{k}') = T_0(k)/A$ for $k=k'$ (on the energy shell). The normalization constant $A = 2\pi^{d/2}/\Gamma(d/2)$ is the area of a d-dimensional "sphere" with unit radius. The s-wave approximation is justified for a gas of hydrogen atoms at temperatures of a few hundreds of millikelvins or less. The spin-transport coefficients Ω and K in Eq.(12) can be expressed as thermal averages over the real part of the T-matrix and the squared modulus of the T-matrix, respectively.

The T-matrix can be written in terms of the s-wave phase shift $\delta^0(k)$:

$$T_0(k) = \frac{-2}{\pi}\frac{\hbar^2}{m\,k^{d-2}}e^{i\delta^0(k)}\sin[\delta^0(k)]. \tag{13}$$

Using this equation we find for the spin transport coefficients Ω and K:

$$\Omega = \frac{2^{d/2}\hbar\lambda^{d-2n}}{d\ m}\int_0^\infty d\xi\, e^{-\xi^2}(2\xi)^3 \cos[\delta^0(\sqrt{2\pi}\,\xi/\lambda)]\,\sin[\delta^0(\sqrt{2\pi}\,\xi/\lambda)] \qquad (14)$$

$$K = \frac{2^{d/2}\hbar\lambda^{d-2n}}{d\ m}\int_0^\infty d\xi\, e^{-\xi^2}(2\xi)^3 \left[\sin[\delta^0(\sqrt{2\pi}\,\xi/\lambda)]\right]^2, \qquad (15)$$

with $\lambda=(2\pi\hbar^2/mk_BT)^{1/2}$, the thermal De Broglie wavelength of the particles.

We reduce the above-derived coupled equations (8) and (12) describing the spin transport to one single spin-diffusion equation in the following way. First, we define the "rotating" spin polarization (dimensionless spin density):

$$P_{\alpha\beta}(\underline{r},t) \equiv e^{i(E^0_\alpha - E^0_\beta)t/\hbar}\,\sigma_{\alpha\beta}(\underline{r},t)/n \qquad (16)$$

and the "rotating" spin-polarization current:

$$\underline{S}_{\alpha\beta}(r,t) \equiv e^{i(E^0_\alpha - E^0_\beta)t/\hbar}\,\underline{J}_{\alpha\beta}(\underline{r},t)/n. \qquad (17)$$

In these equations E^0_α is the energy of the hyperfine level α averaged over the volume. In agreement with experimental circumstances we suppose the deviations $\delta E_\alpha(\underline{r}) = E_\alpha(\underline{r}) - E^0_\alpha$ small compared to thermal energies, and also small compared to $\hbar K$. Physically this means that inhomogeneities in the external field do not influence the thermal motion of the particles, and that the spin currents relax at time scales much shorter than the time scale needed to dephase them in the field inhomogeneities. Furthermore, within a few interatomic collision times the spin current is relaxed to its (local) equilibrium value, while the spin density (a conserved quantity during collisions) changes significantly only over much longer time scales. Therefore, the spin current follows adiabatically the varying spin density. Mathematically this means that we may substitute the stationary value of the spin current following from the spin current evolution equation in the evolution equation for the spin density. Using the above assumptions we find that this quasi-stationary value of the spin current satisfies the equation

$$\underline{S}_{\alpha\beta} = -D_0\underline{\nabla}_r P_{\alpha\beta} + i\epsilon\mu \sum_\gamma (P_{\alpha\gamma}\underline{S}_{\gamma\beta} - \underline{S}_{\alpha\gamma}P_{\gamma\beta}), \qquad (18)$$

with the spindiffusion constant $D_0 \equiv k_BT/mK$,[5] and the dimensionless coefficient $\mu \equiv \Omega/K$. We obtain a single transport equation when we construct a closed expression

for $\underline{S}_{\alpha\beta}$ satisfying Eq.(18), and substitute it in the time evolution equation for the spinpolarization:

$$\frac{\partial}{\partial t} P_{\alpha\beta} + \underline{\nabla}_r \cdot \underline{S}_{\alpha\beta} + \frac{i}{\hbar}(\delta E_\alpha - \delta E_\beta) P_{\alpha\beta} = 0, \tag{19}$$

[Cf. Eq.(8)]. In the absence of oscillating external fields, the polarization matrix is diagonal, $P_{\alpha\beta}(\underline{r},t) = P_{\alpha\alpha}(\underline{r},t)\delta_{\alpha\beta}$, so that Eq.(18) yields a diagonal spin-current matrix, which when substituted in Eq.(19) yields

$$\frac{\partial}{\partial t} P_{\alpha\alpha} = D_0 \nabla^2 P_{\alpha\alpha}. \tag{20}$$

For weak external oscillating fields (small tipping-angle pulses) we may linearize around this unperturbed situation, and write

$$P_{\alpha\beta}(\underline{r},t) = P^0_\alpha(\underline{r},t)\delta_{\alpha\beta} + P'_{\alpha\beta}(\underline{r},t), \tag{21}$$

with $|P'_{\alpha\beta}|<<1$. To first order in $P'_{\alpha\beta}$ we find a solution to Eq.(18) which, substituted in Eq.(19), gives the desired spin-diffusion equation

$$\frac{\partial}{\partial t} P'_{\alpha\beta} + \frac{i}{\hbar}(\delta E_\alpha - \delta E_\beta) P'_{\alpha\beta} = \frac{D_0}{1 - i\epsilon\mu(P^0_\alpha - P^0_\beta)} \nabla^2 P'_{\alpha\beta}. \tag{22}$$

This so-called linearized spin-wave equation is a direct generalization of the corresponding equation for two-level systems in 3D derived by Lhuillier and Laloë.[5] Notice that the form of this equation is independent of the number of spatial dimensions, only the values of the spin-transport coefficients D_0 and μ depend on the dimensionality. Equation (22) is a diffusion equation with a complex diffusion constant. It describes very well the results of the Cornell spin-wave experiment[7] on bulk (3D) atomic hydrogen gas. Thereby the theoretical values of μ and D_0 obtained for a 3D H↓-atom gas by Lhuillier[8] were confirmed. In the following we will calculate these parameters for a 2D H↓-atom gas.

First, we show that the dimensionless coefficient μ is related to the quality factor Q of the spinwaves. To do this, we assume homogeneous external fields, so that the Larmor-precession term on the left-hand side of Eq.(22) vanishes, and by substituting $P_{\alpha\beta}=\exp[i(\underline{k}.\underline{r}+\omega(k)t)]$ we easily obtain the spin-wave dispersion relation,

$$\omega(k) = \frac{-D_0 k^2}{1+\mu^2(P^0_\alpha - P^0_\beta)^2}[\epsilon\mu(P^0_\alpha - P^0_\beta) - i],$$

Hence, off-diagonal elements of the polarization matrix undergo damped oscillations with quality factor

$$Q = \frac{|\mathrm{Re}\ \omega(k)|}{\mathrm{Im}\ \omega(k)} = |\mu(P^0_\alpha - P^0_\beta)|.$$

In experiments with atomic hydrogen the spin-polarization is almost complete, $|P^0_\alpha - P^0_\beta| \simeq 1$, and the spin-wave quality factor is given by the absolute value of the coefficient μ.

Spin–wave quality factor in 2D and 3D

As we are interested in the possible occurrence of spin waves in the two-dimensional hydrogen gas adsorbed on a superfluid helium film, we study μ for general spatial dimensionality $d \geq 2$. Using Eqs.(14) and (15) we find

$$\mu = \frac{\Omega}{K} = \frac{\langle \cos\ \delta^0(k) \sin\ \delta^0(k) \rangle}{\langle \sin^2 \delta^0(k) \rangle}, \tag{23}$$

with thermal averaging

$$\langle f(k) \rangle \equiv \int_0^\infty d\xi\, e^{-\xi^2} \xi^3 f(\sqrt{2\pi}\,\xi/\lambda). \tag{24}$$

In order to get a closed expression for μ, we use the effective range expansion for general dimension $d \geq 2$ as introduced by Verhaar *et al.*,[9]

$$\cot \delta_0(k) = \begin{cases} \dfrac{-2\ \Gamma^2(d/2)}{\pi\ (d-2)} \left[\dfrac{2}{a_d k}\right]^{d-2} [1 + O(k^2)], & d > 2, \\ \dfrac{-2}{\pi} \left[-\gamma + \ln\left[\dfrac{2}{a_2 k}\right]\right]\ [1 + O(k^2)], & d = 2, \end{cases} \tag{25}$$

with a_d the scattering length and $\gamma = 0.57721...$ Euler's constant. For dimension $d > 2$ this leads to the low-temperature limit[10]

$$\mu = \frac{-d\ \Gamma^3(d/2)\ (2/\pi)^{d/2}}{2(d-2)\ \Gamma(d)} \left[\frac{\lambda}{a_d}\right]^{d-2}, \quad d > 2, \tag{26}$$

which for d=3 reduces to the well-known result[6]

$$\mu = \frac{-3\sqrt{2}}{16}\frac{\lambda}{a_3}, \quad d = 3. \tag{27}$$

The μ-coefficient for d=2 cannot be obtained from the limit d→2 in Eq.(26) [notice that this would lead to the result $\mu \to \infty$, i.e., undamped spin waves]. A closed expression describing the low-temperature behavior of μ in 2D can be obtained from Eq.(23) and Eq.(25) for d=2, when making use of the slow variation of $\delta^0(k)$ for small k-values. Thanks to this slow variation the thermal integrals in Eq.(23) can be approximated using a one-point generalized Gauss-integration formula. This leads to the result[10]

$$\mu = \frac{2}{\pi}\left[\gamma - \ln\left(\frac{4\sqrt{2}}{3\pi}\frac{\lambda}{a_2}\right)\right]. \tag{28}$$

In the relevant regime $\lambda >> a_d$, Eqs.(26) and (27) show that spin waves are more damped in lower spatial dimensions. In the zero-temperature limit we find that μ diverges as $\sim T^{-(d-2)/2}$ for d>2, and $\sim \ln(T)$ for d=2. In Fig.1 μ is shown for bulk (d=3) and adsorbed (d=2) H↓ gas as a function of temperature. The full curves represent the values obtained by numerical thermal averaging in Eq.(23) using effective range expansions for $\cot(\delta^0)$ including the effective range [$O(k^2)$] term,[9] and the dashed curves represent the simple expressions (27) and (28) with the calculated values $a_2 = 1.22\times10^{-10}$m and $a_3 = 0.71\times10^{-10}$m. As can be seen very clearly in Fig.1, the simple expression (26) very accurately describes the spin-transport coefficient μ in 2D

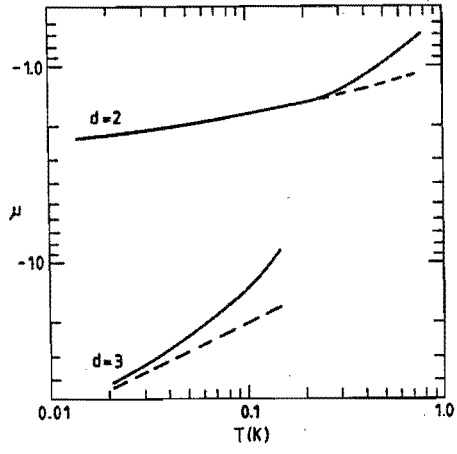

Fig.1: Coefficient μ versus temperature for two- and three-dimensional H↓ *gas. Full curves: including effective-range terms, dashed curves: without effective range terms [Eqs.(27) and (28)].*

H↓ gas for all relevant temperatures ($T \lesssim 0.4$ K). The above analysis makes clear that, in principle, spin waves can propagate in 2D gases of adsorbed H↓ atoms. The low Q value associated with 2D spin waves makes clear, however, that these spin waves will be much less pronounced than in 3D gases. The possibilities for observation of spin waves in 2D H↓ gas will be discussed in detail in the next section.

References

(1) S. Hess, Z. Naturforschung 22A, 1871 (1967).

(2) W. Glöckle, *The Quantum Mechanical Few-Body Problem* (Springer-Verlag, Berlin, 1983).

(3) L.P.H. de Goey, Ph.D. Thesis, Eindhoven University of Technology, The Netherlands, 1988 (unpublished).

(4) E.M. Lifshitz and L.P. Pitaevskii, Vol.10 of *Landau and Lifshitz: Course of Theoretical Physics* (Pergamon Press, 1981).

(5) On a fundamental level there is a problem associated with the introduction of Navier-Stokes transport coefficients for 2D gases. In particular, computer experiments on dense 2D gases show that the average mean square displacement of the particles may be not proportional with time, so that a diffusion coefficient cannot be defined [see for instance: B.J. Adler and T.E. Wainwright, Phys. Rev. A 1, 18 (1970), *ibid.* 4, 233 (1971)]. These deviations from simple hydrodynamic behavior arise at high densities due to a slow decay of the velocity autocorrelation function, indicating a breakdown of the molecular-chaos assumption. For dilute gases such a behavior has not been observed, and consequently these effects are absent, or at least insignificant.

(6) C. Lhuillier and F. Laloë, J. Phys. (Paris) 43, 197 (1982); 43, 225 (1982).

(7) B.R. Johnson, J.S. Denker, N. Bigelow, L.P. Lévy, J.H. Freed, and D.M. Lee, Phys. Rev. Lett. 52, 1512 (1984).

(8) C. Lhuillier, J. Phys. (Paris) 44, 1 (1983).

(9) B.J. Verhaar, L.P.H. de Goey, J.P.H.W. van den Eijnde, and E.J.D. Vredenbregt, Phys. Rev. A 32, 1424 (1985).

(10) J.M.V.A. Koelman, H.J.M.F. Noteborn, L.P.H. de Goey, and B.J. Verhaar, in *Proceedings of the European Conference on Atomic and Molecular Physics* (ECAMP), 1985, edited by W.J. Merz and G. Thomas (European Conference Abstracts, 1985, Vol. 9B, p.151).

Section 4.4

Spin waves in H↓ adsorbed on a superfluid ^{4}He film

J.M.V.A. Koelman, H.J.M.F. Noteborn, L.P.H. de Goey,
B.J. Verhaar, and J.T.M. Walraven[x]

Department of Physics, Eindhoven University of Technology,
Postbus 513, 5600 MB Eindhoven, The Netherlands
[x]*Natuurkundig Laboratorium, Universiteit van Amsterdam,*
1018 XE Amsterdam, The Netherlands

[Published in Phys. Rev. B. 32, 7195 (1985)]

The possibilities for observation and the properties are discussed for two-dimensional spin waves in a nondegenerate spin-polarized atomic hydrogen gas adsorbed on a superfluid helium film. We present results for the spin-transport parameters D_0 en μ, based on two-dimensional effective-range theory. The spin-wave quality factor is an order of magnitude smaller than in the volume case.

Introduction

Spin waves in ferromagnets and other dense systems have been known since the 1950s. In such systems the De Broglie wavelength of the constituents is at least comparable to the distance between nearest neighbors. The associated quantum exchange interaction generated by identical-particle symmetrization is known to play a crucial role in the propagation of spin waves. Some years ago Bashkin[1] and Lhuillier and Laloë[2] pointed to the less obvious possibility of spin waves in very dilute nondegenerate gases. The existence of spin waves was demonstrated a year ago in spin-polarized atomic hydrogen[3,4] and at about the same time[5] in spin-polarized ^{3}He. This discovery led us to investigate the possibility of such waves propagating in the two-dimensional H↓ gas adsorbed on a superfluid helium film.

Such surface spin waves would be interesting for their own sake, but also from a more general point of view. Taking into account the important role of surface atoms in the decay of H↓ in stabilization experiments, it is of vital importance to confirm the accepted picture that the collisions of adsorbed H atoms are not influenced significantly by the dynamics of the helium film. By now it becomes clear[6] that the decay of the atomic density at the surface is not primarily due to two-body dipolar relaxation and thus the latter process does not produce the useful information on the above-mentioned properties which would otherwise have been obtained. The three-

body surface collision processes which one now tends to hold responsible for the decay are probably too complicated to yield such reliable information. On the contrary, surface properties derived from one- and two-body processes such as spin waves are indispensable for reliable calculations[7] of three-body decay at the surface. When it is possible to measure specific transport coefficients such as D_0 and μ (see below) for surface spin waves, this would yield valuable information on the H↓ + H↓ surface scattering. A preliminary report on the present work was presented in Ref. 8.

Previous detailed enquiries[9] into the extent of three dimensionality of the H-H collision process at a superfluid ^{4}He surface, as well as the development of a two-dimensional effective-range theory,[10] provide us with sufficient insight to calculate the properties of spin waves in adsorbed H↓ assuming a static ^{4}He surface. Recently, Bashkin[11] also discussed the possibilities for observation of spin waves in adsorbed H↓. He used a scaling procedure to relate the two-body surface scattering process to that in three dimensions. The premisses for applying this scaling transformation are certainly not fulfilled for H↓ on ^{4}He, in which we are primarily interested in this paper in view of the experience from Ref. 9: the width d of the atomic wave functions perpendicular to the surface is of the order of the range of the H-H triplet interaction. If one would nevertheless apply it to that case, the result for the spin-wave quality factor is of the order of d/a independent of temperature, where a is the three-dimensional (3D) scattering length. This value is a factor of 5 larger than that to be obtained in the following from a more reliable approach, a factor which may be of crucial importance in connection with the prospects for observation of surface spin waves on ^{4}He. Contrary to Bashkin we shall also pay attention to the consequences of the adsorption-desorption kinetics for the observability of surface spin waves.

Surface spin waves

On the atomic scale H↓ spin waves are due to the "identical spin rotation" (ISR) effect: In the case of complete polarization and small tipping angles the effective spins precess in a two-body collision about their sum over an angle $-2\epsilon\delta^0(k)$, where $\epsilon = +1$ (-1) for bosons (fermions) and $\delta^0(k)$ is the s-wave phase shift calculated for a spin-independent potential. Low temperatures are essential for the ISR to lead to a coherent spin transport through the medium. On one hand to avoid collisions with k values for which $|2\delta^0(k)| = O(1)$. On the other hand, to avoid p and higher waves which also perturb the simple ISR behavior.

On the macroscopic scale the collective spin dynamics is described by spin-wave equations in which two important parameters are D_0, the spin-diffusion constant in the unpolarized gas, and μ, measuring the influence of the particle indistinguishability on the spin transport properties. In d dimensions we have for a nondegenerate spin-

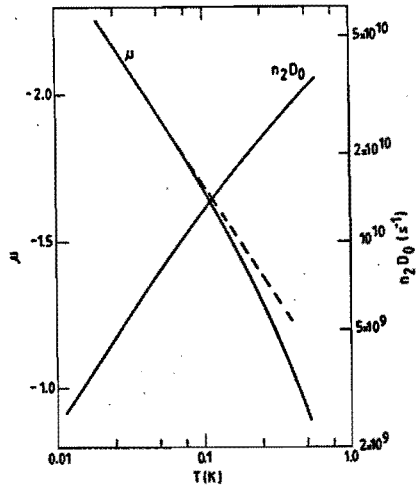

Fig.1. *Two-dimensional spin–transport coefficients* n_2D_0 *and* μ *versus temperature. The broken line indicates the low-temperature limit for* μ *which depends logarithmically on temperature.*

polarized gas,

$$n_dD_0 = \frac{2\pi d\,\hbar}{2^{d/2}m\lambda^d}\left[\int_0^\infty d\xi\, e^{-\xi^2}(2\xi)^3\sin^2\left[\delta^0\left(\frac{\sqrt{2\pi}}{\lambda}\xi\right)\right]\right]^{-1}, \tag{1}$$

$$\mu = \frac{\int_0^\infty d\xi\, e^{-\xi^2}\xi^3\cos\left[\delta^0\left(\frac{\sqrt{2\pi}}{\lambda}\xi\right)\right]\,\sin\left[\delta^0\left(\frac{\sqrt{2\pi}}{\lambda}\xi\right)\right]}{\int_0^\infty d\xi\, e^{-\xi^2}\,\xi^3\sin^2\left[\delta^0\left(\frac{\sqrt{2\pi}}{\lambda}\xi\right)\right]}, \tag{2}$$

where λ is the thermal wavelength and n_d is de d-dimensional particle density. Turning to d = 2 we use the effective-range expression[10]

$$\cot[\delta_0(k)] = \frac{2}{\pi}\left[\gamma+\ln\left(\frac{1}{2}ka\right)\right] + \frac{1}{2\pi}r_e^2k^2, \tag{3}$$

with γ = 0.57721... = Euler's constant, while $a = 2.3a_0$ and $r_e = 14.3a_0$, the two-dimensional scattering length and effective range, respectively. These values were calculated using a potential obtained by averaging the H-H triplet potential over the

finite extension of the atomic wave functions perpendicular to the surface (so-called $2\frac{1}{2}$D model[9]). Figure 1 shows n_2D_0 and μ as functions of temperature. For low temperatures ($T < 0.2$ K) these coefficients go to the values

$$\mu \simeq (2/\pi)[\gamma+\ln(3\pi a/4\sqrt{2}\lambda)],$$

and

$$n_2D_0 \simeq (\pi\hbar/2m\lambda^2)/\sin^2(\operatorname{arccot}|\mu|).$$

The value for μ, as well as the corresponding spin-wave quality factor, following from the first of these equations, is considerably smaller than the bulk value. Note, furthermore, that μ shows a weak temperature dependence, which is due to the typical logarithmic k dependence of the phase shift in two dimensions.

To investigate under what conditions H$\downarrow$ spin waves might be observable in the adsorbed phase we consider a Cornell-type NMR experiment using a cell with a large surface to volume ratio and most of the surface parallel to the (linear) magnetic field gradient in the x direction. Of the remaining small surface part one end is at $x = 0$ and the other at $x = L$. Following Ref. 4 we denote the component of the polarization along $\underline{B}$ by σ_0 and its positive circular component in the frame rotating with the Larmor frequency at $x = 0$ by $\delta\sigma_+$. For the geometry considered we are interested in the lowest transverse (yz-independent) mode, being the only transverse mode coupled to the NMR resonator. We thus have $\delta\sigma_+(\underline{r},t) = F(x,t)$, where F satisfies the boundary condition, based on the smallness of the end surfaces,

$$\left.\frac{\partial F}{\partial x}\right|_{x=0} = \left.\frac{\partial F}{\partial x}\right|_{x=L} = 0, \tag{4}$$

and the mode expansion

$$F(x,t) = \sum_k F^k(x)e^{-i\omega_k t}, \tag{5}$$

in which $F^k(x)$ satisfies

$$\frac{d^2F^k}{dx^2} = \frac{\epsilon\mu\sigma_0-i}{D_0}\left[\omega_k - \frac{Gx}{\hbar}\right]F^k, \tag{6}$$

and the boundary conditions (4). In Eq. (6), $Gx/\hbar$ is the shift of the Larmor frequency due to the field gradient.

Without $\epsilon\mu\sigma_0$ term, Eq. (6) represents spin diffusion in an inhomogeneous field. The $\epsilon\mu\sigma_0$ term arises from the ISR effect. Its form can be understood qualitatively by considering the net effect on a spin of competing ISR precessions around neighboring spins. Clearly, this net effect vanishes for spatially constant or linearly varying polarization $\underline{\sigma}(x,t)$. The first nonvanishing contribution comes from the second derivative. This can be visualized by studying the behavior of a single spin due to two neighboring spins. The net ISR effect vanishes when the latter are tilted over the same angle in opposite directions relative to the first one. Only deviations from this situation contribute. The corresponding molecular field term in the equation for $\partial\underline{\sigma}/\partial t$ gives rise to the above-mentioned $\epsilon\mu\sigma_0$ term in Eq. (6).

For frequencies ω_k small relative to $L|G|/\hbar$ the solutions of Eqs. (6) and (4) can be expressed[12] in Airy functions Ai, each of which corresponds to a (complex) spinwave eigenfrequency,

$$\omega_k = \pm a_k \left[\frac{D_0 G^2/\hbar^2}{|\mu\sigma_0|\overline{+}i}\right]^{1/3}, \tag{7}$$

with a_k defined as the kth zero of Ai', being negative real for all values $k = 1,2,\ldots$. In Eq. (7) and in the following the upper sign refers to the case $\epsilon\mu\sigma_0 > 0$ and the lower sign to $\epsilon\mu\sigma_0<0$. Writing ω_k as $\Omega_k - i\Gamma_k$, Ω_k and Γ_k are products of a_k and k-independent quantities:

$$\Omega_k = \pm a_k \Lambda\cos\Theta, \quad \Gamma_k = -a_k\Lambda\sin\Theta. \tag{8}$$

The distance between eigenfrequencies is determined by the constant

$$\Lambda = \left[\frac{D_0^2 G^4/\hbar^4}{\mu^2\sigma_0^2 + 1}\right]^{1/6}, \tag{9}$$

while the quality factor $Q = |\Omega_k|/\Gamma_k = \cot\Theta$ is determined by the constant

$$\Theta = \tfrac{1}{3}\,\mathrm{arccot}\,|\mu\sigma_0|. \tag{10}$$

The observed spectrum associated with Eq. (5) is a sum over Lorentz profiles centered at the frequencies Ω_k with half-width Γ_k. Notice that $\omega=0$ corresponds to the highest (lowest) Larmor frequency in the sample in case $\epsilon\mu\sigma_0>0$ (<0). Hence for negative polarization ($\sigma_0<0$) and repulsive ($\mu<0$) bosons ($\epsilon=+1$) the spin-wave frequencies Ω_k of the most weakly damped spin waves add positively to the mean Larmor frequency, so that the sharpest spin-wave peaks appear on the high-frequency side of the resonance spectrum.

Adsorption–desorption kinetics

In the foregoing analysis we assumed the surface spin transport to be decoupled from that in the bulk. In what circumstances does the adsorption-desorption kinetics allow for such a decoupling? We consider the following two time scales: $\tau_d = 1/\Gamma_1$, i.e., the damping time of the most weakly damped surface wave, and the mean residency time of atoms on the surface:

$$\tau_{res} = \frac{\pi m \lambda^2}{8 \hbar a} e^{E_B/k_B T} . \tag{11}$$

We take[13] the sticking probability α equal to 0.03 and the binding energy[14] in temperature units E_B/k_B equal to 1.0 K.

The adsorption-desorption kinetics does not influence the surface spin-wave phenomenon if

$$\tau_{res} >> \tau_d. \tag{12}$$

We define the auxiliary time constant $\tau' = (n_2)^{1/2}\hbar/|G|$. This is the time which would be needed by two H atoms at the average interparticle distance to undergo a relative spin precession of 1 rad. For typical densities $n_2 \approx 10^9$ cm^{-2} and field gradients $|\nabla B| \approx 10^{-4}$ T cm^{-1}, τ' is of the order of 1s.

For complete polarization we then have

$$\tau_d = \frac{-(\mu^2+1)^{1/6}(\tau')^{2/3}}{a_1(n_2 D_0)^{1/3} \sin(\frac{1}{3} \operatorname{arccot}|\mu|)} . \tag{13}$$

Figure 2 shows τ_d for various values of τ', as well as τ_{res}, as a function of temperature. Clearly, for the above mentioned n_2 and $|\nabla B|$ values condition (12) is fulfilled for temperatures below 0.08 K. Considering from now on this regime, the spin-wave peaks have a typical width $\tau_d^{-1} \approx 10^2$ s^{-1}. This value is comparable to that for bulk spin waves, as is the total width $L|G|/\hbar \approx 10^4$ s^{-1} (dimension $L \approx 1$ cm) of the NMR absorption spectrum. Due to the lower $|\mu|$ value, however, the quality factor is an order of magnitude smaller than for bulk spin waves. Thus, surface spin-wave peaks in the spectrum are as narrow as in the volume case, but their mutual distance is smaller.

From the point of view of observability it is also of importance to point out that the surface resonance spectrum is shifted over 2.5×10^4 Hz by the surface hyperfine frequency shift relative to the volume spectrum. For the overall intensity of the surface signal the total number of atoms is of interest. It is larger or comparable to the number of volume atoms for surface to volume ratios $A/V > 7$ cm^{-1} ($T \simeq 0.08$ K).

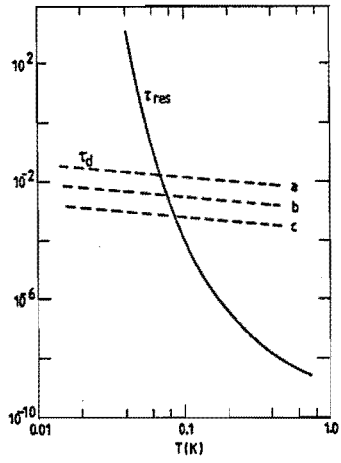

Fig.2. *The times τ_d and τ_{res} as a function of temperature (vertical scale in seconds) for $\tau' = 10$ s (curve a), 1 s (curve b), and 0.1 s (curve c).*

With a high-field ($\simeq$ 8T) NMR spectrometer the minimum detectable number[15] of H atoms is of order 3×10^{13}. For detection of spin waves using small tipping angles, substantially larger quantities are required. This implies the necessity of large surface area within the resonator, possibly a large number of sheets or a ribbon. It seems questionable whether sufficient surface area may be realized in practice. In principle, a large gain in sensitivity may be realized by working at B = 0.65 T, where the NMR frequency is field independent to first order.[16] Since this implies a different excitation and detection scheme it is not further discussed here. We also have to take into account the requirement that τ_d should be small relative to the recombination time for H atoms at the surface. The experimental value[6] for L_s indicates, however, that this requirement is amply fulfilled.

References

(1) E.P. Bashkin, Pis'ma Zh. Eksp. Teor. Fiz. 33, 11 (1981) [JETP Lett. 33, 8 (1981)].

(2) C. Lhuillier and F. Laloë, J. Phys. (Paris) 43, 197 (1982); 43, 225 (1982); C. Lhuillier, *ibid.* 44, 1 (1983).

(3) B. R. Johnson, J.S. Denker, N. Bigelow, L.P. Lévy, J.H. Freed, and D.M. Lee, Phys. Rev. Lett. 52, 1508 (1984); 53, 302 (1984).

(4) L.P. Lévy and A.E. Ruckenstein, Phys. Rev. Lett. 52, 1512 (1984).

(5) P.J. Nacher, G. Tastevin, M. Leduc, S.B. Crampton, and F. Laloë, J. Phys. (Paris) Lett. 45, L441 (1984).

(6) H.F. Hess, D.A. Bell, G.P. Kochanski, D. Kleppner, and T.J. Greytak, Phys. Rev. Lett. 52, 1520 (1984); M.W. Reynolds, I. Shinkoda, W.N. Hardy, A.J. Berlinsky, F. Bridges, and B.W. Statt, Phys. Rev. B 31, 7503 (1985); R. Sprik, J.T.M. Walraven, and I.F. Silvera, Phys. Rev. B 32, 5668 (1985).

(7) L.P.H. de Goey, J.P.J. Driessen, B.J. Verhaar, and J.T.M. Walraven, Phys. Rev. Lett. 53, 1919 (1984).

(8) J.M.V.A. Koelman, H.J.M.F. Noteborn, L.P.H. de Goey, and B.J. Verhaar, in *Proceeding of the European Conference on Atomic and Molecular Physics, 1985*, edited by W.J. Merz and G. Thomas (European Conference Abstracts, 1985), Vol. 9B, p. 151.

(9) J.P.H.W. van den Eijnde, C.J. Reuver, and B.J. Verhaar, Phys. Rev. B 28, 6309 (1983), J.P.H.W. van den Eijnde, Ph.D. thesis, Eindhoven University of Technology, The Netherlands, 1984 (unpublished).

(10) B.J. verhaar, J.P.H.W. van den Eijnde, M.A.J. Voermans, and M.M.J. Schaffrath, J. Phys. A 17, 595 (1984); B.J. Verhaar, L.P.H. de Goey, J.P.H.W. van den Eijnde, and E.J.D. Vredenbregt, Phys. Rev. A 32, 1424 (1985).

(11) E.P. Bashkin, Pis'ma Zh. Eksp. Teor. Fiz. 40, 383 (1984) [JETP Lett. 40, 1197 (1985)].

(12) J.H. Freed, Ann. Phys. (Paris) 10, 901 (1985).

(13) A.J. Berlinsky, M. Morrow, R. Jochemsen, and W.N. Hardy, Physica 109&110B, 2111 (1982).

(14) D.S. Zimmerman and A.J. Berlinsky, Can. J. Phys. 61, 508 (1983).

(15) B.R. Johnson, Ph.D. thesis, Cornell University, 1984 (unpublished).

(16) W.N. Hardy, M. Morrow, R. Jochemsen, and A.J. Berlinsky, Physica 109&110B, 1964 (1982).

CHAPTER 5
CONCLUDING REMARKS

This thesis deals with collision phenomena in atomic hydrogen and deuterium gases. Substantial insight has been obtained into the role played by the nuclear spin dynamics during collisions between low energy ground state hydrogen (deuterium) atoms. On the basis of this insight several new effects have been predicted:

- The formation of an ultra-stable nuclear spin-polarized state due to spin-exchange collisions between magnetically trapped deuterium atoms.
- Shifts of the hydrogen maser frequency due to the nuclear spin dynamics during H+H spin-exchange collisions.
- Nuclear spin waves in two-dimensional atomic hydrogen gas due to the spin-rotation effect associated with low energy collisions between identical particles.

Of course, these predictions have to prove their value while confronted with experimental results. In this respect it is promising that these predictions form a strong enough challenge for experimentalists to put effort in their experimental verification.

For instance, the Amsterdam group working on spin-polarized quantum gases is currently working[1] on the trapping of deuterium atoms. In a preliminary attempt by the Amsterdam group[1] to load deuterium atoms in a magnetic trap no clear signal of trapped deuterium atoms was observed. This was probably due to the specific trap geometry used, which was optimized for trapping hydrogen atoms and which was not deep enough to decouple the stronger adsorbing deuterium atoms from the walls. By using deeper traps and/or optical manipulation techniques[2], some interesting experimental results with magnetically confined deuterium atoms may be expected in the near future.

Also the predicted H-maser frequency shifts are likely to be confronted with experiments in the near future. The U.B.C. group is currently improving the frequency-stability measurements of their cryogenic hydrogen maser by using two reference room-temperature hydrogen masers.[3] This should make it possible to study experimentally the collision frequency shifts of the cryogenic H maser predicted in this thesis.

The M.I.T. group studied two-dimensional hydrogen atom gas adsorbed on a fritted glass "sponge" covered with superfluid ^{4}He.[4] They did not observe the surface spin waves predicted in this thesis. This negative result is understandable taking into account the very rapid decay of the hydrogen atoms observed in this experiment. The anomalously short lifetimes of the atoms is attributed[4] to spin relaxation by magnetic impurities inside the "sponge". The same experiment with a better

characterized substrate should make it possible to observe spin waves in 2D hydrogen atom gas.

References

(1) J.T.M. Walraven, private communication.

(2) T.W. Hijmans, O.J. Luiten, I.D. Setija, and J.T.M. Walraven, Proc. of the Third International Conf. on Spin-Polarized Quantum Systems, Torino, 1988 (World-Scientific Publ.).

(3) W.N. Hardy, M.D. Hürlimann, and R.W. Cline, Jap. J. Appl. Phys. 26, 2065 (1987) Suppl. 26-3 (Proc. Int. Conf. on Low Temp. Physics, Kyoto, 1987).

(4) L. Pollack, S. Buchman, Y.M. Xiao, H.F. Hess, G.P. Kochanski, and T.J. Greytak, Phys. Rev. B 34, 461 (1986).

SUMMARY

Collision phenomena are of outmost importance in spin-polarized atomic hydrogen and deuterium gases. On the one hand, it appears that low energy collisions between even such simple particles as H atoms give rise to a very rich variety of physical phenomena. On the other hand, via the occurrence of interatomic collisions, nature puts very strict limits to the physical regimes which can be explored with these quantum gases.

As an illustration, the decay due to interatomic collisions thwarted till now all attempts to reach the low-temperature, high-density regime where effects due to degeneracy are expected to show up. In chapter 2 of this thesis a simple way out is presented for the case of Fermi gases: In spin-polarized Fermi systems at very low temperatures collisions are much less effective than in Bose systems. Working out these ideas for the Fermi gas consisting of magnetically confined deuterium atoms some interesting possibilities show up. It appears that fast spin-exchange collisions automatically lead to a completely spin-polarized gas for which the spin-relaxation limited lifetime increases dramatically with decreasing temperature. As also the ratio of internal thermalization rate over decay rate increases with decreasing temperature, this gas can be cooled by forced evaporation down to unheard-of low temperatures.

In chapter 3 it is shown that interatomic collisions also play a decisive role in determining the frequency stability of cryogenic hydrogen masers. Especially the hyperfine-interaction induced dynamics of the nuclear spins during collisions, which inevitably shows up at lower collision energies, strongly limits the improvement in frequency stability attainable by H masers operating at lower temperatures. This is because of frequency shifts associated with this nuclear spin dynamics, which are nonlinear in the atomic linewidth. These shifts are not compensated for by the usual methods of tuning the microwave cavities of oscillating hydrogen-maser frequency standards which eliminate only the shifts proportional to the atomic linewidth. At room temperature these nonlinear shifts are much less prominent but still measurable with state-of-the-art hydrogen masers.

In chapter 4 the phenomenon of spin waves is studied. These collective oscillations of the nuclear spins occurring in a hydrogen-atom gas with polarized electronic spins are also associated with the nuclear spin dynamics during collisions. In contrast to the nuclear spin dynamics relevant for H masers, this dynamics of the nuclear spins is not induced by an interaction which couples to the nuclear spin degrees of freedom, but instead by particle indistinguishability effects. It is shown that the resulting spin waves are not restricted to bulk (3D) gases, but can also propagate in 2D gases adsorbed on a substrate. In adsorbed gases the spin-wave characteristic coefficients

acquire a logarithmic temperature dependence typical for 2D. The case of a 2D hydrogen-atom gas adsorbed on a superfluid ^{4}He film is considered in some detail. Taking into account the adsorption-desorption kinetics the regime where spin waves should be observable in adsorbed H gas is determined.

SAMENVATTING

Botsingsverschijnselen zijn van groot belang in spingepolariseerd atomair waterstof gas en deuterium gas. Enerzijds blijkt dat lage energie botsingen tussen zo eenvoudige deeltjes als waterstofatomen aanleiding geven tot een zeer rijke verscheidenheid aan fysische verschijnselen. Anderzijds limiteert de natuur, door middel van interatomaire botsingen, in zeer sterke mate de fysische regimes waarin deze quantumgassen onderzocht kunnen worden.

Dit laatste kan geïllustreerd worden aan de hand van het verval ten gevolge van interatomaire botsingen. Tot op heden verijdelt dit verval alle pogingen tot het bereiken van het lage-temperatuur, hoge-dichtheid regime waar effekten tengevolge van degeneratie verwacht worden waarneembaar te zijn. In hoofdstuk 2 van dit proefschrift wordt een eenvoudige uitweg gepresenteerd voor het geval van Fermi-gassen: bij zeer lage temperaturen zijn botsingen in spingepolariseerde Fermi-systemen veel minder effectief dan in Bose-systemen. Een aantal interessante mogelijkheden treden naar voren wanneer we deze ideeën uitwerken voor het Fermi-gas bestaande uit magnetisch opgesloten deuteriumatomen. Het blijkt dat snelle spin-exchange botsingen vanzelf leiden tot een compleet spingepolariseerd gas waarvan de door spin-relaxatie gelimiteerde levensduur drastisch toeneemt met afnemende temperatuur. Dit gas kan door middel van geforceerd afdampen gekoeld worden tot ongekend lage temperaturen, aangezien bij afnemende temperatuur ook de thermalisatie-snelheid tèn gevolge van interatomaire botsingen toeneemt ten opzichte van de vervalssnelheid.

In hoofdstuk 3 wordt aangetoond dat interatomaire botsingen ook een beslissende rol spelen met betrekking tot de frequentie stabiliteit van cryogene waterstof-masers. Met name de door de hyperfijnwisselwerking geïnduceerde dynamika van de nucleare spins gedurende botsingen, welke onvermijdelijk de kop opsteekt bij lagere botsingsenergieën, limiteert sterk de verbetering in frequentie stabiliteit die haalbaar is met H-masers werkend bij lagere temperaturen. Dit vanwege de met de nucleare spindynamika geassocieerde frequentieverschuiving, welke niet-lineair is in de atomaire lijnbreedte. Deze verschuiving kan niet geëlimineerd worden met de gebruikelijke methoden voor het afstellen van de microgolf trilholten van oscillerende waterstof-masers: deze elimineren alleen verschuivingen die evenredig zijn met de atomaire lijnbreedte. Bij kamertemperatuur is de niet-lineaire verschuiving minder opvallend maar, met de huidige stand van zaken op het gebied van waterstof masers, nog altijd meetbaar.

In hoofdstuk 4 wordt het verschijnsel spingolven bestudeerd. Deze collectieve oscillaties van de nucleare spins die waargenomen zijn in een gas bestaande uit waterstof atomen met gepolariseerde electronenspins zijn eveneens geassocieerd met nucleaire spin dynamika tijdens botsingen. In tegenstelling tot de nucleare spin dynamika relevant in H masers, is in dit geval de dynamica van de nucleare spins niet geïnduceerd door een wisselwerking welke koppelt met de nucleare spin vrijheids-graden, maar in plaats daarvan door deeltjes-ononderscheidbaarheids-effekten. Er wordt aangetoond dat de resulterende spingolven niet beperkt zijn tot drie-dimensionale (3D) gassen, maar ook kunnen propageren in 2D gassen geadsorbeerd aan een substraat. In geadsorbeerde gassen verkrijgen de karakteristieke spingolf-coëfficienten een logaritmische temperatuur afhankelijkheid typisch voor 2D. Het geval van 2D atomair waterstofgas geadsorbeerd aan een superfluïde ^{4}He film wordt in detail beschouwd. De adsorptie-desorptie kinetiek in de beschouwing betrekkend wordt het regime bepaald waarin spingolven waarneembaar zullen zijn in geadsorbeerd H gas.

NAWOORD

Velen ben ik dank verschuldigd voor hun aandeel in het welslagen van het hier beschreven onderzoek. Met name wil ik noemen mijn beide promotoren Boudewijn Verhaar en Jook Walraven die mij in de gelegenheid stelden in een zeer stimulerende omgeving aan boeiend onderzoek te werken, en vervolgens garant stonden voor een bijzonder inspirerende begeleiding. Mijn collega promovendi Philip de Goey en Henk Stoof dank ik voor de vele boeiende diskussies en de zeer vruchtbare samenwerking. Verder hebben afstudeerder Jom Luiten en een groot aantal stagiairs op enthousiaste wijze direkt of indirekt bijgedragen aan dit onderzoek. Furthermore, I would like to thank Stuart Crampton for his stimulating participation in the H-maser project.

Bij het vervaardigen van dit proefschrift zijn een aantal mensen bijzonder behulpzaam geweest. Ik dank Ria Coopmans en Prisca Koelman voor de hulp bij het tikwerk, Behnam Farid voor het doornemen van de tekst, Ruth Gruijters voor het vervaardigen van de illustraties, en Klaas Kopinga voor zijn hulp bij de conversie naar het nieuwe tekstverwerkings systeem.

STELLINGEN

behorende bij het proefschrift van

J.M.V.A. Koelman

Eindhoven, 13 december 1988

1. Dubbel spin-gepolariseerd atomair deuterium is het meest stabiele magnetisch opsluitbare neutrale gas.

Dit proefschrift, hoofdstuk 2.

2. Geforceerd afdampen van wandvrij opgesloten deuteriumatomen in een magneetveldminimum biedt de mogelijkheid tot het bereiken van ongekend lage temperaturen.

Dit proefschrift, hoofdstuk 2.

3. In een willekeurig tweedimensionaal gebied met oppervlakte $\frac{1}{2}N\sqrt{3}$ (N geheel positief) kunnen N+1 punten geplaatst worden zodanig dat de afstand tussen ieder paar punten groter dan of gelijk is aan 1.

4. De nuldoorgangen van de botsingsdoorsneden welke de verschuiving van de H+H 21cm-lijn karakteriseren, kunnen in principe gebruikt worden voor de definitie van een temperatuurschaal die vanuit theoretisch oogpunt voordelen biedt ten opzichte van bestaande temperatuurschalen.

F. Laloë, privé mededeling.

5. De door Berlinsky en Hardy voorspelde frequentiestabiliteit van de cryogene H-maser van 2 op 10^{18} is niet realistisch.

A.J. Berlinsky and W.N. Hardy, Proc. 13th Annual Precise Time and Time Interval (PTTI) Applications and Planning Meeting, Washington D.C. 1982 [NASA Conf. Publ. No. 2220, 1982, p. 547].

6. Gesloten uitdrukkingen voor vervalsconstanten en transportcoëfficienten in 2D en 3D quantumgassen kunnen gevonden worden met behulp van gegeneraliseerde Gauss-Laguerre integratie.

Dit proefschrift, hoofdstuk 2 en 4.

7. De invloed van afwijkingen van de adiabatische Born-Oppenheimer benadering op H+H of D+D botsingen kan eenvoudig afgeschat worden door in de uitdrukkingen gebaseerd op de adiabatische benadering de kernmassa te vervangen door de atoommassa.

P.R. Bunker, C.J. McLarnon and R.E. Moss, Mol. Phys. 33, 425 (1977);
Dit proefschrift, hoofdstuk 3.

8. De "ontaarde interne toestanden benadering" geeft, mits op de juiste grootheid toegepast, zelfs bij willekeurig lage botsingsenergieën een zeer nauwkeurige beschrijving van botsingen tussen grondtoestands H atomen.

Dit proefschrift, hoofdstuk 2 en 3.

9. Op een separabele Hilbertruimte is gegeven een verzameling positieve operatoren $\{R_{ij}\}$ met de eigenschap dat $\Sigma_{i,j} R_{ij} = I$. Indien de marginale operatoren $P_m = \Sigma_j R_{mj}$ en $Q_n = \Sigma_i R_{in}$ niet commuteren zijn beide geen projecties. Dit resultaat geeft aan dat de introductie van gemeenschapelijke metingen van incompatibele observabelen in de quantummechanica impliceert dat meetresultaten van een enkelvoudige observabele in het algemeen niet door middel van projecties kunnen worden gerepresenteerd.

W.M. de Muynck and J.M.V.A. Koelman, Phys. Lett. 98A, 1 (1983).

10. In het "mozaïekbeeld" zoals dat in een groot aantal centrale antenne inrichtingen geïmplementeerd is kunnen fractale objecten waargenomen worden met Hausdorff-dimensies variërend van 0.50 tot 1.95. Dergelijke mozaïekbeelden zijn bij uitstek geschikt om de leek begrip van fractalen bij te brengen.

B.B. Mandelbrot, "The fractal geometry of nature", W.H. Freeman and company, New York, 1983.

11. Ter onderdrukking van randeffecten verdient het aanbeveling het oosterse bordspel Go te spelen met gebruikmaking van periodieke randvoorwaarden.

12. Ter vermijding van kostbare hardwarematige oplossingen dan wel arbeidsintensieve permutatiehandelingen, verdient het aanbeveling om tekstverwerkingspakketten te voorzien van de mogelijkheid om printers zodanig aan te sturen dat een dokument bestaande uit meerdere pagina's in volgorde van afnemend paginanummer wordt afgedrukt.